Title

Search for dark matter produced in association with a single top quark in s=13 TeV pp collisions with the ATLAS detector

Journal

European Physical Journal C, 81(10)

ISSN

1434-6044

Authors

Aad, G
Abbott, B
Abbott, DC
et al.

Publication Date

2021-10-01

DOI

10.1140/epjc/s10052-021-09566-y

Peer reviewed

Eur. Phys. J. C (2021) 81:860
https://doi.org/10.1140/epjc/s10052-021-09566-y

THE EUROPEAN PHYSICAL JOURNAL C

Regular Article - Experimental Physics

Search for dark matter produced in association with a single top quark in $\sqrt{s} = 13$ TeV pp collisions with the ATLAS detector

ATLAS Collaboration[⋆]

CERN, 1211 Geneva 23, Switzerland

Received: 19 November 2020 / Accepted: 23 August 2021 / Published online: 1 October 2021

Abstract This paper presents a search for dark matter in the context of a two-Higgs-doublet model together with an additional pseudoscalar mediator, a, which decays into the dark-matter particles. Processes where the pseudoscalar mediator is produced in association with a single top quark in the 2HDM+a model are explored for the first time at the LHC. Several final states which include either one or two charged leptons (electrons or muons) and a significant amount of missing transverse momentum are considered. The analysis is based on proton–proton collision data collected with the ATLAS experiment at $\sqrt{s} = 13$ TeV during LHC Run 2 (2015–2018), corresponding to an integrated luminosity of 139 fb^{-1}. No significant excess above the Standard Model predictions is found. The results are expressed as 95% confidence-level limits on the parameters of the signal models considered.

1 Introduction

Strong evidence for the existence of a new, non-luminous matter component of the universe, dark matter (DM), arises from astrophysical observations such as precise measurements of the cosmic microwave background and from gravitational lensing measurements. Through its gravitational interactions, it is suggested that DM constitutes up to 26% of the matter–energy content of the universe [1,2]. The nature and properties of DM remain largely unknown in the context of the Standard Model (SM) of particle physics. Under the hypothesis that DM behaves like a weakly interacting massive particle (WIMP) [3], searches are performed using multiple, complementary approaches. At hadron colliders, searches for WIMP-like DM production crucially rely on one or more visible particles being produced in association with the sought-after invisible DM candidate. The experimental signature for DM candidates is missing transverse momentum ($\vec{p}_{\mathrm{T}}^{\,\mathrm{miss}}$, its modulus denoted by $E_{\mathrm{T}}^{\mathrm{miss}}$) in collision events. Several models have been proposed in the past decades, with the details of the DM–SM production process depending on the model assumptions.

A class of simplified models for DM searches at the LHC is considered in this paper. It involves a two-Higgs-doublet extended sector together with an additional pseudoscalar mediator to DM, the 2HDM+a model [4,5]. This class of models represents one of the simplest ultraviolet-complete and renormalisable frameworks for investigating the broad phenomenology predicted by spin-0 mediator-based DM models [5–19]. For the present study, a type-II [20,21] coupling structure of the Higgs sector to third-generation fermions is considered. The CP eigenstates are identified with the mass eigenstates, i.e. two scalars h and H, two pseudoscalars A and a, and charged scalars $H^{\pm}$. Three mixing angles are defined in the model: α denotes the mixing angle between the two CP-even weak spin-0 eigenstates, $\tan\beta$ is the ratio of the vacuum expectation values (VEVs) of the two Higgs doublets and θ represents the mixing angle of the two CP-odd weak spin-0 eigenstates. The alignment ($\cos(\beta-\alpha) = 0$) and decoupling limit is assumed, such that the lightest CP-even state of the Higgs sector, h, can be identified with the SM Higgs boson and the electroweak VEV is set to 246 GeV. The pseudoscalar mediator a couples the DM particles, χ, to the SM and mixes with the pseudoscalar partner of the SM Higgs boson, A. Following the prescriptions in Ref. [5], the masses of the heavy CP-even Higgs boson H and charged bosons $H^{\pm}$ are set equal to the mass of the heavy CP-odd partner A.

This set of models offers a rich phenomenology, with a variety of final states that might arise depending on the production and decay modes of the various bosons composing the Higgs sector, as investigated in Ref. [22]. A recent study [23] has shown that final-state events characterised by the presence of $E_{\mathrm{T}}^{\mathrm{miss}}$ and a single top quark provide promising sensitivity to 2HDM+a models. As in SM single top production, three different types of processes contribute at leading order (LO) in QCD: t-channel production, s-channel production and associated production with a W boson (tW). In the following, these are collectively referred to as DMt

⋆ e-mail: atlas.publications@cern.ch

processes. The t-channel process $pp \to tj\chi\bar{\chi}$ receives its dominant contributions from the two diagrams shown in Fig. 1a, b. These two diagrams interfere destructively, ensuring the perturbative unitarity of the $pp \to tj\chi\bar{\chi}$ process. The magnitude of the interference decreases with increasing $H^{\pm}$ mass. In the case of the tW production channel, the two diagrams shown in Fig. 1c, d provide the dominant contributions to the DMt cross section. As in t-channel production, these two diagrams interfere destructively. When the decays $H^{\pm} \to W^{\pm}a$ are kinematically possible, the charged Higgs bosons are produced on-shell and the cross section of $pp \to tW\chi\bar{\chi}$, assuming $H^{\pm}$ masses of a few hundred GeV, increases to produce a sizeable event rate. Finally, s-channel production is relevant in regions of the parameter space characterised by low $H^{\pm}$ masses (< 300 GeV) and it is not directly targeted by the analysis, but its contribution to the signal is taken into account.

This paper presents a dedicated search for single top quarks produced in association with DM candidates, exploiting final-state signatures characterised by the presence of: large $E_{\mathrm{T}}^{\mathrm{miss}}$; jets, possibly arising from the fragmentation of b-hadrons (b-jets); and one or two charged leptons, either electrons or muons ($\ell = e, \mu$). The analysis is conducted using proton–proton (pp) collisions at a centre-of-mass energy $\sqrt{s} = 13$ TeV produced at the LHC and collected by ATLAS between 2015 and 2018, for a dataset corresponding to 139 fb^{-1}. Three analysis channels, characterised by different lepton or jet multiplicities, are optimised to target different processes: $\mathrm{tW_{1L}}$ and $\mathrm{tW_{2L}}$ (single-lepton and dilepton final states, respectively) for the tW+DM events and $\mathrm{tj_{1L}}$ for t-channel DM production. The results are interpreted in the context of 2HDM+a models, considering various assumptions about the most relevant parameters, m_a, $m_{H^{\pm}}$, and $\tan\beta$. Furthermore, the mutually exclusive $\mathrm{tW_{1L}}$ and $\mathrm{tW_{2L}}$ analysis channels are statistically combined to maximise the sensitivity to tW+DM processes.

Previous searches for 2HDM+a models targeted associated production of DM candidates with Higgs or Z bosons [24], as well as DM and a $t\bar{t}$ pair (referred to as DM$t\bar{t}$) (see Ref. [25] for CMS and Ref. [22] and references therein for ATLAS). This search is targeting the unexplored models within ATLAS where DM produced in association with single top quarks(for CMS results, see Ref. [26]). The analysis is also sensitive to DM$t\bar{t}$ processes in regions of the parameter space where the DMt and DM$t\bar{t}$ production rates are similar.

2 ATLAS detector

The ATLAS detector [27] is a multipurpose particle detector with a forward–backward symmetric cylindrical geometry and nearly 4π coverage in solid angle.[1] The inner tracking detector consists of pixel and microstrip silicon detectors covering the pseudorapidity region $|\eta| < 2.5$, surrounded by a transition radiation tracker which enhances electron identification in the region $|\eta| < 2.0$. A new inner pixel layer, the insertable B-layer [28,29], was added at a mean radius of 3.3 cm during the period between Run 1 and Run 2 of the LHC. The inner detector is surrounded by a thin superconducting solenoid providing an axial 2 T magnetic field and by a fine-granularity lead/liquid-argon (LAr) electromagnetic calorimeter covering $|\eta| < 3.2$. A steel/scintillator-tile calorimeter provides hadronic coverage in the central pseudorapidity range ($|\eta| < 1.7$). The endcap and forward regions ($1.5 < |\eta| < 4.9$) of the hadron calorimeter are made of LAr active layers with either copper or tungsten as the absorber material. A muon spectrometer with an air-core toroid magnet system surrounds the calorimeters. Three layers of high-precision tracking chambers provide coverage in the range $|\eta| < 2.7$, while dedicated fast chambers allow triggering in the region $|\eta| < 2.4$. The ATLAS trigger system consists of a hardware-based level-1 trigger followed by a software-based high-level trigger [30].

3 Data and Monte Carlo simulation

The data analysed in this paper correspond to an integrated luminosity of 139 fb^{-1} of pp collision data collected between 2015 and 2018 by the ATLAS detector with a centre-of-mass energy of 13 TeV and a 25 ns proton bunch crossing interval. The uncertainty in the combined 2015–2018 integrated luminosity is 1.7% [31], obtained using the LUCID-2 detector [32] for the primary luminosity measurements. All detector subsystems were required to be operational during data taking. The average number of interactions in the same and nearby bunch crossings (pile-up) increased from $\langle\mu\rangle = 13.4$ (2015 dataset) to $\langle\mu\rangle = 36.1$ (2018 dataset), with a highest $\langle\mu\rangle = 37.8$ (2017 dataset) and an average $\langle\mu\rangle = 33.7$.

Candidate events were recorded using a combined set of triggers [30] based on the presence of missing transverse momentum or charged leptons ($\ell = e, \mu$). The $E_{\mathrm{T}}^{\mathrm{miss}}$ trigger [33] is fully efficient for events with reconstructed

[1] ATLAS uses a right-handed coordinate system with its origin at the nominal interaction point in the centre of the detector. The positive x-axis is defined by the direction from the interaction point to the centre of the LHC ring, with the positive y-axis pointing upwards, while the beam direction defines the z-axis. Cylindrical coordinates (r, ϕ) are used in the transverse plane, ϕ being the azimuthal angle around the z-axis. The pseudorapidity η is defined in terms of the polar angle θ by $\eta = -\ln\tan(\theta/2)$. Rapidity is defined as $y = 0.5\ln[(E+p_z)/(E-p_z)]$ where E denotes the energy and p_z is the component of the momentum along the beam direction. The angular distance ΔR is defined as $\sqrt{(\Delta y)^2 + (\Delta\phi)^2}$.

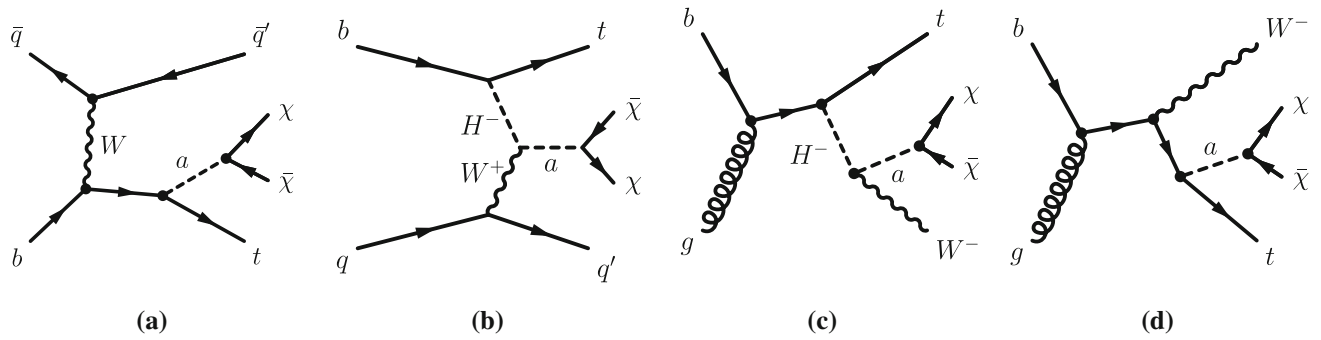

Fig. 1 Representative diagrams of the dark-matter particle χ pair production from the 2HDM+a model considered in this analysis: **a**, **b** through the t-channel, and **c**, **d** through the tW channel

$E_{\mathrm{T}}^{\mathrm{miss}} > 250$ GeV and it was used for the single-lepton analysis channels. Furthermore, an OR between $E_{\mathrm{T}}^{\mathrm{miss}}$ and single-lepton triggers was used for the $\mathrm{tj_{1L}}$ channel for events with reconstructed $E_{\mathrm{T}}^{\mathrm{miss}} < 250$ GeV. Triggers based on a single muon (electron) require the presence of a muon (electron) with transverse momentum p_{T} (transverse energy E_{T}) above certain thresholds, and impose data quality and lepton isolation requirements. The lowest p_{T} (E_{T}) threshold without trigger prescaling is 24 (26) GeV for muons (electrons) and includes a lepton isolation requirement that is not applied for triggers with higher thresholds. In the two-lepton channel, lower thresholds for electrons and muons must be applied to retain sensitivity to the signal. A combined set of two-lepton triggers was used, with the muon (electron) p_{T} (E_{T}) trigger threshold depending on the data-taking period. The lepton trigger threshold ranged between 8 and 22 GeV for muons, and between 12 and 24 GeV for electrons. The analysis selections are chosen to guarantee maximum trigger efficiency, generally above 95%. Trigger matching requirements [30] are applied where the lepton(s) must lie in the vicinity of the corresponding trigger-level object.

Dedicated Monte Carlo (MC) simulated samples are used to model SM processes and estimate the expected signal yields. All samples were produced using the ATLAS simulation infrastructure [34] and GEANT4 [35], or a faster simulation based on a parameterisation of the calorimeter response and GEANT4 for the other detector systems [34]. The simulated events are reconstructed with the same algorithms as used for data. They contain a realistic modelling of pile-up interactions with pile-up profiles matching the ones of each dataset between 2015 and 2018, obtained by overlaying minimum-bias events simulated using the soft QCD processes of PYTHIA 8.186 [36] with the NNPDF2.3 LO set of parton distribution functions (PDFs) [37] and the A3 [38] set of tuned parameters (tune).

Signal MC samples for single top quark production in association with DM include tW, t-channel and s-channel processes. Samples were produced either varying the $(m_a, m_{H^\pm})$ parameters and assuming $\tan\beta$ equal to unity, or varying the $(\tan\beta, m_{H^\pm})$ parameters and setting $m_a = 250$ GeV. Details of other parameter value assumptions are provided in Sect. 7. The samples were generated from leading-order (LO) matrix elements using the MADGRAPH5_aMC@NLO [39] v2.6.2 generator interfaced to PYTHIA 8.212 [40] with the A14 tune [41] for the modelling of parton showering (PS), hadronisation and the description of the underlying event. Parton luminosities are provided by the five-flavour scheme NNPDF3.0 NLO [42] PDF set. Signal cross sections are calculated to LO accuracy in QCD. Additional simulated samples are used for DM$t\bar{t}$ processes. They were generated using LO matrix elements, with up to one extra parton using the MADGRAPH5_aMC@NLO v2.6.7 generator interfaced to PYTHIA 8.244 with the same PDF set and tune as used for the tW, t- and s-channel processes. The top quark decay was simulated using MADSPIN [43]. In this case, signal cross sections are calculated to next-to-leading-order (NLO) accuracy using the same version of MADGRAPH5_aMC@NLO as suggested in Ref. [16].

Background samples were simulated using different MC event generators, accurate at NLO or higher order, depending on the process. All background processes are normalised to the best available theoretical calculation of their respective cross sections. The event generators, the accuracy of theoretical cross sections, the underlying-event parameter tunes, and the PDF sets used in simulating the SM background processes most relevant for this analysis are summarised in Table 1. For all samples, except those generated using SHERPA [44–48], the EVTGEN v1.2.0 [49] program was used to simulate the properties of the b- and c-hadron decays.

4 Event reconstruction and object definitions

Common event-quality criteria and object reconstruction definitions are applied for all analysis channels, including standard data-quality requirements to select events taken during optimal detector operation. In addition, in each analysis channel, dedicated selection criteria, which are specific to

Table 1 List of generators used for the different SM background processes. Diboson includes WW, WZ and ZZ production. Information is given about the underlying-event tunes, the PDF sets and the perturbative QCD highest-order accuracy (LO, NLO, next-to-next-to-leading order (NNLO), and next-to-next-to-leading-log (NNLL)) used for the normalisation of the different samples. Diboson cross sections are taken directly from SHERPA

Process	Generator	PDF set	PS and frag./hadr.	UE tune	Cross-section accuracy
Top pair ($t\bar{t}$)	POWHEG-BOX v2 [50–53]	NNPDF 3.0 NLO	PYTHIA 8	A14	NNLO+NNLL [54]
Single-top t-channel	POWHEG-BOX v1 [55]	NNPDF 3.0 NLO	PYTHIA 8	A14	NNLO+NNLL [56]
Single-top s- and Wt-channel	POWHEG-BOX v2 [57]	NNPDF 3.0 NLO	PYTHIA 8	A14	NNLO+NNLL [58, 59]
V+jets ($V = W/Z$)	SHERPA 2.2.1 [44–48]	NNPDF 3.0 NNLO	SHERPA	Default	NNLO [60]
Diboson	SHERPA 2.2.1 or 2.2.2	NNPDF 3.0 NNLO	SHERPA	Default	NLO
$t\bar{t}+V$, $V = W, Z, h$	MADGRAPH5_aMC@NLO 2.3.3	NNPDF 3.0 NLO	PYTHIA 8	A14	NLO [39, 61]
tWZ	MADGRAPH5_aMC@NLO 2.6.7	NNPDF 3.0 NLO	PYTHIA 8	A14	NLO [39]

the objects and kinematics of interest in those final states, are applied as described in Sect. 5.

Events are required to have at least one reconstructed interaction vertex with a minimum of two associated tracks each having $p_{\mathrm{T}} > 500$ MeV. In events with multiple vertices, the one with the highest sum of squared transverse momenta of associated tracks is chosen as the primary vertex [62]. A set of baseline quality criteria are applied to reject events with non-collision backgrounds or detector noise [63].

Two levels of object identification requirements are defined for leptons and jets: baseline and signal. Baseline leptons and jets are selected with looser identification criteria, and are used in computing the missing transverse momentum as well as in resolving possible reconstruction ambiguities. Signal leptons and jets are a subset of the baseline objects, with tighter quality requirements which are used to define the search regions. Isolation criteria, defined with a list of tracking-based and calorimeter-based variables, are used to select signal leptons by discriminating between semileptonic heavy-flavour decays and jets misidentified as leptons.

Electron candidates are reconstructed from energy deposits in the electromagnetic calorimeter that are matched to charged-particle tracks in the inner detector (ID) [64]. Baseline electrons are required to satisfy $p_{\mathrm{T}} > 10$ GeV and $|\eta| < 2.47$, excluding the transition region between the barrel and endcap calorimeters ($1.37 < |\eta| < 1.52$). They are identified using the 'loose' likelihood identification operating point as described in Ref. [64]. The number of hits in the innermost pixel layer is used to discriminate between electrons and converted photons. The longitudinal impact parameter z_0 relative to the primary vertex is required to satisfy $|z_0 \sin\theta| < 0.5$ mm. Signal electrons are required to also satisfy $p_{\mathrm{T}} > 20$ GeV and the 'tight' likelihood identification criteria as defined in Ref. [64]. The significance of the transverse impact parameter d_0 must satisfy $|d_0/\sigma(d_0)| < 5$ for signal electrons. Signal electrons with $p_{\mathrm{T}} < 200$ GeV are further refined using the 'FCLoose' isolation working point, while those with larger p_{T} are required to pass the 'FCHighPtCaloOnly' isolation working point, as described in Ref. [64]. Corrections for energy contributions due to pile-up are applied.

Muon candidates are reconstructed from matching tracks in the ID and muon spectrometer, refined through a global fit which uses the hits from both subdetectors [65]. Baseline muons must have $p_{\mathrm{T}} > 10$ GeV and $|\eta| < 2.5$, and satisfy the 'medium' identification criteria. Like the electrons, their longitudinal impact parameter z_0 relative to the primary vertex is required to satisfy $|z_0 \sin\theta| < 0.5$ mm. Signal muons are defined with tighter requirements on their transverse momentum and transverse impact parameter significance: $p_{\mathrm{T}} > 20$ GeV and $|d_0/\sigma(d_0)| < 3$. The 'FCLoose' isolation working point is also required for signal muons [65].

Jets are reconstructed from topological clusters of energy depositions in the calorimeters using the anti-k_t algorithm [66], with a radius parameter $R = 0.4$ [67]. The average energy contribution from pile-up is subtracted according to the jet area and the jets are calibrated as described in Ref. [68]. To further reduce the effect of pile-up interactions, the jets with $|\eta| < 2.4$ and $p_{\mathrm{T}} < 120$ GeV are required to satisfy the 'medium' working point of the jet vertex tagger (JVT), a tagging algorithm that identifies jets originating from the primary vertex using track information [69,70]. Baseline jets are selected in the region $|\eta| < 4.5$ and have $p_{\mathrm{T}} > 20$ GeV. The selection of signal jets requires them to be in the region $|\eta| < 2.5$ and to have $p_{\mathrm{T}} > 30$ GeV.

Jets containing b-hadrons are identified as arising from b-quarks ('b-tagged') using a multivariate algorithm (MV2c10), based on the track impact parameters, the presence of displaced secondary vertices and the reconstructed flight path of b- and c-hadrons inside the jet [71]. These b-tagged jets are reconstructed in the region $|\eta| < 2.5$ and have $p_{\mathrm{T}} > 20$ GeV. The b-tagging working point provides an efficiency of 77% for jets containing b-hadrons in simulated $t\bar{t}$ events, with average rejection of 110 and 4.9 for light-flavour jets and jets containing c-hadrons, respectively [72].

To resolve the reconstruction ambiguities between electrons, muons and jets, an overlap removal procedure is applied to baseline objects in a prioritised sequence as follows. First, if an electron shares the same ID track with another electron, the one with lower p_{T} is discarded. Any electron sharing the same ID track with a muon is rejected. Next, jets that are not b-tagged are rejected if they lie within $\Delta R = 0.2$ of an electron. Similarly, jets that are not b-tagged are rejected if they lie within $\Delta R = 0.2$ of a muon if the jet has fewer than three associated tracks or the muon is matched to the jet through ghost association [73]. Finally, electrons and muons that are close to a remaining jet are discarded if their distance from the jet is $\Delta R < \min(0.4, 0.04 + 10\ \mathrm{GeV}/p_{\mathrm{T}})$ as a function of the lepton p_{T}.

The missing transverse momentum $\vec{p}_{\mathrm{T}}^{\,\mathrm{miss}}$, with magnitude $E_{\mathrm{T}}^{\mathrm{miss}}$, is calculated as the negative vectorial sum of the transverse momentum of all baseline reconstructed objects (electrons, muons, jets and photons [74]) and the soft term. The soft term includes all tracks associated with the primary vertex but not matched to any reconstructed physics object. Tracks not associated with the primary vertex are not considered in the $E_{\mathrm{T}}^{\mathrm{miss}}$ calculation, improving the $E_{\mathrm{T}}^{\mathrm{miss}}$ resolution by suppressing the effect of pile-up [75,76].

To compensate for differences between data and simulation in trigger, particle identification and reconstruction efficiency, correction factors that are usually functions of the relevant kinematic variables are derived from data and applied to the samples of simulated events.

5 Analysis strategy

The search is conducted in three independent analysis channels differing in lepton and jet multiplicities to maximise the sensitivity to distinct signal processes. The $\mathrm{tW_{1L}}$ analysis channel targets tW+DM events where one of the W bosons (directly produced or arising from the top quark decay) decays leptonically (Sect. 5.2). The $\mathrm{tW_{2L}}$ analysis channel targets the same signal processes, but considers events where both W bosons decay leptonically (Sect. 5.3). The two selections are designed to be mutually exclusive. The results of these two analysis channels are statistically combined to maximise the sensitivity to the tW+DM processes. Finally, the $\mathrm{tj_{1L}}$ analysis targets t-channel production of DM candidates and requires a single lepton in each event (Sect. 5.4). In all analysis channels, large missing transverse momentum and jets are required. Event selections and background estimation methods specific to each analysis channel are described in this section, as are the definitions of the signal, control, and validation regions (SR, CR, and VR, respectively).

Dedicated CRs are designed in each analysis channel for the major SM background processes in order to predict their expected contribution in the SRs. The CRs and SRs are mutually exclusive, with the CRs enriched in the major background processes relevant to each analysis channel while minimising the contamination from signal. The potential signal contamination in the CRs is found to be negligible, at the level of $< 3\%$ of the total SM expectation for all analysis channels.

The expected SM backgrounds are first determined independently for each channel, with a profile likelihood fit [77] in a background-only fit. In this fit, normalisation factors of the backgrounds, for which dedicated CRs are defined, are adjusted simultaneously to match the data in the associated CRs. The input to the background-only fit includes the number of events observed in the associated CRs and the number of events predicted by simulation in each CR for all background processes. They are both described by Poisson statistics. The systematic uncertainties, described in Sect. 6, are included in the fit as nuisance parameters. They are constrained by Gaussian distributions with widths corresponding to the sizes of the uncertainties and are treated as correlated, when appropriate, between the various regions. The product of the various probability density functions forms the likelihood, which the fit maximises by adjusting the background normalisation and the nuisance parameters.

Normalisation and nuisance parameters obtained from the background-only fit to the control regions are then extrapolated [77] to the SRs to quantify potential excess in data. The reliability of the MC extrapolation of the SM background estimates outside of the control regions is verified in dedicated validation regions. Statistically independent from the corresponding CRs and SRs, these VRs are designed to probe a kinematic region closer to that of the SRs. The potential signal contamination in the VRs is at the level of $< 1\%$ of the total SM expectation for most validation regions, and between 8% and 15% in a few validation regions in the $\mathrm{tW_{1L}}$ analysis channel.

In the absence of a significant event excess in the SRs, as determined after the background-only fit, simultaneous fits of the CRs and SRs are performed to constrain the parameters of the targeted signal models as well as a generic beyond the standard model (BSM), referred to as model-dependent and model-independent signal fits as detailed in Sect. 7.

5.1 Kinematic requirements and event variables

The event selection criteria in each analysis channel are defined using the physics objects described in Sect. 4 and the event variables defined in this section.

The following variables are defined using simple combinations of the physics objects in the events.

- N_{jet} is the number of jets with $|\eta| < 2.5$ and $p_{\text{T}} > 30$ GeV.
- $N_{\text{jet}}^{\text{forward}}$ is the number of jets in the forward region, $2.5 < |\eta| < 4.5$ and $p_{\text{T}} > 30$ GeV.
- $N_{b\text{-jet}}$ is the number of b-jets with $|\eta| < 2.5$ and p_{T} above a given threshold defined in each analysis channel.
- The minimum azimuthal distance $\Delta\phi_{\text{min}}$ between the $\vec{p}_{\text{T}}^{\text{miss}}$ and the $\vec{p}_{\text{T}}$ of each of the four leading jets in the event is useful for rejecting events with mismeasured jet energies leading to $E_{\text{T}}^{\text{miss}}$ in the event, and is defined as:

$$\Delta\phi_{\text{min}} = \min_{i\leq 4}\Delta\phi\left(\vec{p}_{\text{T}}^{\text{miss}}, \vec{p}_{\text{T},i}^{\text{jet}}\right),$$

  where $\min_{i\leq 4}$ selects the jet that minimises $\Delta\phi$.
- $m_{\ell\ell}$ is the invariant mass of the dilepton system in the event.
- An iterative reclustering approach as defined in Ref. [78] is used to reconstruct the hadronically decaying W bosons. All the signal jets in the event are first reclustered using the anti-k_t algorithm with a large radius parameter of $R = 3.0$. The radius of each large-radius jet is then iteratively reduced to an optimal radius, $R(p_{\text{T}}) = 2 \times m_W/p_{\text{T}}$. The mass of the reclustered jet, $m_W^{\text{reclustered}}$, is used in the $\text{tW}_{1\text{L}}$ channel.
- $m_{\ell_1 b_1}$ is the invariant mass of the leading lepton and b-jet in the event.

A set of variables based on transverse mass are defined in order to distinguish between the signal and SM background processes in the following.

- The transverse mass formed by the $\vec{p}_{\text{T}}^{\text{miss}}$ and the leading lepton in the event, $m_{\text{T}}^{\text{lep}}$, is used to reduce the W+jets and semileptonic $t\bar{t}$ backgrounds. It is defined as:

$$m_{\text{T}}^{\text{lep}} = \sqrt{2p_{\text{T}}^{\ell}E_{\text{T}}^{\text{miss}}\left(1-\cos\Delta\phi(\vec{p}_{\text{T}}^{\ell}, \vec{p}_{\text{T}}^{\text{miss}})\right)}.$$

- Similarly, the transverse mass $m_{\text{T}}^{\ell b}$ is formed by the $\vec{p}_{\text{T}}^{\text{miss}}$ and the system of the leading lepton and b-jet in the event to suppress the $W + b$ background, and is defined as:

$$m_{\text{T}}^{\ell b} = \sqrt{2p_{\text{T}}^{\ell_1+b_1}E_{\text{T}}^{\text{miss}}\left(1-\cos\Delta\phi(\vec{p}_{\text{T}}^{\ell_1+b_1}, \vec{p}_{\text{T}}^{\text{miss}})\right)}.$$

- Closely related to $m_{\text{T}}^{\text{lep}}$, the stransverse mass m_{T2} [79,80] is used to bound the masses of pair-produced particles, such as in $t\bar{t}$ production, each of which decays so as to produce a visible particle that can be detected and an invisible particle that contributes to the missing transverse momentum. In the case of a dilepton final state, it is defined by:

$$m_{\text{T2}}(\vec{p}_{\text{T}}^{\ell_1}, \vec{p}_{\text{T}}^{\ell_2}, \vec{p}_{\text{T}}^{\text{miss}}) = \min_{\vec{q}_{\text{T}}}\left[\max\left(m_{\text{T}}^{\text{lep}}(\vec{p}_{\text{T}}^{\ell_1}, \vec{q}_{\text{T}}), m_{\text{T}}^{\text{lep}}(\vec{p}_{\text{T}}^{\ell_2}, \vec{p}_{\text{T}}^{\text{miss}} - \vec{q}_{\text{T}})\right)\right],$$

  where $\vec{q}_{\text{T}}$ is the transverse momentum vector that minimises the larger of the two transverse masses $m_{\text{T}}^{\text{lep}}$, and $\vec{p}_{\text{T}}^{\ell_1}$ and $\vec{p}_{\text{T}}^{\ell_2}$ are the leading and subleading transverse momenta of the two leptons in the pair. For the dileptonic $t\bar{t}$ background events, m_{T2} has a kinematic endpoint at m_W.
- The asymmetric stransverse mass am_{T2} [81,82], a variation of m_{T2}, is used in the $\text{tW}_{1\text{L}}$ final state to reduce the number of dileptonic $t\bar{t}$ background events where one of the leptons is undetected. For these events, am_{T2} has a kinematic endpoint at the top quark mass.

To improve the selection of single-top events in the $\text{tW}_{2\text{L}}$ channel, the following quantities based on invariant mass are defined.

- $m_{b\ell}^{\text{min}}$ is the minimum invariant mass found by combining the leading b-jet with each of the leptons, $m_{b\ell}^{\text{min}} = \min(m_{b_1\ell_1}, m_{b_1\ell_2})$. An upper endpoint at approximately 153 GeV or 160−170 GeV is expected for the events with one or two leptonic top quark decays, respectively.
- To further reduce the background with two leptonic top quark decays, such as $t\bar{t}$ and $t\bar{t}V$, $m_{b\ell}^{\text{t}}$, an extended variation of $m_{b\ell}^{\text{min}}$, is used in the $\text{tW}_{2\text{L}}$ final state. It is defined as:

$$m_{b\ell}^{\text{t}} = \min[\max(m_{\ell_1 j_1}, m_{\ell_2 j_2}), \max(m_{\ell_1 j_2}, m_{\ell_2 j_1})],$$

  where $m_{\ell_n j_m}$ is the invariant mass of lepton ℓ_n and jet j_m, where j_1 and j_2 are the two jets with highest b-tag discriminator value. For the $t\bar{t}$ and $t\bar{t}V$ backgrounds where both top quarks decay leptonically, $m_{b\ell}^{\text{t}}$ has a kinematic endpoint at approximately 160−170 GeV.

Additional variables based on angular separations of the objects are used in the $\text{tj}_{1\text{L}}$ analysis to suppress SM background contributions, as defined below.

- $\Delta\eta(\ell_1, b_1)$, $\Delta\phi(\ell_1, b_1)$, and $\Delta R(\ell_1, b_1)$: the pseudorapidity difference, azimuthal angle difference, and angular distance between the leading lepton and b-jet in the event.
- $\Delta\phi(\ell_1, \vec{p}_{\text{T}}^{\text{miss}})$: the azimuthal angle difference between the $\vec{p}_{\text{T}}^{\text{miss}}$ and the leading lepton in the event.

Table 2 summarises the trigger and preselection requirements for all analysis channels, in terms of lepton, jet and

Table 2 Summary of the trigger and preselection requirements for the three analysis channels. Opposite-sign leptons are indicated as (OS). Events with extra baseline leptons are vetoed in addition

Variable	$\mathrm{tW_{1L}}$	$\mathrm{tW_{2L}}$	$\mathrm{tj_{1L}}$
Trigger	$E_{\mathrm{T}}^{\mathrm{miss}}$	Dilepton	$E_{\mathrm{T}}^{\mathrm{miss}}$ OR one-lepton
$N_{\ell}^{\mathrm{signal}}$	$= 1$	$= 2$ (OS)	$= 1$
$p_{\mathrm{T}}(\ell_1)$ (GeV)	> 30	> 25	> 30
$p_{\mathrm{T}}(\ell_2)$ (GeV)	–	> 20	–
N_{jet}	≥ 3	≥ 1	$\in [1, 4]$
p_{T}(jet) (GeV)	> 30	> 30	> 30
$N_{b\text{-jet}}$	≥ 1	≥ 1	$\in [1, 2]$
$p_{\mathrm{T}}(b_1)$ (GeV)	> 50	> 50	> 50
$E_{\mathrm{T}}^{\mathrm{miss}}$ (GeV)	> 250	> 200	> 200
$m_{\mathrm{T}}^{\mathrm{lep}}$ (GeV)	> 30	–	> 60
$m_{\ell\ell}$ (GeV)	–	$\geq 40, \notin [71, 111]$ $(ee/\mu\mu)$	–
$\Delta\phi_{\mathrm{min}}$ (rad)	> 0.5	–	> 0.5

b-jet multiplicities, as well as transverse momenta and global kinematic variables. Events with extra baseline leptons are vetoed in addition.

5.2 Single-lepton $\mathrm{tW_{1L}}$ analysis channel

Events with exactly one electron or muon are first selected for the SR if they also contain at least three jets, exactly one of which must be b-tagged, and satisfy the preselection requirements described in Table 2. The dominant SM background contributions in the channel are $t\bar{t}$, W+jets, and single top (Wt channel) production. Discriminating variables, $E_{\mathrm{T}}^{\mathrm{miss}}$, $m_{\mathrm{T}}^{\mathrm{lep}}$, $m_W^{\mathrm{reclustered}}$ and the asymmetric stransverse mass am_{T2} as described in Sect. 5.1, are used to further separate the signal from backgrounds. A 'genetic algorithm' [83] is used to optimise a baseline signal region defined as in Table 3. To increase the sensitivity to different signal model parameters, a binned $E_{\mathrm{T}}^{\mathrm{miss}}$ distribution is used as the final input for the statistical analysis. The binning is chosen to be [250, 300] GeV, [300, 400] GeV, [400, 500] GeV, [500, 600] GeV and ≥ 600 GeV, referred to as Bins [0−4].

The acceptance times detector efficiency for the tW+DM signal processes after applying all selection criteria is between 0.3% and 5.1% in the parameter space of $\tan\beta = 1$, $m_a \in [100, 450]$ GeV and $m_{H^{\pm}} \in [400, 1500]$ GeV, and between 0.2% and 4.8% in the parameter space of $m_a = 250$ GeV, $\tan\beta \in [0.5, 30]$ and $m_{H^{\pm}} \in [400, 1500]$ GeV.

Dominant background contributions from the $t\bar{t}$ and W+jets processes are estimated using MC simulation and the dedicated CRs. The contribution from multijet production, where the lepton is a misidentified jet or originates from a heavy-flavour hadron decay or photon conversion, is found to be negligible. The remaining sources of background (single-top, Z+jets, diboson, $t\bar{t}V$, and tWZ production, as well as rarer processes such as triboson, $t\bar{t}t\bar{t}$, and $t\bar{t}WW$), are estimated from simulation.

Dedicated control regions $\mathrm{CR_{tW_{1L}}(t\bar{t})}$ and $\mathrm{CR_{tW_{1L}}(W)}$, defined in Table 3, are designed for the $t\bar{t}$ and W+jets background estimations. Compared to the SR, the acceptance for $t\bar{t}$ events is increased in $\mathrm{CR_{tW_{1L}}(t\bar{t})}$ by requiring at least two b-jets, inverting the selection on am_{T2} and removing the requirement on $m_W^{\mathrm{reclustered}}$. To increase the acceptance of the W+jets events and hence the sample size, $\mathrm{CR_{tW_{1L}}(W)}$ is first selected by requiring $40 < m_{\mathrm{T}}^{\mathrm{lep}} < 100$ GeV and $m_W^{\mathrm{reclustered}} < 60$ GeV. To exploit the lepton charge asymmetry of the W+jets events relative to the remaining backgrounds, it is subsequently split into two regions with opposite lepton charges, $\mathrm{CR_{tW_{1L}}(W^+)}$ and $\mathrm{CR_{tW_{1L}}(W^-)}$. Normalisation factors, $\mu_{t\bar{t}}$ and $\mu_{W+\mathrm{jets}}$, defined as the ratio of the number of observed events to the SM prediction, are found to be 0.96 ± 0.08 and 1.01 ± 0.05 after the background-only fit for the $t\bar{t}$ and W+jets processes, respectively.

To validate the $t\bar{t}$ background predictions and the reliability of MC extrapolation in $m_W^{\mathrm{reclustered}}$ and am_{T2}, two validation regions, $\mathrm{VR1_{tW_{1L}}(t\bar{t})}$ and $\mathrm{VR2_{tW_{1L}}(t\bar{t})}$, are defined by reversing the SR selection requirements on am_{T2} and $m_W^{\mathrm{reclustered}}$ respectively, as shown in Table 3. To increase the sample size, the SR selection requirement on the $m_W^{\mathrm{reclustered}}$ is removed in the $\mathrm{VR1_{tW_{1L}}(t\bar{t})}$ region. Similarly, for the W+jets background processes, two validation regions, $\mathrm{VR1_{tW_{1L}}(W)}$ and $\mathrm{VR2_{tW_{1L}}(W)}$, are defined by varying the SR selection requirements on $m_{\mathrm{T}}^{\mathrm{lep}}$ and $m_W^{\mathrm{reclustered}}$ shown in Table 3, respectively. Each of the W+jets validation regions is split into two regions with opposite lepton charge. Figure 2 shows the post-fit $E_{\mathrm{T}}^{\mathrm{miss}}$ distributions in the representative validation regions. Good agreement is observed between data and SM expectation in all validation regions. The observed yield, post-fit background estimates and significance [84] in each CR and VR are shown in Fig. 3 after the background-only fit. Since the W+jets CR is split into two regions with opposite lepton charges sharing the same normalisation factor, the

Table 3 Summary of signal, control and validation region definitions used in the tW_{1L} analysis channel. The '–' entries represent an inclusive selection with no requirements. The W+jets control and validation regions are each split into two regions with opposite lepton charges as described in the text

Variable	SR	CR($t\bar{t}$)	CR(W)	VR1($t\bar{t}$)	VR2($t\bar{t}$)	VR1(W)	VR2(W)
$N_{b\text{-jet}}$	$= 1$	≥ 2	$= 1$	$= 1$	$= 1$	$= 1$	$= 1$
$p_{\mathrm{T}}(b_2)$ [GeV]	< 50	> 50	< 50	< 50	< 50	< 50	< 50
$m_W^{\text{reclustered}}$ [GeV]	> 60	–	< 60	–	< 60	> 60	< 60
$m_{\mathrm{T}}^{\text{lep}}$ [GeV]	> 200	> 200	$\in [40, 100]$	> 200	> 200	$\in [40, 100]$	> 100
am_{T2} [GeV]	> 220	< 220	> 220	< 220	> 220	> 220	> 220

significances in the CRs are shown explicitly. The data event yields are found to be consistent with background expectations.

5.3 Dilepton tW_{2L} analysis channel

Events with exactly two oppositely charged leptons (electron or muon) are first selected for the SR if they also contain at least one signal jet, at least one of which must be b-tagged with $p_{\mathrm{T}} > 50$ GeV, and satisfy the preselection requirements described in Table 2. The dominant SM background contributions in the channel after these selections are from the $t\bar{t}$, $t\bar{t}Z$, and tWZ processes, followed by that of diboson events. The contribution from misidentified or non-prompt lepton backgrounds (referred to as 'Fakes /non-prompt' in Figs. 4 and 5) is found to be negligible in the signal region.

Discriminating variables, $m_{b\ell}^{\min}$, $m_{b\ell}^{\mathrm{t}}$, m_{T2} and $\Delta\phi_{\min}$ as defined in Sect. 5.1, are used to define the final signal region as shown in Table 4.

The acceptance times detector efficiency after applying all selection criteria for the tW+DM signal processes is between 0.07% and 0.7% in the parameter space of $\tan\beta = 1$, $m_a \in [100, 450]$ GeV and $m_{H^\pm} \in [400, 1500]$ GeV, and between 0.05% and 0.6% in the parameter space of $m_a = 250$ GeV, $\tan\beta \in [0.5, 30]$ and $m_{H^\pm} \in [400, 1500]$ GeV.

The contributions from the $t\bar{t}$, $t\bar{t}V$ (with $V = W$ or Z boson) and diboson background processes are estimated from MC simulation and dedicated CRs. The remaining sources of background, including the irreducible tWZ process, which is dominated by the $Z \to \nu\nu$ component, single top quark production, $t\bar{t}h$ production and other rarer processes such as $t\bar{t}t\bar{t}$ and $t\bar{t}WW$, are estimated from simulation.

The acceptance for $t\bar{t}$ events is increased in $\mathrm{CR}_{\mathrm{tW_{2L}}}(\mathrm{t\bar{t}})$ by requiring a low value of m_{T2} and inverting the SR selection criteria on $m_{b\ell}^{\mathrm{t}}$.

The $t\bar{t}V$ contribution is dominated by the $t\bar{t}Z$ component (about 80% of $t\bar{t}V$ in the SR), especially where $Z \to \nu\nu$. A dedicated control region, $\mathrm{CR}_{\mathrm{tW_{2L}}}(\mathrm{t\bar{t}Z})$, is defined by first selecting three leptons, where at least one same-flavour–opposite-charge (SFOS) pair is required to be consistent with coming from a Z boson decay with an invariant mass within a window of [71, 111] GeV. If more than one such pair is present in the event, the pair which has an invariant mass closest to the Z boson mass is chosen. The purity of $t\bar{t}Z$ events is further increased by requiring at least three jets. To reduce the diboson background in this region, events with exactly one b-jet and three jets are rejected.

Due to the presence of three leptons in this region, the background contribution from misidentified or non-prompt leptons becomes non-negligible and is estimated using a data-driven matrix method (MM) as described in Refs. [85,86]. Two types of lepton identification criteria, 'tight' and 'loose' are defined in the evaluation, corresponding to the baseline and signal lepton selections described in Sect. 4. The number of events containing misidentified or non-prompt leptons in the $t\bar{t}Z$ CR is estimated from the number of observed events with tight or loose leptons using as input the probability for loose prompt, misidentified or non-prompt leptons to satisfy the tight criteria. The probability for prompt loose leptons to pass the tight selection is determined from $t\bar{t}Z$ MC simulation. The equivalent probability for loose misidentified or non-prompt leptons to pass the tight selection is measured in a $t\bar{t}$-enriched region with two same-sign leptons (electrons or muons) and a least one b-tagged jet, which is dominated by events with at least one misidentified or non-prompt lepton.

In the $\mathrm{CR}_{\mathrm{tW_{2L}}}(\mathrm{t\bar{t}Z})$ region, to mimic the event topology of the $t\bar{t}Z$ background in the signal region, a corrected $\vec{p}_{\mathrm{T}}^{\,\text{miss}}$ is obtained by vectorially adding the transverse momenta of the SFOS pair, and it is subsequently used to calculate a transverse mass ($m_{\mathrm{T}}^{\text{lep}}$) with the third lepton, referred to as corrected m_{T2}. The two leptons from the SFOS pair are excluded in the calculation of $m_{b\ell}^{\min}$, which effectively becomes the invariant mass of the third lepton and the leading b-jet. To improve the estimation of the dominant background from the WZ process in the $\mathrm{CR}_{\mathrm{tW_{2L}}}(\mathrm{t\bar{t}Z})$, a dedicated WZ CR, $\mathrm{CR}_{\mathrm{tW_{2L}}}(\mathrm{WZ})$, is defined by inverting the $\mathrm{CR}_{\mathrm{tW_{2L}}}(\mathrm{t\bar{t}Z})$ selection requirements on the jet multiplicity and the corrected $m_{b\ell}^{\min}$. This CR is also used to aid in the estimation of all diboson processes in the SR. Normalisation factors $\mu_{t\bar{t}}$, $\mu_{t\bar{t}V}$ and μ_{Diboson} are found to be 1.00 ± 0.03, 0.76 ± 0.26 and 0.80 ± 0.16 after the background-only fit for the $t\bar{t}$, $t\bar{t}V$ and diboson processes, respectively.

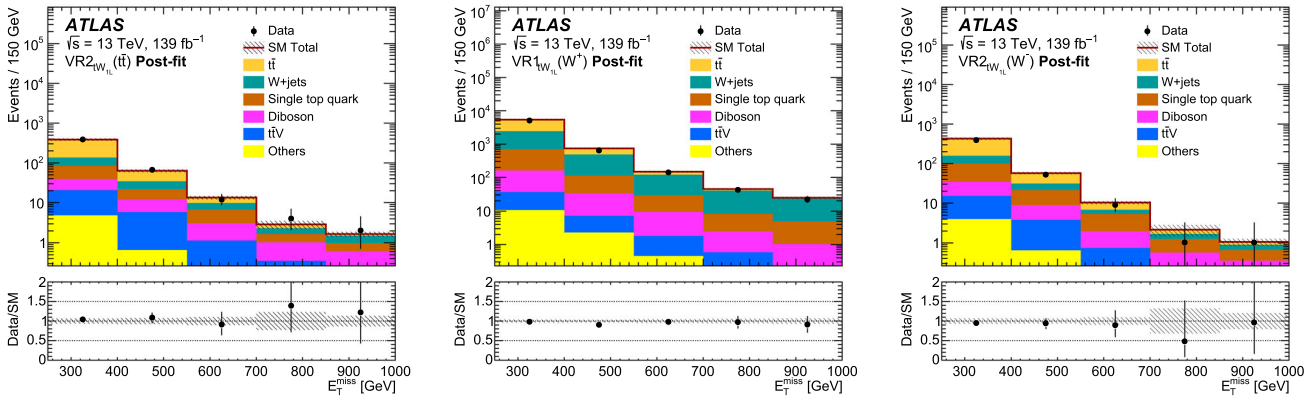

Fig. 2 The $E_{\mathrm{T}}^{\mathrm{miss}}$ distributions after the background-only fit (post-fit) are shown in three representative validation regions: **a** $\mathrm{VR2t_{W_{1L}}}(\mathrm{t\bar{t}})$, **b** $\mathrm{VR1t_{W_{1L}}}(\mathrm{W^{+}})$ and **c** $\mathrm{VR2t_{W_{1L}}}(\mathrm{W^{-}})$. The uncertainty bands plotted include all statistical and systematic uncertainties. The 'Others' category includes contributions from Z+jets and tWZ production, and rare processes such as triboson, $t\bar{t}t\bar{t}$, $t\bar{t}WW$, and Higgs boson production processes. The overflow events, where present, are included in the last bin. The lower panels show the ratio of data to the background prediction. The hatched error bands indicate the combined experimental and MC statistical uncertainties on these background predictions

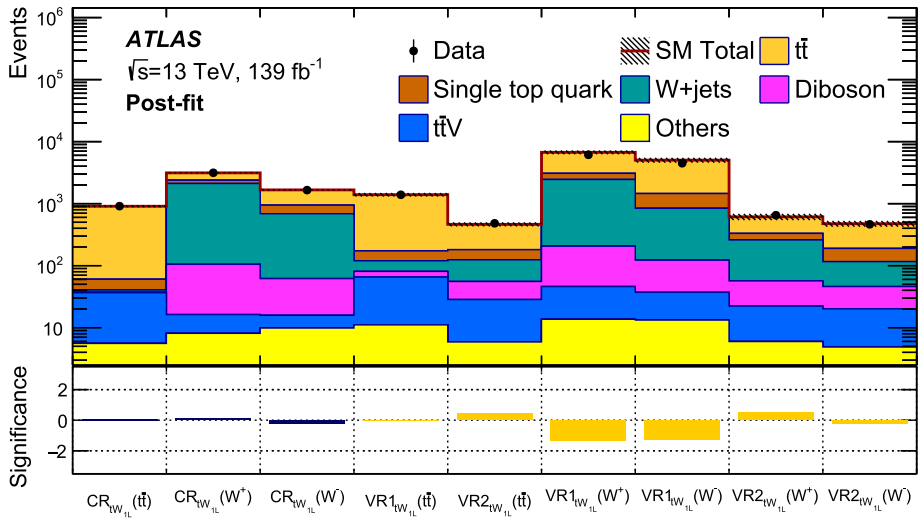

Fig. 3 Comparison of the predicted backgrounds with the observed numbers of events in the CRs and VRs associated with the $\mathrm{tW_{1L}}$ channel. The normalisation of the backgrounds is obtained from the background-only fit to the CRs. The 'Others' category includes contributions from Z+jets and tWZ production, and rare processes such as triboson, $t\bar{t}t\bar{t}$, $t\bar{t}WW$, and Higgs boson production processes. The upper panel shows the observed number of events and the predicted background yield. All uncertainties are included in the uncertainty band. The lower panel shows the significances in each region

A validation region, $\mathrm{VR_{tW_{2L}}}(\mathrm{t\bar{t}})$, is defined in order to validate the $t\bar{t}$ background predictions by applying all the signal selection criteria, apart from requiring lower values of m_{T2}, as shown in Table 4. For the background predictions of the $t\bar{t}V$ and diboson processes, a 3ℓ validation region, $\mathrm{VR_{tW_{2L}}}(3\mathrm{L})$, is defined with selection requirements similar to those of the $\mathrm{CR_{tW_{2L}}}(\mathrm{t\bar{t}Z})$ and $\mathrm{CR_{tW_{2L}}}(\mathrm{WZ})$. To ensure that the $\mathrm{VR_{tW_{2L}}}(3\mathrm{L})$ is orthogonal to those two CRs, the selection on the corrected $m_{b\ell}^{\mathrm{min}}$ variable is varied according to the jet and b-jet multiplicities. For the events with exactly one b-jet, the corrected $m_{b\ell}^{\mathrm{min}}$ is required to be larger than 170 GeV if $N_{\mathrm{jet}} > 3$, or smaller than 170 GeV if $N_{\mathrm{jet}} \leq 3$. For the events with more than one b-jet and $N_{\mathrm{jet}} > 2$, the corrected $m_{b\ell}^{\mathrm{min}}$ is required to be larger than 170 GeV. To increase the sample size in this region, the p_{T} threshold for the b-tagged jets is reduced to 40 GeV.

Figure 4 shows the post-fit kinematic distributions in the validation regions. Good agreement is observed between data and the SM expectation in all validation regions. The observed yield, post-fit background estimates and signifi-

cance [84] in each CR and VR are shown in Fig. 5 after the background-only fit. The data event yields are found to be consistent with background expectations.

5.4 Single-lepton tj_{1L} analysis channel

Events with exactly one electron or muon are first selected for the SR if they also contain 1–4 jets with $p_T > 30$ GeV, one or two of which must be b-tagged, and satisfy the preselection requirements described in Table 2. The fourth jet in the event, if present, is required to have $p_T < 50$ GeV. The second b-tagged jet is required to have $p_T > 30$ GeV. The dominant SM background contributions in this channel are from $t\bar{t}$, W+jets, and single top (Wt channel) production. Discriminating variables, E_T^{miss}, m_T^{lep}, $N_{jet}^{forward}$ and $\Delta\phi(\ell_1, b_1)$ as described in Sect. 5.1, are used to define the signal region as shown in Table 5.

To further improve the sensitivity, a boosted decision tree (BDT), provided by the Toolkit for Multivariate Analysis (TMVA) [87], is trained to distinguish between signal and background processes, using events passing the preselection defined in Table 2. BDT training settings found to be optimal for this analysis include number of trees set to 1500 with a maximum depth of 5 and gradient boosting. Cross-validation is performed to ensure there is no over-training. The following nine kinematic variables defined in Sect. 5.1 are used as input:

- p_T and η of the highest-p_T jet: $p_T(j_1)$ and $\eta(j_1)$.
- The transverse masses: m_T^{lep} and $m_T^{\ell b}$.
- $\eta^{\ell b}$ of the leading lepton and b-jet system.
- The invariant mass of, and angular distances between, the highest-p_T lepton and b-jet: $m_{\ell_1 b_1}$, $\Delta\phi(\ell_1, b_1)$, and $\Delta R(\ell_1, b_1)$.
- The azimuthal separation between the highest-p_T lepton and missing transverse momentum, $\Delta\phi(\ell_1, \vec{p}_T^{miss})$.

To explore the kinematic features in different regions of the signal parameter space, samples with different signal model parameters are used as an ensemble in the training. A binned distribution of the BDT output score above 0.6 is then used to extract the final results in the signal regions. The binning of the distribution is optimised as [0.6, 0.75], [0.75, 0.85], [0.85, 0.9] and [0.9, 1.0], referred to as Bins [0–3].

The acceptance times detector efficiency after applying all selection criteria for t-channel production in the signal models is between 0.37% (0.36%) and 0.73% (0.67%) in the parameter space of $m_a = 250$ GeV, $\tan\beta = 0.3$ (0.5) and $m_{H^\pm} \in [500, 1750]$ GeV.

Similarly to the tW_{1L} analysis channel, dominant backgrounds from the $t\bar{t}$ and W+jets processes are estimated using MC simulation and dedicated CRs. The contribution from multijet production is found to be negligible. The remaining sources of background (single-top, Z+jets, diboson, $t\bar{t}V$, $t\bar{t}h$, tWZ production and rarer processes such as triboson, $t\bar{t}t\bar{t}$, and $t\bar{t}WW$) are estimated from simulation.

Dedicated control regions $CR_{tj_{1L}}(t\bar{t})$ and $CR_{tj_{1L}}(W)$ are designed to estimate the $t\bar{t}$ and W+jets background processes, respectively, as shown in Table 5. Compared to the SR, the acceptance for $t\bar{t}$ events is increased in $CR_{tj_{1L}}(t\bar{t})$ by requiring exactly two b-jets and large $\Delta\phi(\ell_1, b_1)$ values. The contribution from W+jets events in the $CR_{tj_{1L}}(W)$ is enhanced by selecting events with one or two jets, exactly one b-jet, and low m_T^{lep} and large $\Delta\phi(\ell_1, b_1)$ values. No splitting based on the W boson charge is applied. The normalisation factors $\mu_{t\bar{t}}$ and μ_{W+jets} are found to be 1.00 ± 0.27 and 1.10 ± 0.13 for the $t\bar{t}$ and W+jets processes, respectively.

To validate the $t\bar{t}$ background predictions, a validation region $VR_{tj_{1L}}(t\bar{t})$ is defined by requiring a BDT score that is lower than in the SR definition, as shown in Table 5. For the W+jets background, a validation region $VR_{tj_{1L}}(W)$ is defined by requiring a lower m_T^{lep} value than in the SR definition, as shown in Table 5. To ensure orthogonality to the corresponding CRs, events in these two VRs are required to have low $\Delta\phi(\ell_1, b_1)$. Figure 6 shows the post-fit distribution of representative kinematic variables and the BDT score for these two validation regions. Good agreement is observed between data and expectation in all validation regions. The observed yield, post-fit background estimates and significance [84] in each CR and VR are shown in Fig. 7 after the background-only fit. The data event yields are found to be consistent with background expectations.

6 Systematic uncertainties

Several sources of experimental and theoretical systematic uncertainty in the signal and background estimates are considered. Their impact is reduced through the normalisation of the dominant backgrounds in the control regions defined with kinematic selections resembling those of the corresponding signal region. Uncertainties are included as nuisance parameters, common across all regions, with Gaussian constraints in the likelihood fits, taking into account correlations between different regions. Uncertainties due to the numbers of events in the CRs are also included in the fit for each region. The magnitude of the contributions arising from uncertainties on the background normalisation factors μ and on the detector, theoretical modelling and statistics of the MC samples are summarised in Fig. 8 as a relative uncertainty in the total background yield for each SR in the three analysis channels.

Dominant detector-related systematic uncertainties arise from the jet energy scale and resolution, and from the b-tagging efficiency and mis-tagging rates.

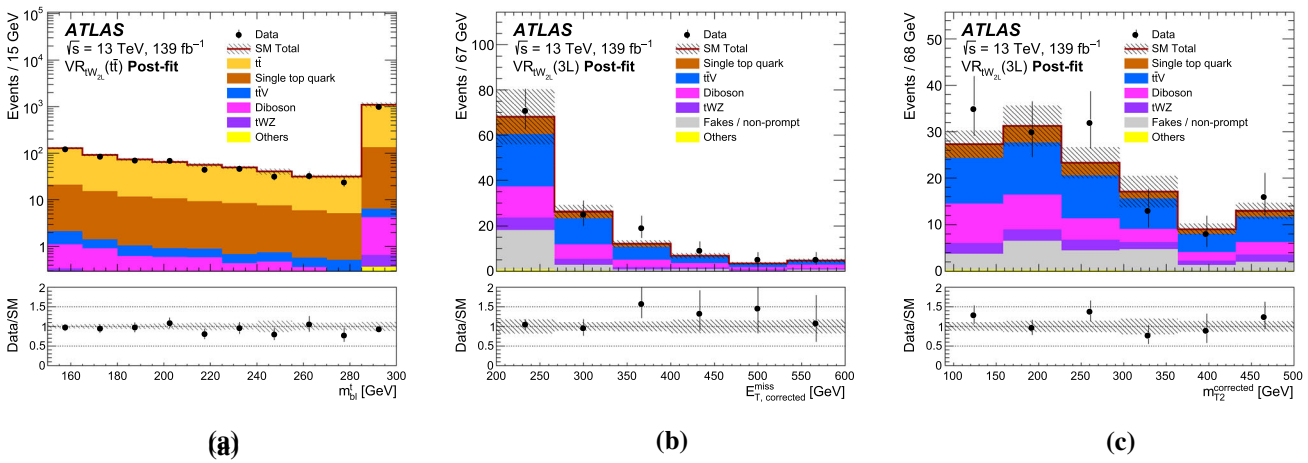

Fig. 4 The kinematic distributions in the $t\bar{t}$ and 3ℓ validation regions of the $\mathrm{tW_{2L}}$ analysis channel after the background-only fit: **a** $m^{\mathrm{t}}_{b\ell}$ in $\mathrm{VR_{tW_{2L}}(t\bar{t})}$, **b** $E_{\mathrm{T}}^{\mathrm{miss}}$ in $\mathrm{VR_{tW_{2L}}(3L)}$ and **c** m_{T2} in $\mathrm{VR_{tW_{2L}}(3L)}$. The uncertainty bands plotted include all statistical and systematic uncertainties. The 'Others' category includes contributions from rare processes such as triboson, $t\bar{t}t\bar{t}$, $t\bar{t}WW$, and Higgs boson production processes. The overflow events, where present, are included in the last bin. Since the $m^{\mathrm{t}}_{b\ell}$ is defined for events with at least two jets, the events with exactly one jet are included in the overflow bin. The lower panels show the ratio of data to the background prediction. The hatched error bands indicate the combined experimental and MC statistical uncertainties on these background predictions

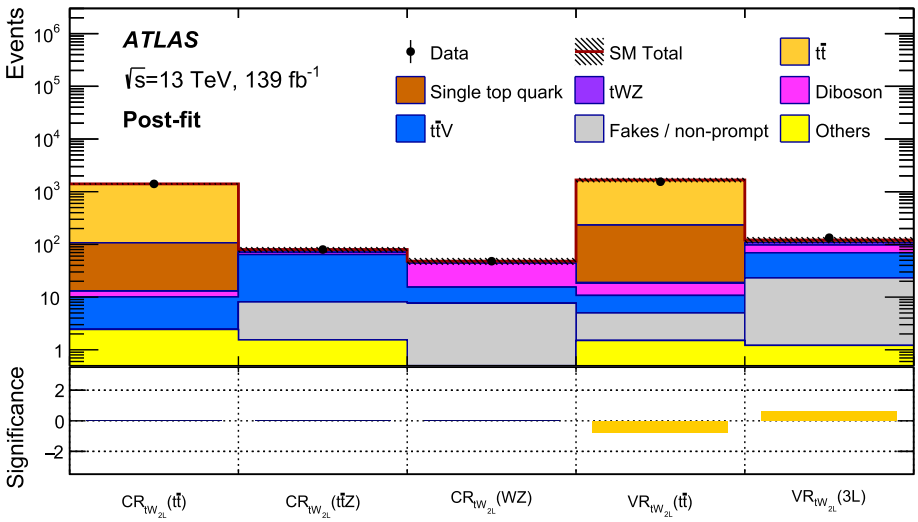

Fig. 5 Comparison of the predicted backgrounds with the observed numbers of events in the CRs and VRs associated with the $\mathrm{tW_{2L}}$ channel. The normalisation of the backgrounds is obtained from the background-only fit to the CRs. The 'Others' category includes contributions from rare processes such as triboson, $t\bar{t}t\bar{t}$, $t\bar{t}WW$, and Higgs boson production processes. The upper panel shows the observed number of events and the predicted background yield. All uncertainties are included in the uncertainty band. The lower panel shows the significances estimated for each region

The uncertainties in the jet energy scale and resolution are based on their respective measurements in data [68] and are derived as a function of the p_{T} and η of the jet, as well as of the pile-up conditions and the jet flavour composition (light-quark, b-quark, or gluon-initiated jets) of the selected jet sample. Their contributions to the SRs are the dominant experimental uncertainty components and are almost equivalent in all analysis channels. The systematic uncertainty in the b-tagging efficiency is the second largest experimental uncertainty. It ranges from 4.5% for b-jets with $p_{\mathrm{T}} \in [35, 40]$ GeV up to 7.5% for b-jets with high p_{T} (> 100 GeV). The b-tagging uncertainty is estimated by varying the η-, p_{T}- and flavour-dependent scale factors applied to each jet in the simulation within a range that reflects the systematic uncertainty in the measured tagging efficiency and mis-tag rates in data [71]. The uncertainties associated with trigger requirements, pile-up modelling, and lepton reconstruction and energy measurements have a small or negligible impact on the final

Table 4 Summary of signal, control and validation region definitions used in the tW_{2L} analysis channel. The '–' entries represent an inclusive selection with no requirements. In the final states with three leptons, the corrected $E_{\mathrm{T}}^{\mathrm{miss}}$, $m_{b\ell}^{\mathrm{min}}$ and m_{T2} variables are used instead as described in the main text. The selection requirement on the corrected $m_{b\ell}^{\mathrm{min}}$ in the VR(3ℓ) region varies according to the jet and b-jet multiplicity as described in the main text. Events with additional baseline leptons are vetoed

Variable	SR	CR($\mathrm{t\bar{t}}$)	CR($\mathrm{t\bar{t}}Z$)	CR(WZ)	VR($\mathrm{t\bar{t}}$)	VR(3ℓ)
N_ℓ^{signal}	$= 2$	$= 2$	$= 3$	$= 3$	$= 2$	$= 3$
	(OS)	(OS)	(≥ 1 SFOS)	(≥ 1 SFOS)	(OS)	(≥ 1 SFOS)
$p_{\mathrm{T}}(\ell_3)$ (GeV)	–	–	> 20	> 20	-	> 20
$m_{ee/\mu\mu}$ (GeV)	$\notin [71, 111]$	$\notin [71, 111]$	$\in [71, 111]$	$\in [71, 111]$	$\notin [71, 111]$	$\in [71, 111]$
N_{jet}	≥ 1	≥ 1	≥ 3	$\in [1, 3]$	≥ 1	≥ 1
$N_{b\text{-jet}}$	≥ 1	≥ 1	≥ 1	$= 1$	≥ 1	≥ 1
			(≥ 2 if $N_{\mathrm{jet}} = 3$)			
$m_{b\ell}^{\mathrm{min}}$ (GeV)	< 170	< 170	< 170	> 170	< 170	varies
$m_{b\ell}^{\mathrm{t}}$ (GeV)	> 150	< 150	–	–	> 150	–
m_{T2} (GeV)	> 130	$\in [40, 80]$	> 90	> 90	$\in [40, 80]$	> 90
$\Delta\phi_{\mathrm{min}}$ (rad)	> 1.1	> 1.1	–	–	> 1.1	–

Table 5 Summary of signal, control and validation region definitions used in the $\mathrm{tj}_{1\mathrm{L}}$ analysis channel. The '–' entries represent an inclusive selection with no requirements

Variable	SR	CR($\mathrm{t\bar{t}}$)	CR(W)	VR($\mathrm{t\bar{t}}$)	VR(W)
N_{jet}	$\in [1, 4]$	$\in [1, 4]$	$\in [1, 2]$	$\in [1, 4]$	$\in [1, 2]$
$N_{b\text{-jet}}$	$\in [1, 2]$	$= 2$	$= 1$	$\in [1, 2]$	$= 1$
$N_{\mathrm{jet}}^{\mathrm{forward}}$	> 0	–	–	–	–
$E_{\mathrm{T}}^{\mathrm{miss}}$ (GeV)	> 225	> 225	> 225	> 225	> 225
$m_{\mathrm{T}}^{\mathrm{lep}}$ (GeV)	> 100	> 100	$\in [60, 100]$	> 100	$\in [60, 100]$
$\Delta\phi(\ell_1, b_1)$ (rad)	< 1.2	> 1.5	> 1.5	< 1.5	< 1.5
BDT score	> 0.6	incl.	incl.	< 0.5	incl.

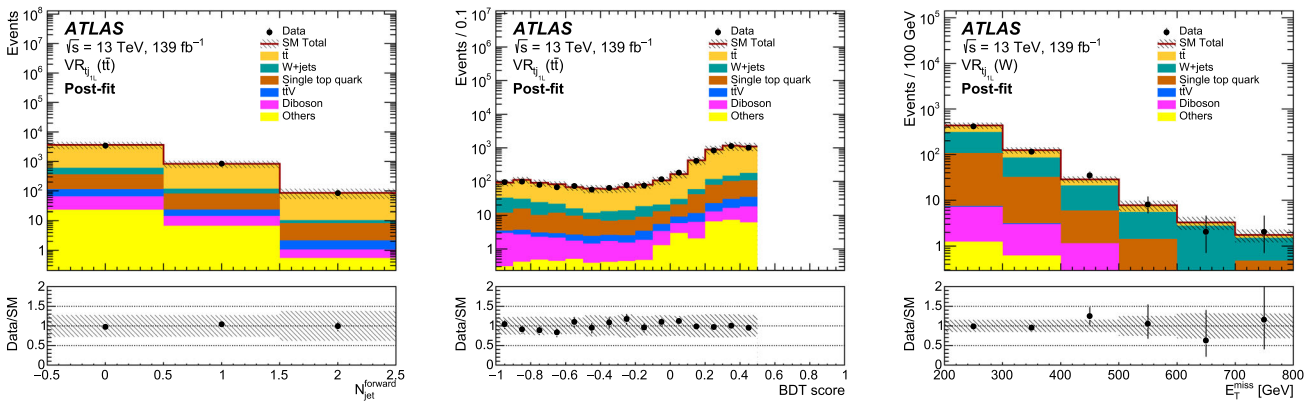

(a) **(b)** **(c)**

Fig. 6 Distributions in the $t\bar{t}$ and W+jets validation regions in the $\mathrm{tj}_{1\mathrm{L}}$ analysis channel: **a** $N_{\mathrm{jet}}^{\mathrm{forward}}$ in $\mathrm{VR}_{\mathrm{tj}_{1\mathrm{L}}}(\mathrm{t\bar{t}})$, **b** BDT score in $\mathrm{VR}_{\mathrm{tj}_{1\mathrm{L}}}(\mathrm{t\bar{t}})$ and **c** $E_{\mathrm{T}}^{\mathrm{miss}}$ in $\mathrm{VR}_{\mathrm{tj}_{1\mathrm{L}}}(\mathrm{W})$. The normalisation of the backgrounds is obtained from the background-only fit to the CRs. The uncertainty bands plotted include all statistical and systematic uncertainties. The 'Others' category includes contributions from Z+jets and tWZ production, and rare processes such as triboson, $t\bar{t}t\bar{t}$, $t\bar{t}WW$, and Higgs boson production processes. The overflow events, where present, are included in the last bin. The lower panels show the ratio of data to the background prediction. The hatched error bands indicate the combined experimental and MC statistical uncertainties on these background predictions

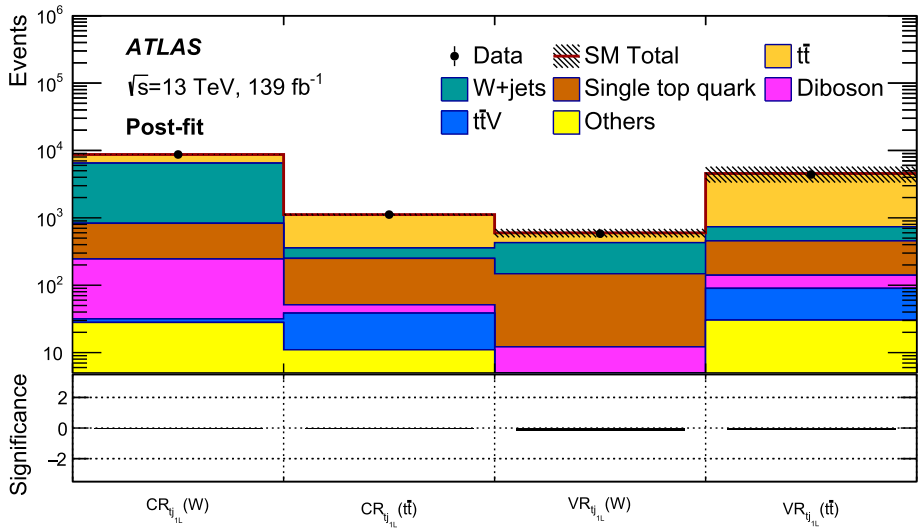

Fig. 7 Comparison of the predicted backgrounds with the observed numbers of events in the CRs and VRs associated with the $\mathrm{tj}_{1\mathrm{L}}$ channel. The normalisation of the backgrounds is obtained from the background-only fit to the CRs. The upper panel shows the observed number of events and the predicted background yield. The 'Others' category includes contributions from Z+jets and tWZ production, and rare processes such as triboson, $t\bar{t}t\bar{t}$, $t\bar{t}WW$, and Higgs boson production processes. All uncertainties are included in the uncertainty band. The lower panel shows the significance for each region

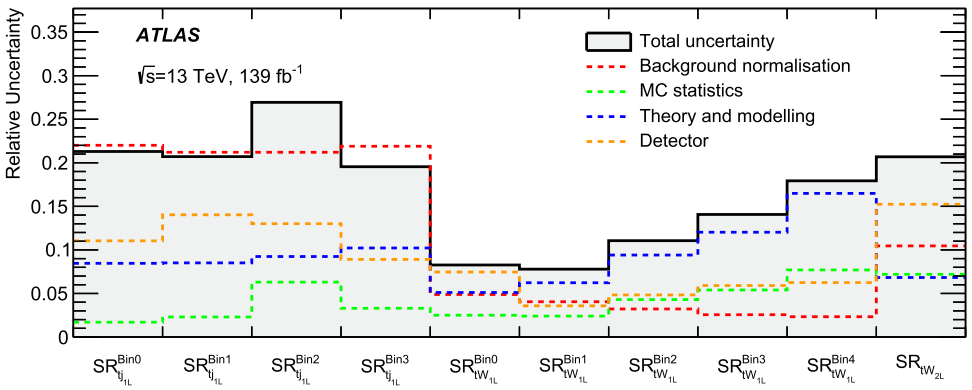

Fig. 8 Relative uncertainties in the total background yield in each SR for the three analysis channels, including the contribution from the different sources of uncertainty. The 'Detector' category contains all detector-related systematic uncertainties and is dominated by the jet energy scale and resolution. The 'Background normalisation' represents the uncertainty in the fitted normalisation factors, including the available event counts in the CRs. Individual uncertainties can be correlated, and do not necessarily add up in quadrature to the total background uncertainty

results; however, the lepton, photon and jet-related uncertainties are propagated to the calculation of the $E_{\mathrm{T}}^{\mathrm{miss}}$, and additional uncertainties due to the energy scale and resolution of the soft term are included in the $E_{\mathrm{T}}^{\mathrm{miss}}$. Finally, uncertainties in estimates of the non-prompt or misidentified leptons background are found to be below 1% in the $\mathrm{tW}_{2\mathrm{L}}$ analysis channel and negligible for single-lepton selections.

Uncertainties in the modelling of the SM background processes in MC simulation and their theoretical cross-section uncertainties are also taken into account. Furthermore, for these processes the 1.7% uncertainty in the combined 2015–2018 integrated luminosity is included.

Modelling uncertainties in the $t\bar{t}$ and single-top backgrounds are dominant in all SRs for the $\mathrm{tW}_{1\mathrm{L}}$ and $\mathrm{tj}_{1\mathrm{L}}$ analysis channels, and the second leading source of uncertainty for the $\mathrm{tW}_{2\mathrm{L}}$ SR. They are computed as the difference between the predictions from nominal samples and those from additional samples differing in hard-scattering generator and parameter settings, or by using internal weights assigned to the events depending on the choice of renormalisation and factorisation scales (μ_{R} and μ_{F}, respectively, varied independently by factors of 2 and 0.5), initial- and final-state radiation parameters, and PDF sets. The impact of the PS and hadronisation model is evaluated by comparing the nominal

generator with a POWHEG- BOX sample interfaced to HERWIG 7 [88,89], using the H7UE set of tuned parameters [89]. To assess the uncertainty due to the choice of hard-scattering generator and matching scheme, an alternative generator setup using MADGRAPH5_aMC@NLO interfaced to PYTHIA 8 is employed. For single-top Wt production, the impact of interference between single-resonant and double-resonant top quark production and on the implementation of the W lineshape in the generator is estimated in all analysis channels by comparing the nominal sample generated using the diagram removal method with alternative samples, including those generated using the diagram subtraction method [90]. For the $\mathrm{tW}_{2\mathrm{L}}$ selection, this results in a 100% uncertainty in the subdominant Wt contribution.

For the $t\bar{t}+W/Z$ background, uncertainties due to parton shower and hadronisation modelling are evaluated by comparing the predictions from MADGRAPH5_aMC@NLO interfaced to PYTHIA 8 and HERWIG 7, while the uncertainties related to the choice of renormalisation and factorisation scales are assessed by varying the corresponding event generator parameters up and down by a factor of two around their nominal values. Their contribution is dominant in the $\mathrm{tW}_{2\mathrm{L}}$ analysis channel and subdominant or small in all other SRs. A similar approach is used to assess the uncertainties in the tWZ process, with an additional 20% uncertainty assigned to account for uncertainties in the effects of interference between the $t\bar{t}+W/Z$ and tWZ processes. The 20% is assigned on the basis of preliminary comparisons of alternative approaches developed to evaluate interference effects in the $t\bar{t}$–tW [91] and $t\bar{t}Z$–tWZ processes [92].

Finally, modelling and normalisation uncertainties in minor backgrounds are also considered. For diboson and W/Z+jets events, they are estimated by varying the renormalisation, factorisation and resummation scales up and down by a factor of two around the values used to generate the nominal samples. For $t\bar{t}WW$, tZ, $t\bar{t}H$, Wh, Zh, $t\bar{t}t\bar{t}$, and triboson production processes, experimental and theoretical uncertainties in the event yields are also evaluated and found to be negligible.

For the DM signal processes, both the experimental and theoretical uncertainties in the expected signal yields are considered, including the aforementioned luminosity uncertainty. Experimental uncertainties are found to be 3–35% (2.5–11%) across the m_a–$m_{H^\pm}$ and m_a–$\tan\beta$ planes for the $\mathrm{tW}_{1\mathrm{L}}$ ($\mathrm{tW}_{2\mathrm{L}}$) analysis channel, and in the range 3–14% as a function of $m_{H^\pm}$ for the $\mathrm{tj}_{1\mathrm{L}}$ selection, independently of $\tan\beta$. In all SRs, the dominant uncertainty in the signal yields is found to be from the jet energy scale and resolution, followed by uncertainties in b-tagging rates. Larger uncertainties for the $\mathrm{tW}_{1\mathrm{L}}$ selections are found for the highest $E_{\mathrm{T}}^{\mathrm{miss}}$-binned region, where MC statistical fluctuations are also relevant. In the modelling of the signal samples, uncertainties due to the variations of the renormalisation and factorisation scales are dominant. They are evaluated using a variation scheme wherein μ_{R} and μ_{F} are scaled simultaneously by either a factor of 2 or 0.5. For the PS and hadronisation uncertainties, alternative samples with varied A14 tune parameter values are used. The effect of each systematic variation on the acceptance and efficiency is evaluated for each analysis channel SR by comparing the variation samples with the corresponding nominal sample. The impact on the total yields for tW+DM, $t\bar{t}$+DM and t-channel production processes is also evaluated for each signal scenario and found to be between 5% and 15%. For the $\mathrm{tW}_{1\mathrm{L}}$ and $\mathrm{tW}_{2\mathrm{L}}$ analysis channels, the uncertainties vary between 5% and 30% across the m_a–$m_{H^\pm}$ and m_a–$\tan\beta$ planes, with the largest values obtained for samples characterised by low values of the $H^\pm$ mass and independently of $\tan\beta$. For the $\mathrm{tj}_{1\mathrm{L}}$ analysis channel, uncertainties are found to be between 15% and 5% as a function of increasing $m_{H^\pm}$ for all $\tan\beta$ values considered.

7 Results

The event yields for all SRs in the three analysis channels are reported in Tables 6 and 7 and are summarised in Fig. 9, where the significance for each of the SRs is also presented. The SM background expectations resulting from background-only fits are shown along with their statistical plus systematic uncertainties. No significant deviations from the expected yields are observed in any of the signal regions considered. The largest background contribution in the $\mathrm{tW}_{1\mathrm{L}}$ and $\mathrm{tj}_{1\mathrm{L}}$ analysis channel SRs arises from $t\bar{t}$ production, whilst the contribution from $t\bar{t}V$ is largest in the $\mathrm{tW}_{2\mathrm{L}}$ SRs, with subdominant contributions from the $t\bar{t}$, single-top (including tWZ) and diboson processes. Other non-negligible background sources are W+jets and Z+jets production.

Figures 10, 11, 12 show comparisons between the observed data and the post-fit SM predictions for some relevant kinematic distributions in the three analysis channels after applying all SR selection requirements except the one on the quantity shown (except for Figs. 10c and 11b, where all events in the SR are shown). For the $\mathrm{tW}_{1\mathrm{L}}$ analysis channel, the $m_{\mathrm{T}}^{\mathrm{lep}}$ and am_{T2} distributions are shown for all values of $E_{\mathrm{T}}^{\mathrm{miss}}$ across the five bins. Similarly, for the $\mathrm{tj}_{1\mathrm{L}}$ analysis channel, the number of forward jets and $E_{\mathrm{T}}^{\mathrm{miss}}$ are shown for all BDT values above 0.6. The expected distributions for representative scenarios with different m_a, $m_{H^\pm}$, and $\tan\beta$ (depending on the analysis channel and SR considered) are shown for illustrative purposes. Reasonable agreement is found between data and SM predictions in all distributions, although a mild excess of data events is found in the $\mathrm{tW}_{2\mathrm{L}}$ distributions, accounting for a discrepancy lower than 2σ considering statistical and systematic uncertainties.

Table 6 Background-only fit results for the tW_{1L} and tW_{2L} signal regions. The backgrounds which contribute only a small amount (rare processes such as triboson, $t\bar{t}\,t\bar{t}$, $t\bar{t}\,WW$ and Higgs boson production processes, and non-prompt or misidentified leptons background) are grouped and labelled as 'Others'. The quoted uncertainties of the fitted SM background include both the statistical and systematic uncertainties

	$SR^{Bin0}_{tW_{1L}}$	$SR^{Bin1}_{tW_{1L}}$	$SR^{Bin2}_{tW_{1L}}$	$SR^{Bin3}_{tW_{1L}}$	$SR^{Bin4}_{tW_{1L}}$	$SR_{tW_{2L}}$
Observed events	182	191	60	24	12	12
Fitted SM bkg events	169 ± 14	171 ± 13	55 ± 6	20.1 ± 2.8	15.6 ± 2.8	5.9 ± 1.2
$t\bar{t}$	101 ± 12	84 ± 12	20 ± 5	5.1 ± 1.7	2.3 ± 1.5	1.2 ± 0.9
Single top	16.3 ± 5.2	17.3 ± 5.2	5.4 ± 3.2	2.0 ± 1.8	$1.7^{+2.0}_{-1.7}$	$0.26^{+0.27}_{-0.26}$
W+jets	28 ± 4	37.0 ± 4.3	14.2 ± 2.4	6 ± 1	5.9 ± 1.1	–
Z+jets	2.0 ± 0.9	1.1 ± 0.7	0.3 ± 0.1	0.15 ± 0.04	0.15 ± 0.02	–
Diboson	7.2 ± 1.7	9.6 ± 2.0	4.6 ± 1.0	2.2 ± 0.5	2.7 ± 0.6	0.5 ± 0.2
$t\bar{t}\,V$	12.3 ± 1.4	19.5 ± 3.5	8.7 ± 1.2	4.0 ± 0.7	2.5 ± 0.5	2.9 ± 0.7
tWZ	1.7 ± 0.2	2.4 ± 0.5	1.17 ± 0.15	0.42 ± 0.09	0.39 ± 0.09	0.8 ± 0.1
Others	0.6 ± 0.1	0.6 ± 0.1	0.17 ± 0.02	0.06 ± 0.02	0.03 ± 0.01	0.16 ± 0.08

Table 7 Background-only fit results for the tj_{1L} signal regions. The backgrounds which contribute only a small amount (Z+jets, rare processes such as tWZ, triboson, $t\bar{t}\,t\bar{t}$, $t\bar{t}\,WW$ and Higgs boson production processes) are grouped and labelled as 'Others'. The quoted uncertainties of the fitted SM background include both the statistical and systematic uncertainties

	$SR^{Bin0}_{tj_{1L}}$	$SR^{Bin1}_{tj_{1L}}$	$SR^{Bin2}_{tj_{1L}}$	$SR^{Bin3}_{tj_{1L}}$
Observed events	360	178	69	29
Fitted SM bkg events	335 ± 74	187 ± 40	67 ± 18	37 ± 7
$t\bar{t}$	280 ± 75	151 ± 42	54 ± 16	30 ± 8
W+jets	14.4 ± 5.1	12.4 ± 8.7	$2.7^{+7.5}_{-2.7}$	<0.1
Single top	27 ± 14	13.2 ± 7.5	5.7 ± 3.7	3.8 ± 2.5
$t\bar{t}V$	5.0 ± 1.6	3.1 ± 1.0	1.4 ± 0.6	1.3 ± 0.5
Diboson	3.3 ± 1.0	2.5 ± 0.8	1.4 ± 0.5	0.8 ± 0.3
Others	4.9 ± 2.4	4.8 ± 2.0	2.0 ± 0.7	1.0 ± 0.4

7.1 Statistical combination of the tW_{1L} and tW_{2L} analysis channels

A statistical combination of results from the tW_{1L} and tW_{2L} channels is performed to maximise the sensitivity to tW+DM models. The simultaneous fit is performed such that the individual background normalisation factors, $\mu^{1L}_{t\bar{t}}$, $\mu^{2L}_{t\bar{t}}$, $\mu_{W+\text{jets}}$ and $\mu_{t\bar{t}V}$, are constrained in the same regions as the respective, individual analyses to avoid extrapolations into a different phase space. Experimental uncertainties in the background and signal are evaluated using the same methods as described in Sect. 5 and correlated across channels. Modelling uncertainties from the same source for a given process are correlated, e.g. all modelling uncertainties for $t\bar{t}$ are correlated across the regions. Signal systematic uncertainties are also correlated for the exclusion fits described in the next section.

The predictions for SM backgrounds are, as expected, equivalent to those of the individual channels. In particular, the values for the $\mu_{t\bar{t}}$ background normalisation factor are found to be consistent for tW_{1L} and tW_{2L} estimates, $\mu^{1L}_{t\bar{t}} = 0.97 \pm 0.08$ and $\mu^{2L}_{t\bar{t}} = 1.00 \pm 0.03$, respectively.

7.2 Model-independent limits

The CL_s technique [93] is used to place 95% confidence level (CL) upper limits on event yields from physics BSM for each signal region (model-independent limits). The profile-likelihood-ratio test statistic is used to exclude the signal-plus-background hypotheses for specific signal models. When normalised to the integrated luminosity of the data sample, results can be interpreted as corresponding upper limits on the visible cross section, σ_{vis}, defined as the product of the BSM production cross section, the acceptance and the selection efficiency of a BSM signal. In the case of the tW_{1L} analysis channel, the $E_{\text{T}}^{\text{miss}}$ bins are defined inclusively, i.e. all events above the lowest bin-threshold in $E_{\text{T}}^{\text{miss}}$ are taken, to retain discovery potential. The SM predictions and their corresponding uncertainties are reported in Table 8. In the case of the tj_{1L} analysis channel, the last bin of the BDT score distribution, 0.9–1.0, is considered.

Table 9 summarises the observed (S^{95}_{obs}) and expected (S^{95}_{exp}) 95% CL upper limits on the number of BSM events and on σ_{vis} for all SRs. The p_0-values, which represent the probability of the SM background to fluctuate to the observed

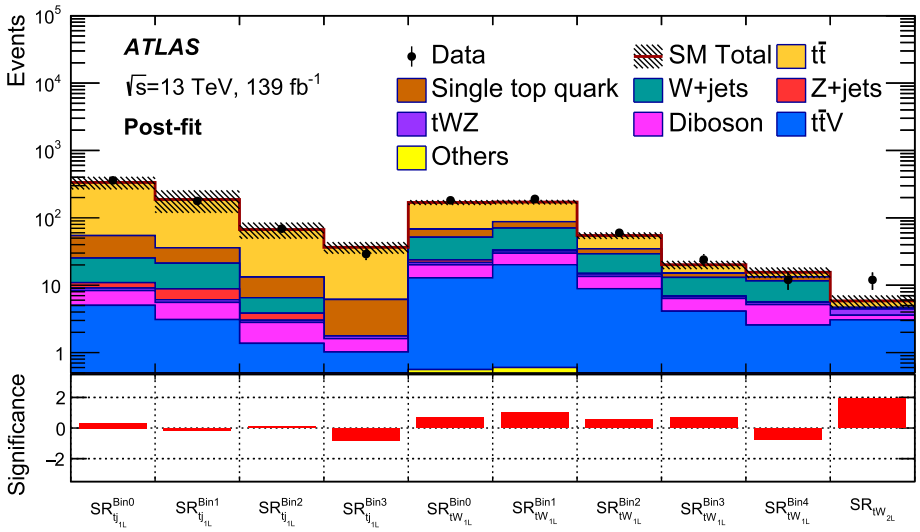

Fig. 9 Results of the background-only fit extrapolated to all SRs. The normalisation of the backgrounds is obtained from the fit to the CRs. The upper panel shows the observed number of events and the predicted background yields. The 'Others' category includes contributions from rare processes such as triboson, $t\bar{t}t\bar{t}$, $t\bar{t}WW$, and Higgs boson production processes. All uncertainties defined in Sect. 6 are included in the uncertainty band. The lower panel shows the significance in each SR. The significance calculation is performed as described in Ref. [84]

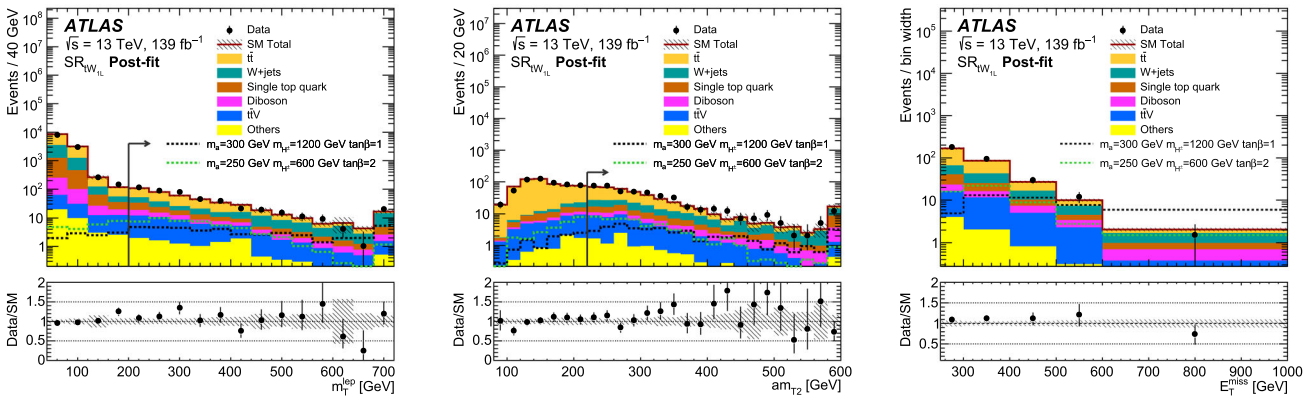

(a) **(b)** **(c)**

Fig. 10 Representative distributions of **a** $m_{\mathrm{T}}^{\mathrm{lep}}$, **b** am_{T2} and **c** $E_{\mathrm{T}}^{\mathrm{miss}}$ in the $\mathrm{tW_{1L}}$ channel. Observed data are compared with the SM background predictions extrapolated from the background-only fit. All SR selections except the one on the quantity shown are applied. The SR requirement is indicated by the arrow. The 'Others' category includes contributions from Z+jets and tWZ production, and rare processes such as triboson, $t\bar{t}t\bar{t}$, $t\bar{t}WW$, and Higgs boson production processes. The expected distributions for representative scenarios with different m_a, $m_{H^\pm}$, and $\tan\beta$ are shown for illustrative purposes. The overflow events, where present, are included in the last bin. The lower panels show the ratio of data to the background prediction. The hatched error bands indicate the combined experimental and MC statistical uncertainties on these background predictions

number of events or higher, are also provided and are capped at $p_0 = 0.5$; the associated significance is provided in parentheses.

7.3 Model-dependent limits

Model-dependent exclusion limits are placed on the common signal parameters m_a, $m_{H^\pm}$, and $\tan\beta$ in the 2HDM+a models considered in the analysis. Following the prescriptions in Ref. [5], the masses of the bosons H, $H^\pm$ and A are set to be equal. The three quartic couplings between the scalar doublets and the a boson (λ_{P1}, λ_{P2} and λ_3) are all set equal to 3, in order to reduce the number of parameters and evade the constraints from electroweak precision measurements [18]. To further reduce the parameter space, unitary couplings between the a boson mediator and the DM particle χ ($g_\chi = 1$) are considered, with the DM particle mass set to $m_\chi = 10$ GeV. The mixing angle θ is fixed at $\sin\theta = 1/\sqrt{2}$, yielding full mixing between the a and A bosons and the largest cross sections for the processes of interest. Two sets of samples are considered,[2] varying either the (m_a, $m_{H^\pm}$) parameters and setting $\tan\beta$ to unity, or vary-

[2] As pointed out in Ref. [5], for the two considered sets of samples, only values $m_{H^\pm} < 600$ GeV provide a bounded-from-below scalar potential [20] for the 2HDM+a model. This constraint can be relaxed up to a factor 2 if the quartic coupling λ_3 assumes a value closer to the perturbativity limit and they can be relaxed further in more general 2HDMs containing additional quartic couplings [94], as discussed in Ref. [95].

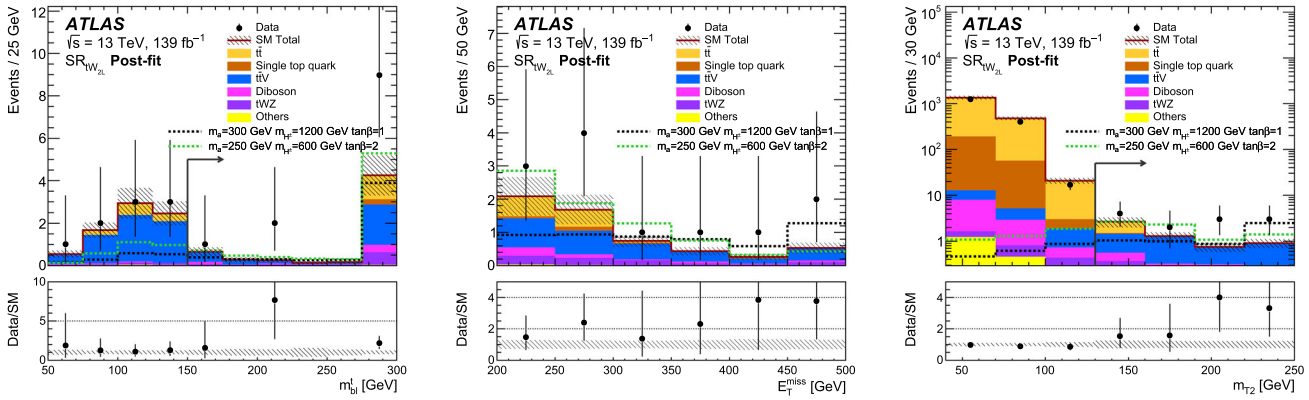

(a) (b) (c)

Fig. 11 Representative distributions of **a** $m_{b\ell}^{\mathrm{t}}$, **b** $E_{\mathrm{T}}^{\mathrm{miss}}$ and **c** m_{T2} in the $\mathrm{tW_{2L}}$ channel. Observed data are compared with the SM background predictions extrapolated from the background-only fit. All SR selections except the one on the quantity shown are applied. The SR requirement is indicated by the arrow. As the $m_{b\ell}^{\mathrm{t}}$ is defined for events with at least two jets, the events with exactly one jet are included in the overflow bin. The 'Others' category includes contributions from rare processes such as triboson, $t\bar{t}t\bar{t}$, $t\bar{t}WW$, and Higgs boson production processes. The expected distributions for representative scenarios with different m_a, $m_{H^\pm}$, and $\tan\beta$ are shown for illustrative purposes. The overflow events, where present, are included in the last bin. The lower panels show the ratio of data to the background prediction. The hatched error bands indicate the combined experimental and MC statistical uncertainties on these background predictions

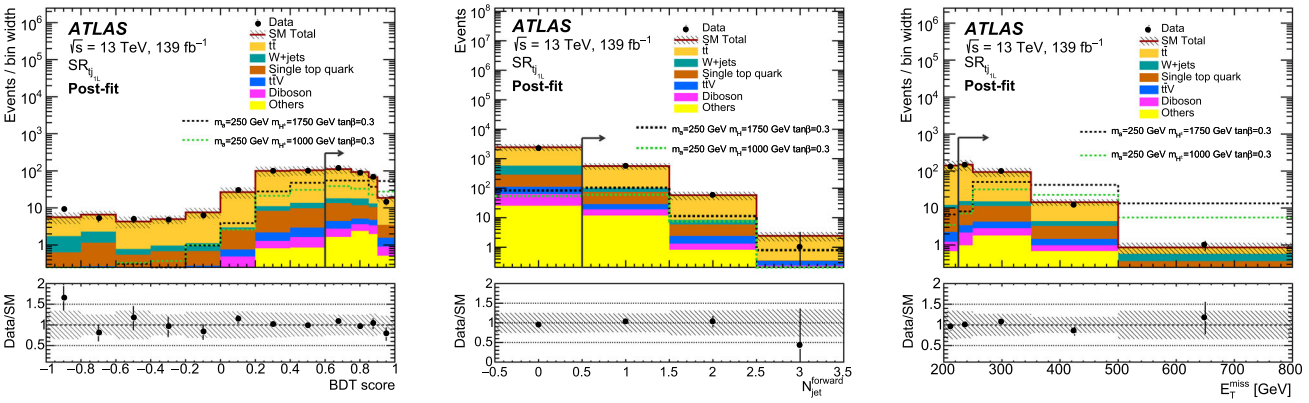

(a) (b) (c)

Fig. 12 Representative distributions of **a** BDT score, **b** $N_{\mathrm{jet}}^{\mathrm{forward}}$ and **c** $E_{\mathrm{T}}^{\mathrm{miss}}$ in the $\mathrm{tj_{1L}}$ channel. Observed data are compared with the SM background predictions extrapolated from the background-only fit. All SR selections except the one on the quantity shown are applied. The SR requirement is indicated by the arrow. The 'Others' category includes contributions from Z+jets and tWZ production, and rare processes such as triboson, $t\bar{t}t\bar{t}$, $t\bar{t}WW$, and Higgs boson production processes. The expected distributions for representative scenarios with different m_a, $m_{H^\pm}$, and $\tan\beta$ are shown for illustrative purposes. The overflow events, where present, are included in the last bin. The lower panels show the ratio of data to the background prediction. The hatched error bands indicate the combined experimental and MC statistical uncertainties on these background predictions

ing the $(m_{H^\pm}, \tan\beta)$ parameters and setting $m_a = 250$ GeV. The fit procedure takes into account correlations in the yield predictions between control and signal regions due to common background normalisation parameters and systematic uncertainties. The experimental systematic uncertainties in the signal are taken into account for the calculation and are assumed to be fully correlated with those in the SM background. The results of the combined fit for the $\mathrm{tW_{1L}}$ and $\mathrm{tW_{2L}}$ channels are interpreted using the sum of the respective signal yield estimates for each generated sample, with overlap between the samples removed according to the procedure illustrated in Ref. [22].

Figure 13a, b show the observed and expected exclusion contours as functions of $(m_a, m_{H^\pm})$ and $(m_{H^\pm}, \tan\beta)$, respectively, for the $\mathrm{tW_{1L}}$ and $\mathrm{tW_{2L}}$ channels, presented both individually and statistically combined. In this case, only the

Table 8 Background-only fit results for $\mathrm{tW}_{1\mathrm{L}}$ signal region bins for model-independent limits. Events with $E_{\mathrm{T}}^{\mathrm{miss}}$ above the lowest bin-threshold are retained in each bin. This is indicated by value X in $\mathrm{SR}_{\mathrm{tW}_{1\mathrm{L}}}^{X}$. The backgrounds which contribute only a small amount (rare processes such as tWZ, triboson, $t\bar{t}\,t\bar{t}$, $t\bar{t}\,WW$ and Higgs boson production processes) are grouped and labelled as 'Others'. The quoted uncertainties of the fitted SM background include both the statistical and systematic uncertainties

	$\mathrm{SR}_{\mathrm{tW}_{1\mathrm{L}}}^{250}$	$\mathrm{SR}_{\mathrm{tW}_{1\mathrm{L}}}^{300}$	$\mathrm{SR}_{\mathrm{tW}_{1\mathrm{L}}}^{400}$	$\mathrm{SR}_{\mathrm{tW}_{1\mathrm{L}}}^{500}$	$\mathrm{SR}_{\mathrm{tW}_{1\mathrm{L}}}^{600}$
Observed events	469	287	96	36	12
Fitted SM bkg events	431 ± 27	262 ± 20	91 ± 10	36 ± 5	15.5 ± 2.8
$t\bar{t}$	213 ± 25	111 ± 18	28 ± 7	7.5 ± 2.9	2.3 ± 1.5
Single top	43 ± 15	27 ± 12	9 ± 7	3.9 ± 3.8	$1.7^{+2.0}_{-1.7}$
W+jets	91 ± 8	63 ± 5	26 ± 3	12.0 ± 1.7	5.9 ± 1.1
Z+jets	3.8 ± 1.0	1.7 ± 0.7	0.6 ± 0.1	0.30 ± 0.05	0.15 ± 0.02
Diboson	26 ± 5	19.0 ± 3.9	9 ± 2	4.8 ± 1.0	2.6 ± 0.6
$t\bar{t}V$	47 ± 3	34.7 ± 2.4	15.3 ± 1.2	6.6 ± 0.5	2.5 ± 0.3
Others	7.5 ± 0.5	5.3 ± 0.4	2.3 ± 0.1	0.9 ± 0.1	0.40 ± 0.05

Table 9 The 95% CL upper limits on the visible cross section ($\langle\epsilon\sigma\rangle_{\mathrm{obs}}^{95}$) and on the number of signal events (S_{obs}^{95}) for all SRs and analysis channels as detailed in the text. The fourth column (S_{exp}^{95}) shows the 95% CL upper limit on the number of signal events, given the expected number (and $\pm 1\sigma$ exclusions of the expectation) of background events. The last two columns indicate the CL_B value, i.e. the confidence level observed for the background-only hypothesis, and the discovery p-value ($p(s=0)$). The associated significance is provided in parentheses

Signal channel	$\langle\epsilon\sigma\rangle_{\mathrm{obs}}^{95}$ [fb]	S_{obs}^{95}	S_{exp}^{95}	CL_B	$p(s=0)$ (Z)
$\mathrm{SR}_{\mathrm{tW}_{1\mathrm{L}}}^{250}$	0.72	100.6	67^{+33}_{-16}	0.85	0.12 (1.16)
$\mathrm{SR}_{\mathrm{tW}_{1\mathrm{L}}}^{300}$	0.51	70.8	54 ± 16	0.85	0.15 (1.02)
$\mathrm{SR}_{\mathrm{tW}_{1\mathrm{L}}}^{400}$	0.24	32.9	29^{+10}_{-6}	0.64	0.30 (0.52)
$\mathrm{SR}_{\mathrm{tW}_{1\mathrm{L}}}^{500}$	0.14	18.9	19^{+8}_{-5}	0.52	0.45 (0.13)
$\mathrm{SR}_{\mathrm{tW}_{1\mathrm{L}}}^{600}$	0.08	10.6	12^{+3}_{-4}	0.24	0.94 (−1.54)
$\mathrm{SR}_{\mathrm{tW}_{2\mathrm{L}}}$	0.10	13.8	$7.3^{+2.9}_{-1.1}$	0.97	0.02 (2.07)
$\mathrm{SR}_{\mathrm{tj}_{1\mathrm{L}}}$ (BDT>0.9)	0.10	14.4	19^{+6}_{-5}	0.24	0.50 (0.00)

DMt contribution of the signal is taken into account to better illustrate the sensitivity to single-top signatures. Figure 14a, b show the observed and expected exclusion contours for the same models, but also include the expected contributions from the DM$t\bar{t}$ process. Figures 13 and 14 also report the 1σ and 2σ uncertainty bands around the observed limit contour, as well as the variations obtained by changing the theoretical cross-section predictions for signal to be 15% above or below the nominal value (as this is expected to be largest uncertainty in the signal yields across the plane). For low $H^{\pm}$ masses, DMt production generally dominates DM$t\bar{t}$ production, due to the contribution from the resonant $H^{\pm}$ diagrams, except when the mass difference $m_{H^{\pm}} - m_a$ is small enough to suppress the branching fraction of $H^{\pm} \to Wa$ decay relative to $H^{\pm} \to t\bar{b}$. On the other hand, DM$t\bar{t}$ contributions are dominant at high $m_{H^{\pm}}$. The width of $H^{\pm}$ also increases at high $m_{H^{\pm}}$, and it is about 20% of its mass for $m_{H^{\pm}} = 1$ TeV. Moreover, as studied in Ref. [22], the DM$t\bar{t}$ cross section is proportional to $1/\tan^2\beta$, whereas the $H^{\pm}$ production cross section has a more complex dependence, with a minimum for $\tan\beta \sim 10$ and an enhancement for high values of $\tan\beta$. For $\tan\beta = 1$ and $m_{H^{\pm}} \sim m_a + m_W$, the DM$t\bar{t}$ cross section also dominates the DMt cross section. Assuming $m_\chi = 10$ GeV and $g_\chi = 1$, masses of a below 190 GeV are excluded at 95% CL for all values of $m_{H^{\pm}}$ in the range 400–1400 GeV, and up to 330 GeV for $m_{H^{\pm}}$ around 800 GeV. When only DMt contributions are taken into account, the constraints on m_a decrease by 20–50 GeV. In the case where $m_a = 250$ GeV, all values of $m_{H^{\pm}}$ between 450 GeV and 1.5 TeV are excluded for $\tan\beta$ around and below unity, and scenarios with $\tan\beta$ below 1.5 are excluded for masses of $H^{\pm}$ around 800 GeV.

The sensitivity of the $\mathrm{tj}_{1\mathrm{L}}$ channel is small compared to the other analysis channels. It targets the t-channel production component of the DMt signal, which has a smaller cross section with respect to the tW+DM process. The observed and expected cross-section limits at 95% CL as a function of $m_{H^{\pm}}$ for two representative values of $\tan\beta$ are shown in Fig. 15 assuming a fixed value of $m_a = 250$ GeV. The limits are shown as a multiple of σ_{BSM}, the theoretical cross section of the t-channel DM production process. For $\tan\beta =$

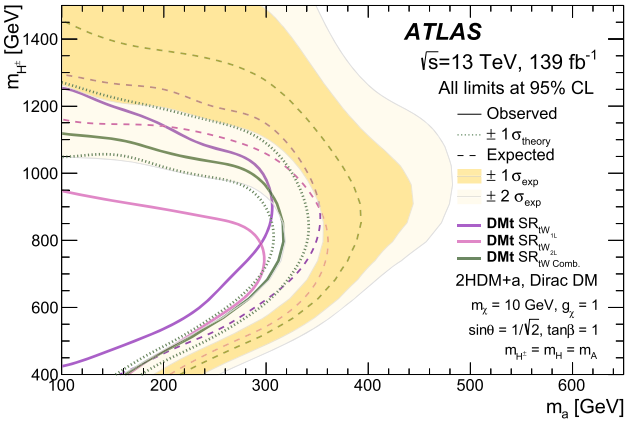

(a) DMt, m_a–$m_{H^\pm}$ plane

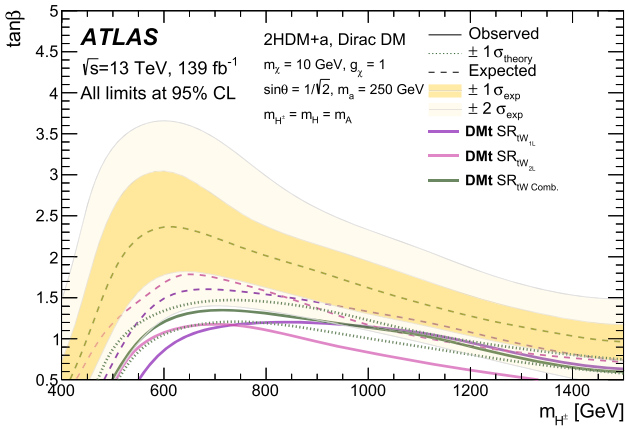

(b) DMt, $m_{H^\pm}$–tan β plane

Fig. 13 The expected and observed exclusion contours as a function of $(m_a, m_{H^\pm})$ (top) and $(m_{H^\pm}, \tan\beta)$ (bottom), assuming only tW+DM contributions, for the individual $\mathrm{tW_{1L}}$ (purple line) and $\mathrm{tW_{2L}}$ (pink line) analysis channels, and for their statistical combination (green line). Experimental and theoretical systematic uncertainties, as described in Sect. 6, are applied to background and signal samples and illustrated by the ±1 standard-deviation and ±2 standard-deviation yellow bands and the green dotted contour lines, respectively, for the statistical combination

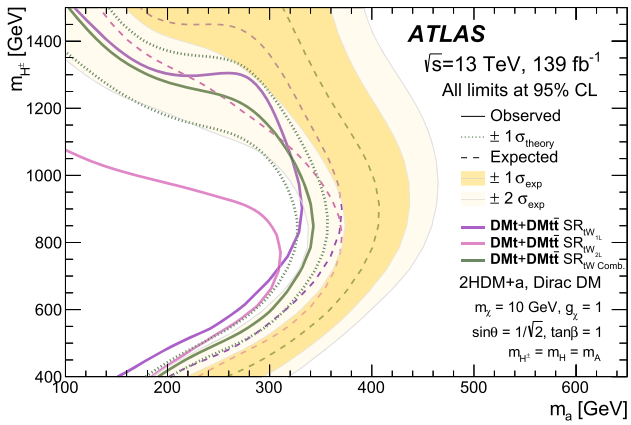

(a) DMt+DM$t\bar{t}$, m_a–$m_{H^\pm}$ plane

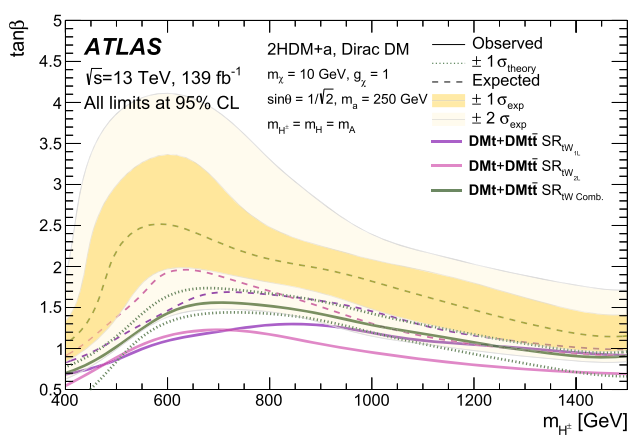

(b) DMt+DM$t\bar{t}$, $m_{H^\pm}$–tan β plane

Fig. 14 The expected and observed exclusion contours as a function of $(m_a, m_{H^\pm})$ (top) and $(m_{H^\pm}, \tan\beta)$ (bottom), assuming DM$t\bar{t}$ and DMt contributions, for the individual $\mathrm{tW_{1L}}$ (purple line) and $\mathrm{tW_{2L}}$ (pink line) analysis channels, and for their statistical combination (green line). Experimental and theoretical systematic uncertainties, as described in Sect. 6, are applied to background and signal samples and illustrated by the ±1 standard-deviation and ±2 standard-deviation yellow bands and the green dotted contour lines, respectively, for the statistical combination

0.3, $H^\pm$ masses above 900 GeV are excluded under these hypotheses, whilst no exclusion is obtained for $\tan\beta = 0.5$.

8 Conclusion

A search for dark matter has been performed in the context of a two-Higgs-doublet model together with an additional pseudoscalar mediator, a, which decays into the dark-matter particles. Processes where the pseudoscalar mediator is produced in association with a single top quark in the 2HDM+a model are explored for the first time at the LHC. Several final states which include either one or two leptons (electrons or muons) and a significant amount of missing transverse momentum are considered. The analysis makes use of proton–proton collision data at $\sqrt{s} = 13$ TeV collected by the ATLAS experiment during LHC Run 2 (2015–2018), corresponding to an integrated luminosity of 139 fb^{-1}. No significant excess above the Standard Model predictions is found. The results are expressed as 95% confidence-level limits on the 2HDM+a signal models considered. Assuming dark-matter particles with mass $m_\chi = 10$ GeV and coupling $g_\chi = 1$ to the mediator, and full mixing between the a and A bosons, masses of a below 200 GeV are excluded at 95% CL for all values of $m_{H^\pm}$ in the range 400–1400 GeV, and up to 330 GeV for $m_{H^\pm}$ around 900 GeV. For $m_a = 250$ GeV, all values of $m_{H^\pm}$ below 1.5 TeV are excluded for $\tan\beta$ below

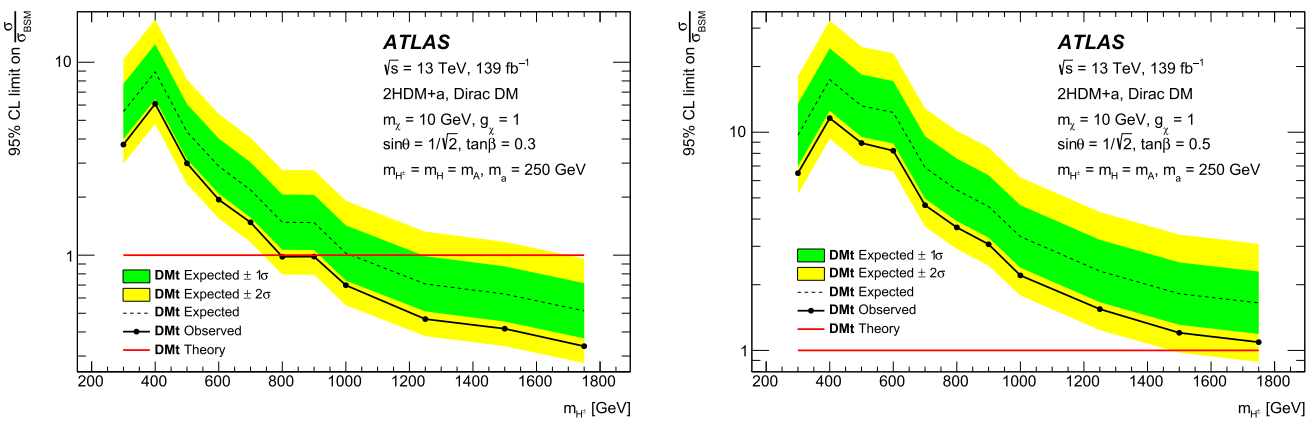

(a) $\tan\beta = 0.3$ **(b)** $\tan\beta = 0.5$

Fig. 15 The expected and observed cross-section exclusion limits as a function of $m_{H^\pm}$ in the $\mathrm{tj}_{1\mathrm{L}}$ analysis channel for signal models with $m_a = 250$ GeV, and **a** $\tan\beta = 0.3$ and **b** $\tan\beta = 0.5$. The theoretical cross section of the t-channel DM production process is denoted by 'Theory'

unity, and scenarios with $\tan\beta$ below 1.5 are excluded for masses of $H^\pm$ around 800 GeV.

Acknowledgements We thank CERN for the very successful operation of the LHC, as well as the support staff from our institutions without whom ATLAS could not be operated efficiently. We acknowledge the support of ANPCyT, Argentina; YerPhI, Armenia; ARC, Australia; BMWFW and FWF, Austria; ANAS, Azerbaijan; SSTC, Belarus; CNPq and FAPESP, Brazil; NSERC, NRC and CFI, Canada; CERN; ANID, Chile; CAS, MOST and NSFC, China; COLCIENCIAS, Colombia; MSMT CR, MPO CR and VSC CR, Czech Republic; DNRF and DNSRC, Denmark; IN2P3-CNRS and CEA-DRF/IRFU, France; SRNSFG, Georgia; BMBF, HGF and MPG, Germany; GSRT, Greece; RGC and Hong Kong SAR, China; ISF and Benoziyo Center, Israel; INFN, Italy; MEXT and JSPS, Japan; CNRST, Morocco; NWO, Netherlands; RCN, Norway; MNiSW and NCN, Poland; FCT, Portugal; MNE/IFA, Romania; JINR; MES of Russia and NRC KI, Russian Federation; MESTD, Serbia; MSSR, Slovakia; ARRS and MIZŠ, Slovenia; DST/NRF, South Africa; MICINN, Spain; SRC and Wallenberg Foundation, Sweden; SERI, SNSF and Cantons of Bern and Geneva, Switzerland; MOST, Taiwan; TAEK, Turkey; STFC, United Kingdom; DOE and NSF, United States of America. In addition, individual groups and members have received support from BCKDF, CANARIE, Compute Canada, CRC and IVADO, Canada; Beijing Municipal Science & Technology Commission, China; COST, ERC, ERDF, Horizon 2020 and Marie Skłodowska-Curie Actions, European Union; Investissements d'Avenir Labex, Investissements d'Avenir Idex and ANR, France; DFG and AvH Foundation, Germany; Herakleitos, Thales and Aristeia programmes co-financed by EU-ESF and the Greek NSRF, Greece; BSF-NSF and GIF, Israel; La Caixa Banking Foundation, CERCA Programme Generalitat de Catalunya and PROMETEO and GenT Programmes Generalitat Valenciana, Spain; Göran Gustafssons Stiftelse, Sweden; The Royal Society and Leverhulme Trust, United Kingdom. The crucial computing support from all WLCG partners is acknowledged gratefully, in particular from CERN, the ATLAS Tier-1 facilities at TRIUMF (Canada), NDGF (Denmark, Norway, Sweden), CC-IN2P3 (France), KIT/GridKA (Germany), INFN-CNAF (Italy), NL-T1 (Netherlands), PIC (Spain), ASGC (Taiwan), RAL (UK) and BNL (USA), the Tier-2 facilities worldwide and large non-WLCG resource providers. Major contributors of computing resources are listed in Ref. [96].

Data Availability Statement This manuscript has no associated data or the data will not be deposited. [Authors' comment: All ATLAS scientific output is published in journals, and preliminary results are made available in Conference Notes. All are openly available, without restriction on use by external parties beyond copyright law and the standard conditions agreed by CERN. Data associated with journal publications are also made available: tables and data from plots (e.g. cross section values, likelihood profiles, selection efficiencies, cross section limits,...) are stored in appropriate repositories such as HEPDATA (http://hepdata.cedar.ac.uk/). ATLAS also strives to make additional material related to the paper available that allows a reinterpretation of the data in the context of new theoretical models. For example, an extended encapsulation of the analysis is often provided for measurements in the framework of RIVET (http://rivet.hepforge.org/). The above sentence is taken from the ATLAS Data Access Policy. Please make reference to it saying that it is a public document that can be dowloaded form here: http://opendata.cern.ch/record/413[opendata.cern.ch.]

Funded by SCOAP[3].

References

1. G. Hinshaw et al., Nine-year Wilkinson microwave anisotropy probe (WMAP) observations: cosmological parameter results. Astrophys. J. Suppl. **208**, 19 (2013). https://doi.org/10.1088/0067-0049/208/2/19. arXiv:1212.5226 [astro-ph.CO]
2. Planck Collaboration, Planck 2018 results. I. Overview and the cosmological legacy of Planck, Astron. Astrophys. **641**,

A1 (2020). https://doi.org/10.1051/0004-6361/201833880. arXiv:1807.06205 [astro-ph.CO]
3. G. Steigman, M.S. Turner, Cosmological constraints on the properties of weakly interacting massive particles. Nucl. Phys. B **253**, 375 (1985). https://doi.org/10.1016/0550-3213(85)90537-1
4. M. Bauer, U. Haisch, F. Kahlhoefer, Simplified dark matter models with two Higgs doublets: I. Pseudoscalar mediators. JHEP **05**, 138 (2017). https://doi.org/10.1007/JHEP05(2017)138. arXiv:1701.07427 [hep-ph]
5. T. Abe et al., LHC Dark Matter Working Group: next-generation spin-0 dark matter models. Phys. Dark Univ. **27**, 100351 (2020). https://doi.org/10.1016/j.dark.2019.100351. arXiv:1810.09420 [hep-ex]
6. P.J. Fox, E. Poppitz, Leptophilic dark matter. Phys. Rev. D **79**, 083528 (2009). https://doi.org/10.1103/PhysRevD.79.083528. arXiv:0811.0399 [hep-ph]
7. S. Cassel, D.M. Ghilencea, G.G. Ross, Electroweak and dark matter constraints on a $Z^{'}$ in models with a hidden valley. Nucl. Phys. B **827**, 256 (2010). https://doi.org/10.1016/j.nuclphysb.2009.10.029. arXiv:0903.1118 [hep-ph]
8. Y. Bai, P.J. Fox, R. Harnik, The Tevatron at the frontier of dark matter direct detection. JHEP **12**, 048 (2010). https://doi.org/10.1007/JHEP12(2010)048. arXiv:1005.3797 [hep-ph]
9. J. Abdallah et al., Simplified models for dark matter searches at the LHC. Phys. Dark Univ. **9–10**, 8 (2015). https://doi.org/10.1016/j.dark.2015.08.001. arXiv:1506.03116 [hep-ph]
10. D. Abercrombie et al., Dark Matter benchmark models for early LHC Run-2 Searches: Report of the ATLAS/CMS Dark Matter Forum. Phys. Dark Univ. **27**, 100371 (2020) ed. by A. Boveia, C. Doglioni, S. Lowette, S. Malik and S. Mrenna. https://doi.org/10.1016/j.dark.2019.100371. arXiv:1507.00966 [hep-ex]
11. K. Cheung, K. Mawatari, E. Senaha, P.-Y. Tseng, T.-C. Yuan, The top window for dark matter. JHEP **10**, 081 (2010). https://doi.org/10.1007/JHEP10(2010)081. arXiv:1009.0618 [hep-ph]
12. U. Haisch, A. Hibbs, E. Re, Determining the structure of dark-matter couplings at the LHC. Phys. Rev. D **89**, 034009 (2014). https://doi.org/10.1103/PhysRevD.89.034009. arXiv:1311.7131 [hep-ph]
13. M.R. Buckley, D. Feld, D. Goncalves, Scalar simplified models for dark matter. Phys. Rev. D **91**, 015017 (2015). https://doi.org/10.1103/PhysRevD.91.015017. arXiv:1410.6497 [hep-ph]
14. M.R. Buckley, D. Goncalves, Constraining the strength and CP structure of dark production at the LHC: the associated top-pair channel. Phys. Rev. D **93**, 034003 (2016). https://doi.org/10.1103/PhysRevD.93.034003. arXiv:1511.06451 [hep-ph]
15. U. Haisch, E. Re, Simplified dark matter top-quark interactions at the LHC. JHEP **06**, 078 (2015). https://doi.org/10.1007/JHEP06(2015)078. arXiv:1503.00691 [hep-ph]
16. M. Backovic et al., Higher-order QCD predictions for dark matter production at the LHC in simplified models with s-channel mediators. Eur. Phys. J. C **75**, 482 (2015). https://doi.org/10.1140/epjc/s10052-015-3700-6. arXiv:1508.05327 [hep-ph]
17. C. Arina et al., A comprehensive approach to dark matter studies: exploration of simplified top-philic models. JHEP **11**, 111 (2016). https://doi.org/10.1007/JHEP11(2016)111. arXiv:1605.09242 [hep-ph]
18. U. Haisch, P. Pani, G. Polesello, Determining the CP nature of spin-0 mediators in associated production of dark matter and tt pairs. JHEP **02**, 131 (2017). https://doi.org/10.1007/JHEP02(2017)131. arXiv:1611.09841 [hep-ph]
19. S. Banerjee et al., Cornering pseudoscalar-mediated dark matter with the LHC and cosmology. JHEP **07**, 080 (2017). https://doi.org/10.1007/JHEP07(2017)080. arXiv:1705.02327 [hep-ph]
20. J.F. Gunion, H.E. Haber, CP-conserving two Higgs doublet model: the approach to the decoupling limit. Phys. Rev. D **67**, 075019 (2003). https://doi.org/10.1103/PhysRevD.67.075019. arXiv:hep-ph/0207010
21. G.C. Branco et al., Theory and phenomenology of two-Higgs-doublet models. Phys. Rep. **516**, 1 (2012). https://doi.org/10.1016/j.physrep.2012.02.002. arXiv:1106.0034 [hep-ph]
22. ATLAS Collaboration, Constraints on mediator-based dark matter and scalar dark energy models using $\sqrt{s} = 13$ TeV pp collision data collected by the ATLAS detector. JHEP **05**, 142 (2019). https://doi.org/10.1007/JHEP05(2019)142. arXiv: 1903.01400 [hep-ex]
23. P. Pani, G. Polesello, Dark matter production in association with a single top-quark at the LHC in a two-Higgs-doublet model with a pseudoscalar mediator. Phys. Dark Univ. **21**, 8 (2018). https://doi.org/10.1016/j.dark.2018.04.006. arXiv:1712.03874 [hep-ph]
24. CMS Collaboration, Search for dark matter produced in association with a leptonically decaying Z boson in proton-proton collisions at $\sqrt{s} = 13$ TeV. Eur. Phys. J. C **81**, 13 (2021). https://doi.org/10.1140/epjc/s10052-020-08739-5. arXiv:2008.04735 [hep-ex]
25. CMS Collaboration, Search for dark matter produced in association with a Higgs boson decaying to a pair of bottom quarks in proton-proton collisions at $\sqrt{s} = 13$ TeV. Eur. Phys. J. C **79**, 280 (2019). https://doi.org/10.1140/epjc/s10052-019-6730-7. arXiv:1811.06562 [hep-ex]
26. CMS Collaboration, Search for dark matter produced in association with a single top quark or a top quark pair in proton-proton collisions at $\sqrt{s} = 13$ TeV. JHEP **03**, 141 (2019). https://doi.org/10.1007/JHEP03(2019)141. arXiv:1901.01553 [hep-ex]
27. ATLAS Collaboration, The ATLAS Experiment at the CERN Large Hadron Collider. JINST **3**, S08003 (2008). https://doi.org/10.1088/1748-0221/3/08/S08003
28. ATLAS Collaboration, ATLAS Insertable B-Layer Technical Design Report, ATLAS-TDR-19; CERN-LHCC-2010-013 (2010). https://cds.cern.ch/record/1291633
29. B. Abbott et al., Production and integration of the ATLAS Insertable B-Layer. JINST **13**, T05008 (2018). https://doi.org/10.1088/1748-0221/13/05/T05008. arXiv:1803.00844 [physics.ins-det]
30. ATLAS Collaboration, Performance of the ATLAS trigger system in 2015. Eur. Phys. J. C **77**, 317 (2017), https://doi.org/10.1140/epjc/s10052-017-4852-3. arXiv:1611.09661 [hep-ex]
31. ATLAS Collaboration, Luminosity determination in pp collisions at $\sqrt{s} = 13$ TeV using the ATLAS detector at the LHC, ATLAS-CONF-2019-021 (2019). https://cds.cern.ch/record/2677054
32. G. Avoni et al., The new LUCID-2 detector for luminosity measurement and monitoring in ATLAS. JINST **13**, P07017 (2018). https://doi.org/10.1088/1748-0221/13/07/P07017
33. ATLAS Collaboration, 2015 start-up trigger menu and initial performance assessment of the ATLAS trigger using Run-2 data, ATL-DAQ-PUB-2016-001 (2016). https://cds.cern.ch/record/2136007
34. ATLAS Collaboration, The ATLAS Simulation Infrastructure. Eur. Phys. J. C **70**, 823 (2010). https://doi.org/10.1140/epjc/s10052-010-1429-9. arXiv:1005.4568 [physics.ins-det]
35. S. Agostinelli et al., Geant4—a simulation toolkit. Nucl. Instrum. Meth. A **506**, 250 (2003). https://doi.org/10.1016/S0168-9002(03)01368-8
36. T. Sjöstrand, S. Mrenna, P. Skands, A brief introduction to PYTHIA 8.1. Comput. Phys. Commun. **178**, 852 (2008). https://doi.org/10.1016/j.cpc.2008.01.036. arXiv:0710.3820 [hep-ph]
37. R.D. Ball et al., Parton distributions with LHC data. Nucl. Phys. B **867**, 244 (2013). https://doi.org/10.1016/j.nuclphysb.2012.10.003. arXiv:1207.1303 [hep-ph]
38. ATLAS Collaboration, The Pythia 8 A3 tune description of ATLAS minimum bias and inelastic measurements incorporating the Donnachie–Landshoff diffractive model, ATL-PHYS-PUB-2016-017 (2016). https://cds.cern.ch/record/2206965
39. J. Alwall et al., The automated computation of tree-level and next-to-leading order differential cross sections, and their matching to

parton shower simulations. JHEP **07**, 079 (2014). https://doi.org/10.1007/JHEP07(2014)079. arXiv:1405.0301 [hep-ph]
40. T. Sjöstrand et al., An introduction to PYTHIA 8.2. Comput. Phys. Commun. **191**, 159 (2015). https://doi.org/10.1016/j.cpc.2015.01.024. arXiv:1410.3012 [hep-ph]
41. ATLAS Collaboration, ATLAS Pythia 8 tunes to 7 TeV data, ATL-PHYS-PUB-2014-021 (2014). https://cds.cern.ch/record/1966419
42. R.D. Ball et al., Parton distributions for the LHC run II. JHEP **04**, 040 (2015). https://doi.org/10.1007/JHEP04(2015)040. arXiv:1410.8849 [hep-ph]
43. P. Artoisenet, R. Frederix, O. Mattelaer, R. Rietkerk, Automatic spin-entangled decays of heavy resonances in Monte Carlo simulations. JHEP **03**, 015 (2013). https://doi.org/10.1007/JHEP03(2013)015. arXiv:1212.3460 [hep-ph]
44. T. Gleisberg, S. Höche, F. Krauss, M. Schönherr, S. Schumann et al., Event generation with SHERPA 1.1. JHEP **02**, 007 (2009). https://doi.org/10.1088/1126-6708/2009/02/007. arXiv:0811.4622 [hep-ph]
45. T. Gleisberg, S. Höche, Comix, a new matrix element generator. JHEP **12**, 039 (2008). https://doi.org/10.1088/1126-6708/2008/12/039. arXiv:0808.3674 [hep-ph]
46. F. Cascioli, P. Maierhofer, S. Pozzorini, Scattering amplitudes with open loops. Phys. Rev. Lett. **108**, 111601 (2012). https://doi.org/10.1103/PhysRevLett.108.111601. arXiv:1111.5206 [hep-ph]
47. S. Schumann, F. Krauss, A parton shower algorithm based on Catani–Seymour dipole factorisation. JHEP **03**, 038 (2008). https://doi.org/10.1088/1126-6708/2008/03/038. arXiv:0709.1027 [hep-ph]
48. S. Höche, F. Krauss, M. Schönherr, F. Siegert, QCD matrix elements + parton showers: the NLO case. JHEP **04**, 027 (2013). https://doi.org/10.1007/JHEP04(2013)027. arXiv:1207.5030 [hep-ph]
49. D.J. Lange, The EvtGen particle decay simulation package. Nucl. Instrum. Meth. A **462**, 152 (2001). https://doi.org/10.1016/S0168-9002(01)00089-4
50. S. Frixione, P. Nason, G. Ridolfi, A positive-weight next-to-leading-order Monte Carlo for heavy flavour hadroproduction. JHEP **09**, 126 (2007). https://doi.org/10.1088/1126-6708/2007/09/126. arXiv:0707.3088 [hep-ph]
51. P. Nason, A new method for combining NLO QCD with shower Monte Carlo algorithms. JHEP **11**, 040 (2004). https://doi.org/10.1088/1126-6708/2004/11/040. arXiv:hep-ph/0409146
52. S. Frixione, P. Nason, C. Oleari, Matching NLO QCD computations with parton shower simulations: the POWHEG method. JHEP **11**, 070 (2007). https://doi.org/10.1088/1126-6708/2007/11/070. arXiv:0709.2092 [hep-ph]
53. S. Alioli, P. Nason, C. Oleari, E. Re, A general framework for implementing NLO calculations in shower Monte Carlo programs: the POWHEG BOX. JHEP **06**, 043 (2010). https://doi.org/10.1007/JHEP06(2010)043. arXiv:1002.2581 [hep-ph]
54. M. Czakon, A. Mitov, Top++: a program for the calculation of the top-pair cross-section at hadron colliders. Comput. Phys. Commun. **185**, 2930 (2014). https://doi.org/10.1016/j.cpc.2014.06.021. arXiv:1112.5675 [hep-ph]
55. R. Frederix, E. Re, P. Torrielli, Single-top t-channel hadroproduction in the four-flavour scheme with POWHEG and aMC@NLO. JHEP **09**, 130 (2012). https://doi.org/10.1007/JHEP09(2012)130. arXiv:1207.5391 [hep-ph]
56. N. Kidonakis, Next-to-next-to-leading-order collinear and soft gluon corrections for t-channel single top quark production. Phys. Rev. D **83**, 091503 (2011). https://doi.org/10.1103/PhysRevD.83.091503. arXiv:1103.2792 [hep-ph]
57. E. Re, Single-top Wt-channel production matched with parton showers using the POWHEG method. Eur. Phys. J. C **71**, 1547 (2011). https://doi.org/10.1140/epjc/s10052-011-1547-z. arXiv:1009.2450 [hep-ph]
58. N. Kidonakis, Two-loop soft anomalous dimensions for single top quark associated production with a W− or H−. Phys. Rev. D **82**, 054018 (2010). https://doi.org/10.1103/PhysRevD.82.054018. arXiv:1005.4451 [hep-ph]
59. N. Kidonakis, Next-to-next-to-leading logarithm resummation for s-channel single top quark production. Phys. Rev. D **81**, 054028 (2010). https://doi.org/10.1103/PhysRevD.81.054028. arXiv:1001.5034 [hep-ph]
60. S. Catani, L. Cieri, G. Ferrera, D. de Florian, M. Grazzini, Vector boson production at hadron colliders: a fully exclusive QCD calculation at next-to-next-to-leading order. Phys. Rev. Lett. **103**, 082001 (2009). https://doi.org/10.1103/PhysRevLett.103.082001. arXiv:0903.2120 [hep-ph]
61. D. de Florian et al., Handbook of LHC Higgs Cross Sections: 4. Deciphering the Nature of the Higgs Sector (2016). https://doi.org/10.23731/CYRM-2017-002. arXiv:1610.07922 [hep-ph]
62. ATLAS Collaboration, Vertex reconstruction performance of the ATLAS detector at $\sqrt{s}$ = 13 TeV, ATL-PHYS-PUB-2015-026 (2015). https://cds.cern.ch/record/2037717
63. ATLAS Collaboration, Selection of jets produced in 13 TeV proton-proton collisions with the ATLAS detector. ATLAS-CONF-2015-029 (2015). https://cds.cern.ch/record/2037702
64. ATLAS Collaboration, Electron reconstruction and identification in the ATLAS experiment using the 2015 and 2016 LHC proton–proton collision data at $\sqrt{s}$ = 13 TeV. Eur. Phys. J. C **79**, 639 (2019). https://doi.org/10.1140/epjc/s10052-019-7140-6. arXiv:1902.04655 [hep-ex]
65. ATLAS Collaboration, Muon reconstruction performance of the ATLAS detector in proton–proton collision data at $\sqrt{s}$ = 13 TeV. Eur. Phys. J. C **76**, 292 (2016). https://doi.org/10.1140/epjc/s10052-016-4120-y. arXiv:1603.05598 [hep-ex]
66. ATLAS Collaboration, Topological cell clustering in the ATLAS calorimeters and its performance in LHC Run 1. Eur. Phys. J. C **77**, 490 (2017). https://doi.org/10.1140/epjc/s10052-017-5004-5. arXiv: 1603.02934 [hep-ex]
67. M. Cacciari, G.P. Salam, G. Soyez, The $anti-k_t$ jet clustering algorithm. JHEP **04**, 063 (2008). https://doi.org/10.1088/1126-6708/2008/04/063. arXiv:0802.1189 [hep-ph]
68. ATLAS Collaboration, Jet energy scale measurements and their systematic uncertainties in proton–proton collisions at $\sqrt{s}$ = 13 TeV with the ATLAS detector. Phys. Rev. D **96**, 072002 (2017). https://doi.org/10.1103/PhysRevD.96.072002. arXiv:1703.09665 [hep-ex]
69. ATLAS Collaboration, Performance of pile-up mitigation techniques for jets in pp collisions at $\sqrt{s}$ = 8 TeV using the ATLAS detector. Eur. Phys. J. C **76**, 581 (2016). https://doi.org/10.1140/epjc/s10052-016-4395-z. arXiv:1510.03823 [hep-ex]
70. M. Cacciari, G.P. Salam, G. Soyez, FastJet user manual. Eur. Phys. J. C **72**, 1896 (2012). https://doi.org/10.1140/epjc/s10052-012-1896-2. arXiv:1111.6097 [hep-ph]
71. ATLAS Collaboration, ATLAS b-jet identification performance and efficiency measurement with $t\bar{t}$ events in pp collisions at $\sqrt{s}$ = 13 TeV. Eur. Phys. J. C **79**, 970 (2019). https://doi.org/10.1140/epjc/s10052-019-7450-8. arXiv:1907.05120 [hep-ex]
72. ATLAS Collaboration, Optimisation and performance studies of the ATLAS b-tagging algorithms for the 2017–18 LHC run. ATL-PHYS-PUB-2017-013 (2017). https://cds.cern.ch/record/2273281
73. M. Cacciari, G.P. Salam, G. Soyez, The catchment area of jets. JHEP **04**, 005 (2008). https://doi.org/10.1088/1126-6708/2008/04/005. arXiv:0802.1188 [hep-ph]
74. ATLAS Collaboration, Measurement of the photon identification efficiencies with the ATLAS detector using LHC Run 2 data collected in 2015 and 2016. Eur. Phys. J. C **79**, 205 (2019). https://doi.org/10.1140/epjc/s10052-019-6650-6. arXiv:1810.05087 [hep-ex]

75. ATLAS Collaboration, Performance of missing transverse momentum reconstruction with the ATLAS detector using proton–proton collisions at $\sqrt{s} = 13$ TeV. Eur. Phys. J. C **78**, 903 (2018). https://doi.org/10.1140/epjc/s10052-018-6288-9. arXiv:1802.08168 [hep-ex]
76. ATLAS Collaboration, E_T^{miss} performance in the ATLAS detector using 2015–2016 LHC pp collisions. ATLAS-CONF-2018-023 (2018). https://cds.cern.ch/record/2625233
77. M. Baak et al., HistFitter software framework for statistical data analysis. Eur. Phys. J. C **75**, 153 (2015). https://doi.org/10.1140/epjc/s10052-015-3327-7. arXiv:1410.1280 [hep-ex]
78. ATLAS Collaboration, Search for top-squark pair production in final states with one lepton, jets, and missing transverse momentum using 36.1 fb^{-1} of $\sqrt{s} = 13$ TeV pp collision data with the ATLAS detector. JHEP **06**, 108 (2018). https://doi.org/10.1007/JHEP06(2018)108. arXiv:1711.11520 [hep-ex]
79. C. Lester, D. Summers, Measuring masses of semi-invisibly decaying particles pair produced at hadron colliders. Phys. Lett. B **463**, 99 (1999). https://doi.org/10.1016/S0370-2693(99)00945-4. arXiv:hep-ph/9906349
80. A. Barr, C. Lester, P. Stephens, A variable for measuring masses at hadron colliders when missing energy is expected; m_{T2}: the truth behind the glamour. J. Phys. G **29**, 2343 (2003). https://doi.org/10.1088/0954-3899/29/10/304. arXiv:hep-ph/0304226 [hep-ph]
81. P. Konar, K. Kong, K.T. Matchev, M. Park, Dark matter particle spectroscopy at the LHC: generalizing M_{T2} to asymmetric event topologies. JHEP **04**, 086 (2010). https://doi.org/10.1007/JHEP04(2010)086. arXiv:0911. 4126 [hep-ph]
82. C.G. Lester, B. Nachman, Bisection-based asymmetric M_{T2} computation: a higher precision calculator than existing symmetric methods. JHEP **03**, 100 (2015). https://doi.org/10.1007/JHEP03(2015)100. arXiv:1411.4312 [hep-ph]
83. K. Sastry, D. Goldberg, G. Kendall, 'Genetic Algorithms', Search Methodologies: Introductory Tutorials in Optimization and Decision Support Techniques, ed. by E. K. Burke and G. Kendall, Springer US (2005). ISBN: 978-0-387-28356-2. https://doi.org/10.1007/0-387-28356-0_4
84. G. Choudalakis, D. Casadei, Plotting the differences between data and expectation. Eur. Phys. J. Plus **127**, 25 (2012). https://doi.org/10.1140/epjp/i2012-12025-y. arXiv:1111.2062 [physics.data-an]
85. ATLAS Collaboration, Measurement of the top quark-pair production cross section with ATLAS in pp collisions at $\sqrt{s}$ = 7 TeV. Eur. Phys. J. C **71**, 1577 (2011). https://doi.org/10.1140/epjc/s10052-011-1577-6. arXiv: 1012.1792 [hep-ex]
86. ATLAS Collaboration, Measurement of the top quark pair production cross section in pp collisions at $\sqrt{s}$ = 7 TeV in dilepton final states with ATLAS. Phys. Lett. B **707**, 459 (2012). https://doi.org/10.1016/j.physletb.2011.12.055. arXiv:1108.3699 [hep-ex]
87. A. Hoecker et al., TMVA—Toolkit for Multivariate Data Analysis. arXiv: physics/0703039 [physics.data-an] (2007)
88. M. Bähr et al., Herwig++ physics and manual. Eur. Phys. J. C **58**, 639 (2008). https://doi.org/10.1140/epjc/s10052-008-0798-9. arXiv:0803.0883 [hep-ph]
89. J. Bellm et al., Herwig 7.0/Herwig++ 3.0 release note. Eur. Phys. J. C **76**, 196 (2016). https://doi.org/10.1140/epjc/s10052-016-4018-8. arXiv:1512.01178 [hep-ph]
90. S. Frixione, E. Laenen, P. Motylinski, C. White, B.R. Webber, Single-top hadroproduction in association with a W boson. JHEP **07**, 029 (2008). https://doi.org/10.1088/1126-6708/2008/07/029
91. F. Demartin, B. Maier, F. Maltoni, K. Mawatari, M. Zaro, tWH associated production at the LHC. Eur. Phys. J. C **77**, 34 (2017). https://doi.org/10.1140/epjc/s10052-017-4601-7. arXiv:1607.05862 [hep-ph]
92. O. Bessidskaia Bylund, Modelling Wt and tWZ production at NLO for ATLAS analyses, 9th International Workshop on Top Quark. Physics (2016). arXiv:1612.00440 [hep-ph]
93. A.L. Read, Presentation of search results: the CLS technique. J. Phys. G **28**, 2693 (2002). https://doi.org/10.1088/0954-3899/28/10/313
94. M. Bauer, M. Klassen, V. Tenorth, Universal properties of pseudoscalar mediators in dark matter extensions of 2HDMs. JHEP **07**, 107 (2018). https://doi.org/10.1007/JHEP07(2018)107. arXiv:1712.06597 [hep-ph]
95. U. Haisch, G. Polesello, Searching for heavy Higgs bosons in the $t\bar{t}Z$ and tbW final states. JHEP **09**, 151 (2018). https://doi.org/10.1007/JHEP09(2018)151. arXiv:1807.07734 [hep-ph]
96. ATLAS Collaboration, ATLAS Computing Acknowledgements ATL-SOFT-PUB-2020-001. https://cds.cern.ch/record/2717821

ATLAS Collaboration

G. Aad[102], B. Abbott[128], D. C. Abbott[103], A. Abed Abud[36], K. Abeling[53], D. K. Abhayasinghe[94], S. H. Abidi[167], O. S. AbouZeid[40], N. L. Abraham[156], H. Abramowicz[161], H. Abreu[160], Y. Abulaiti[6], B. S. Acharya[67a,67b,o], B. Achkar[53], L. Adam[100], C. Adam Bourdarios[5], L. Adamczyk[84a], L. Adamek[167], J. Adelman[121], A. Adiguzel[12c], S. Adorni[54], T. Adye[143], A. A. Affolder[145], Y. Afik[160], C. Agapopoulou[65], M. N. Agaras[38], A. Aggarwal[119], C. Agheorghiesei[27c], J. A. Aguilar-Saavedra[139a,139f,ac], A. Ahmad[36], F. Ahmadov[80], W. S. Ahmed[104], X. Ai[18], G. Aielli[74a,74b], S. Akatsuka[86], M. Akbiyik[100], T. P. A. Åkesson[97], E. Akilli[54], A. V. Akimov[111], K. Al Khoury[65], G. L. Alberghi[23a,23b], J. Albert[176], M. J. Alconada Verzini[161], S. Alderweireldt[36], M. Aleksa[36], I. N. Aleksandrov[80], C. Alexa[27b], T. Alexopoulos[10], A. Alfonsi[120], F. Alfonsi[23a,23b], M. Alhroob[128], B. Ali[141], S. Ali[158], M. Aliev[166], G. Alimonti[69a], C. Allaire[36], B. M. M. Allbrooke[156], B. W. Allen[131], P. P. Allport[21], A. Aloisio[70a,70b], F. Alonso[89], C. Alpigiani[148], E. Alunno Camelia[74a,74b], M. Alvarez Estevez[99], M. G. Alviggi[70a,70b], Y. Amaral Coutinho[81b], A. Ambler[104], L. Ambroz[134], C. Amelung[36], D. Amidei[106], S. P. Amor Dos Santos[139a], S. Amoroso[46], C. S. Amrouche[54], F. An[79], C. Anastopoulos[149], N. Andari[144], T. Andeen[11], J. K. Anders[20], S. Y. Andrean[45a,45b], A. Andreazza[69a,69b], V. Andrei[61a], C. R. Anelli[176], S. Angelidakis[9], A. Angerami[39], A. V. Anisenkov[122a,122b], A. Annovi[72a], C. Antel[54], M. T. Anthony[149], E. Antipov[129], M. Antonelli[51], D. J. A. Antrim[18], F. Anulli[73a], M. Aoki[82], J. A. Aparisi Pozo[174], M. A. Aparo[156], L. Aperio Bella[46], N. Aranzabal[36], V. Araujo Ferraz[81a], R. Araujo Pereira[81b], C. Arcangeletti[51], A. T. H. Arce[49], J-F. Arguin[110], S. Argyropoulos[52], J.-H. Arling[46], A. J. Armbruster[36], A. Armstrong[171], O. Arnaez[167], H. Arnold[120], Z. P. Arrubarrena Tame[114], G. Artoni[134], H. Asada[117], K. Asai[126], S. Asai[163], T. Asawatavonvanich[165], N. Asbah[59], E. M. Asimakopoulou[172], L. Asquith[156], J. Assahsah[35d], K. Assamagan[29], R. Astalos[28a], R. J. Atkin[33a], M. Atkinson[173], N. B. Atlay[19], H. Atmani[65], P. A. Atmasiddha[106], K. Augsten[141], V. A. Austrup[182], G. Avolio[36], M. K. Ayoub[15a], G. Azuelos[110,aj], D. Babal[28a], H. Bachacou[144], K. Bachas[162], F. Backman[45a,45b], P. Bagnaia[73a,73b], M. Bahmani[85], H. Bahrasemani[152], A. J. Bailey[174], V. R. Bailey[173], J. T. Baines[143], C. Bakalis[10], O. K. Baker[183], P. J. Bakker[120], E. Bakos[16], D. Bakshi Gupta[8], S. Balaji[157], R. Balasubramanian[120], E. M. Baldin[122a,122b], P. Balek[180], F. Balli[144], W. K. Balunas[134], J. Balz[100], E. Banas[85], M. Bandieramonte[138], A. Bandyopadhyay[19], Sw. Banerjee[181,j], L. Barak[161], W. M. Barbe[38], E. L. Barberio[105], D. Barberis[55a,55b], M. Barbero[102], G. Barbour[95], T. Barillari[115], M-S. Barisits[36], J. Barkeloo[131], T. Barklow[153], R. Barnea[160], B. M. Barnett[143], R. M. Barnett[18], Z. Barnovska-Blenessy[60a], A. Baroncelli[60a], G. Barone[29], A. J. Barr[134], L. Barranco Navarro[45a,45b], F. Barreiro[99], J. Barreiro Guimarães da Costa[15a], U. Barron[161], S. Barsov[137], F. Bartels[61a], R. Bartoldus[153], G. Bartolini[102], A. E. Barton[90], P. Bartos[28a], A. Basalaev[46], A. Basan[100], A. Bassalat[65,ag], M. J. Basso[167], R. L. Bates[57], S. Batlamous[35e], J. R. Batley[32], B. Batool[151], M. Battaglia[145], M. Bauce[73a,73b], F. Bauer[144], P. Bauer[24], H. S. Bawa[31], A. Bayirli[12c], J. B. Beacham[49], T. Beau[135], P. H. Beauchemin[170], F. Becherer[52], P. Bechtle[24], H. C. Beck[53], H. P. Beck[20,q], K. Becker[178], C. Becot[46], A. Beddall[12d], A. J. Beddall[12a], V. A. Bednyakov[80], M. Bedognetti[120], C. P. Bee[155], T. A. Beermann[182], M. Begalli[81b], M. Begel[29], A. Behera[155], J. K. Behr[46], F. Beisiegel[24], M. Belfkir[5], A. S. Bell[95], G. Bella[161], L. Bellagamba[23b], A. Bellerive[34], P. Bellos[9], K. Beloborodov[122a,122b], K. Belotskiy[112], N. L. Belyaev[112], D. Benchekroun[35a], N. Benekos[10], Y. Benhammou[161], D. P. Benjamin[6], M. Benoit[29], J. R. Bensinger[26], S. Bentvelsen[120], L. Beresford[134], M. Beretta[51], D. Berge[19], E. Bergeaas Kuutmann[172], N. Berger[5], B. Bergmann[141], L. J. Bergsten[26], J. Beringer[18], S. Berlendis[7], G. Bernardi[135], C. Bernius[153], F. U. Bernlochner[24], T. Berry[94], P. Berta[100], A. Berthold[48], I. A. Bertram[90], O. Bessidskaia Bylund[182], N. Besson[144], S. Bethke[115], A. Betti[42], A. J. Bevan[93], J. Beyer[115], S. Bhatta[155], D. S. Bhattacharya[177], P. Bhattarai[26], V. S. Bhopatkar[6], R. Bi[138], R. M. Bianchi[138], O. Biebel[114], D. Biedermann[19], R. Bielski[36], K. Bierwagen[100], N. V. Biesuz[72a,72b], M. Biglietti[75a], T. R. V. Billoud[141], M. Bindi[53], A. Bingul[12d], C. Bini[73a,73b], S. Biondi[23a,23b], C. J. Birch-sykes[101], M. Birman[180], T. Bisanz[36], J. P. Biswal[3], D. Biswas[181,j], A. Bitadze[101], C. Bittrich[48], K. Bjørke[133], T. Blazek[28a], I. Bloch[46], C. Blocker[26], A. Blue[57], U. Blumenschein[93], G. J. Bobbink[120], V. S. Bobrovnikov[122a,122b], S. S. Bocchetta[97], D. Bogavac[14], A. G. Bogdanchikov[122a,122b], C. Bohm[45a], V. Boisvert[94], P. Bokan[172,53], T. Bold[84a], A. E. Bolz[61b], M. Bomben[135], M. Bona[93], J. S. Bonilla[131], M. Boonekamp[144], C. D. Booth[94], A. G. Borbély[57], H. M. Borecka-Bielska[91], L. S. Borgna[95], A. Borisov[123], G. Borissov[90], D. Bortoletto[134], D. Boscherini[23b], M. Bosman[14], J. D. Bossio Sola[104], K. Bouaouda[35a], J. Boudreau[138], E. V. Bouhova-Thacker[90], D. Boumediene[38], A. Boveia[127], J. Boyd[36], D. Boye[33c], I. R. Boyko[80], A. J. Bozson[94], J. Bracinik[21],

N. Brahimi[60d], G. Brandt[182], O. Brandt[32], F. Braren[46], B. Brau[103], J. E. Brau[131], W. D. Breaden Madden[57], K. Brendlinger[46], R. Brener[160], L. Brenner[36], R. Brenner[172], S. Bressler[180], B. Brickwedde[100], D. L. Briglin[21], D. Britton[57], D. Britzger[115], I. Brock[24], R. Brock[107], G. Brooijmans[39], W. K. Brooks[146d], E. Brost[29], P. A. Bruckman de Renstrom[85], B. Brüers[46], D. Bruncko[28b], A. Bruni[23b], G. Bruni[23b], M. Bruschi[23b], N. Bruscino[73a,73b], L. Bryngemark[153], T. Buanes[17], Q. Buat[155], P. Buchholz[151], A. G. Buckley[57], I. A. Budagov[80], M. K. Bugge[133], O. Bulekov[112], B. A. Bullard[59], T. J. Burch[121], S. Burdin[91], C. D. Burgard[120], A. M. Burger[129], B. Burghgrave[8], J. T. P. Burr[46], C. D. Burton[11], J. C. Burzynski[103], V. Büscher[100], E. Buschmann[53], P. J. Bussey[57], J. M. Butler[25], C. M. Buttar[57], J. M. Butterworth[95], P. Butti[36], W. Buttinger[143], C. J. Buxo Vazquez[107], A. Buzatu[158], A. R. Buzykaev[122a,122b], G. Cabras[23a,23b], S. Cabrera Urbán[174], D. Caforio[56], H. Cai[138], V. M. M. Cairo[153], O. Cakir[4a], N. Calace[36], P. Calafiura[18], G. Calderini[135], P. Calfayan[66], G. Callea[57], L. P. Caloba[81b], A. Caltabiano[74a,74b], S. Calvente Lopez[99], D. Calvet[38], S. Calvet[38], T. P. Calvet[102], M. Calvetti[72a,72b], R. Camacho Toro[135], S. Camarda[36], D. Camarero Munoz[99], P. Camarri[74a,74b], M. T. Camerlingo[75a,75b], D. Cameron[133], C. Camincher[36], S. Campana[36], M. Campanelli[95], A. Camplani[40], V. Canale[70a,70b], A. Canesse[104], M. Cano Bret[78], J. Cantero[129], T. Cao[161], Y. Cao[173], M. Capua[41a,41b], R. Cardarelli[74a], F. Cardillo[174], G. Carducci[41a,41b], I. Carli[142], T. Carli[36], G. Carlino[70a], B. T. Carlson[138], E. M. Carlson[176,168a], L. Carminati[69a,69b], R. M. D. Carney[153], S. Caron[119], E. Carquin[146d], S. Carrá[46], G. Carratta[23a,23b], J. W. S. Carter[167], T. M. Carter[50], M. P. Casado[14,g], A. F. Casha[167], E. G. Castiglia[183], F. L. Castillo[174], L. Castillo Garcia[14], V. Castillo Gimenez[174], N. F. Castro[139a,139e], A. Catinaccio[36], J. R. Catmore[133], A. Cattai[36], V. Cavaliere[29], V. Cavasinni[72a,72b], E. Celebi[12b], F. Celli[134], K. Cerny[130], A. S. Cerqueira[81a], A. Cerri[156], L. Cerrito[74a,74b], F. Cerutti[18], A. Cervelli[23a,23b], S. A. Cetin[12b], Z. Chadi[35a], D. Chakraborty[121], J. Chan[181], W. S. Chan[120], W. Y. Chan[91], J. D. Chapman[32], B. Chargeishvili[159b], D. G. Charlton[21], T. P. Charman[93], M. Chatterjee[20], C. C. Chau[34], S. Che[127], S. Chekanov[6], S. V. Chekulaev[168a], G. A. Chelkov[80,ae], B. Chen[79], C. Chen[60a], C. H. Chen[79], H. Chen[15c], H. Chen[29], J. Chen[60a], J. Chen[39], J. Chen[26], S. Chen[136], S. J. Chen[15c], X. Chen[15b], Y. Chen[60a], Y-H. Chen[46], H. C. Cheng[63a], H. J. Cheng[15a], A. Cheplakov[80], E. Cheremushkina[123], R. Cherkaoui El Moursli[35e], E. Cheu[7], K. Cheung[64], T. J. A. Chevalérias[144], L. Chevalier[144], V. Chiarella[51], G. Chiarelli[72a], G. Chiodini[68a], A. S. Chisholm[21], A. Chitan[27b], I. Chiu[163], Y. H. Chiu[176], M. V. Chizhov[80], K. Choi[11], A. R. Chomont[73a,73b], Y. Chou[103], Y. S. Chow[120], L. D. Christopher[33e], M. C. Chu[63a], X. Chu[15a,15d], J. Chudoba[140], J. J. Chwastowski[85], L. Chytka[130], D. Cieri[115], K. M. Ciesla[85], V. Cindro[92], I. A. Cioară[27b], A. Ciocio[18], F. Cirotto[70a,70b], Z. H. Citron[180,k], M. Citterio[69a], D. A. Ciubotaru[27b], B. M. Ciungu[167], A. Clark[54], P. J. Clark[50], S. E. Clawson[101], C. Clement[45a,45b], L. Clissa[23a,23b], Y. Coadou[102], M. Cobal[67a,67c], A. Coccaro[55b], J. Cochran[79], R. Coelho Lopes De Sa[103], H. Cohen[161], A. E. C. Coimbra[36], B. Cole[39], A. P. Colijn[120], J. Collot[58], P. Conde Muiño[139a,139h], S. H. Connell[33c], I. A. Connelly[57], S. Constantinescu[27b], F. Conventi[70a,ak], A. M. Cooper-Sarkar[134], F. Cormier[175], K. J. R. Cormier[167], L. D. Corpe[95], M. Corradi[73a,73b], E. E. Corrigan[97], F. Corriveau[104,aa], M. J. Costa[174], F. Costanza[5], D. Costanzo[149], G. Cowan[94], J. W. Cowley[32], J. Crane[101], K. Cranmer[125], R. A. Creager[136], S. Crépé-Renaudin[58], F. Crescioli[135], M. Cristinziani[24], V. Croft[170], G. Crosetti[41a,41b], A. Cueto[5], T. Cuhadar Donszelmann[171], H. Cui[15a,15d], A. R. Cukierman[153], W. R. Cunningham[57], S. Czekierda[85], P. Czodrowski[36], M. M. Czurylo[61b], M. J. Da Cunha Sargedas De Sousa[60b], J. V. Da Fonseca Pinto[81b], C. Da Via[101], W. Dabrowski[84a], F. Dachs[36], T. Dado[47], S. Dahbi[33e], T. Dai[106], C. Dallapiccola[103], M. Dam[40], G. D'amen[29], V. D'Amico[75a,75b], J. Damp[100], J. R. Dandoy[136], M. F. Daneri[30], M. Danninger[152], V. Dao[36], G. Darbo[55b], O. Dartsi[5], A. Dattagupta[131], T. Daubney[46], S. D'Auria[69a,69b], C. David[168b], T. Davidek[142], D. R. Davis[49], I. Dawson[149], K. De[8], R. De Asmundis[70a], M. De Beurs[120], S. De Castro[23a,23b], N. De Groot[119], P. de Jong[120], H. De la Torre[107], A. De Maria[15c], D. De Pedis[73a], A. De Salvo[73a], U. De Sanctis[74a,74b], M. De Santis[74a,74b], A. De Santo[156], J. B. De Vivie De Regie[65], D. V. Dedovich[80], A. M. Deiana[42], J. Del Peso[99], Y. Delabat Diaz[46], D. Delgove[65], F. Deliot[144], C. M. Delitzsch[7], M. Della Pietra[70a,70b], D. Della Volpe[54], A. Dell'Acqua[36], L. Dell'Asta[74a,74b], M. Delmastro[5], C. Delporte[65], P. A. Delsart[58], S. Demers[183], M. Demichev[80], G. Demontigny[110], S. P. Denisov[123], L. D'Eramo[121], D. Derendarz[85], J. E. Derkaoui[35d], F. Derue[135], P. Dervan[91], K. Desch[24], K. Dette[167], C. Deutsch[24], M. R. Devesa[30], P. O. Deviveiros[36], F. A. Di Bello[73a,73b], A. Di Ciaccio[74a,74b], L. Di Ciaccio[5], C. Di Donato[70a,70b], A. Di Girolamo[36], G. Di Gregorio[72a,72b], A. Di Luca[76a,76b], B. Di Micco[75a,75b], R. Di Nardo[75a,75b], K. F. Di Petrillo[59], R. Di Sipio[167], C. Diaconu[102], F. A. Dias[120], T. Dias Do Vale[139a], M. A. Diaz[146a], F. G. Diaz Capriles[24], J. Dickinson[18], M. Didenko[166],

E. B. Diehl[106], J. Dietrich[19], S. Díez Cornell[46], C. Diez Pardos[151], A. Dimitrievska[18], W. Ding[15b], J. Dingfelder[24], S. J. Dittmeier[61b], F. Dittus[36], F. Djama[102], T. Djobava[159b], J. I. Djuvsland[17], M. A. B. Do Vale[147], M. Dobre[27b], D. Dodsworth[26], C. Doglioni[97], J. Dolejsi[142], Z. Dolezal[142], M. Donadelli[81c], B. Dong[60c], J. Donini[38], A. D'onofrio[15c], M. D'Onofrio[91], J. Dopke[143], A. Doria[70a], M. T. Dova[89], A. T. Doyle[57], E. Drechsler[152], E. Dreyer[152], T. Dreyer[53], A. S. Drobac[170], D. Du[60b], T. A. du Pree[120], Y. Duan[60d], F. Dubinin[111], M. Dubovsky[28a], A. Dubreuil[54], E. Duchovni[180], G. Duckeck[114], O. A. Ducu[36], D. Duda[115], A. Dudarev[36], A. C. Dudder[100], E. M. Duffield[18], M. D'uffizi[101], L. Duflot[65], M. Dührssen[36], C. Dülsen[182], M. Dumancic[180], A. E. Dumitriu[27b], M. Dunford[61a], S. Dungs[47], A. Duperrin[102], H. Duran Yildiz[4a], M. Düren[56], A. Durglishvili[159b], D. Duschinger[48], B. Dutta[46], D. Duvnjak[1], G. I. Dyckes[136], M. Dyndal[36], S. Dysch[101], B. S. Dziedzic[85], M. G. Eggleston[49], T. Eifert[8], G. Eigen[17], K. Einsweiler[18], T. Ekelof[172], H. El Jarrari[35e], V. Ellajosyula[172], M. Ellert[172], F. Ellinghaus[182], A. A. Elliot[93], N. Ellis[36], J. Elmsheuser[29], M. Elsing[36], D. Emeliyanov[143], A. Emerman[39], Y. Enari[163], M. B. Epland[49], J. Erdmann[47], A. Ereditato[20], P. A. Erland[85], M. Errenst[182], M. Escalier[65], C. Escobar[174], O. Estrada Pastor[174], E. Etzion[161], G. E. Evans[139a], H. Evans[66], M. O. Evans[156], A. Ezhilov[137], F. Fabbri[57], L. Fabbri[23a,23b], V. Fabiani[119], G. Facini[178], R. M. Fakhrutdinov[123], S. Falciano[73a], P. J. Falke[24], S. Falke[36], J. Faltova[142], Y. Fang[15a], Y. Fang[15a], G. Fanourakis[44], M. Fanti[69a,69b], M. Faraj[67a,67c], A. Farbin[8], A. Farilla[75a], E. M. Farina[71a,71b], T. Farooque[107], S. M. Farrington[50], P. Farthouat[36], F. Fassi[35e], P. Fassnacht[36], D. Fassouliotis[9], M. Faucci Giannelli[50], W. J. Fawcett[32], L. Fayard[65], O. L. Fedin[137,p], W. Fedorko[175], A. Fehr[20], M. Feickert[173], L. Feligioni[102], A. Fell[149], C. Feng[60b], M. Feng[49], M. J. Fenton[171], A. B. Fenyuk[123], S. W. Ferguson[43], J. Ferrando[46], A. Ferrari[172], P. Ferrari[120], R. Ferrari[71a], D. E. Ferreira de Lima[61b], A. Ferrer[174], D. Ferrere[54], C. Ferretti[106], F. Fiedler[100], A. Filipčič[92], F. Filthaut[119], K. D. Finelli[25], M. C. N. Fiolhais[139a,139c,a], L. Fiorini[174], F. Fischer[114], J. Fischer[100], W. C. Fisher[107], T. Fitschen[21], I. Fleck[151], P. Fleischmann[106], T. Flick[182], B. M. Flierl[114], L. Flores[136], L. R. Flores Castillo[63a], F. M. Follega[76a,76b], N. Fomin[17], J. H. Foo[167], G. T. Forcolin[76a,76b], B. C. Forland[66], A. Formica[144], F. A. Förster[14], A. C. Forti[101], E. Fortin[102], M. G. Foti[134], D. Fournier[65], H. Fox[90], P. Francavilla[72a,72b], S. Francescato[73a,73b], M. Franchini[23a,23b], S. Franchino[61a], D. Francis[36], L. Franco[5], L. Franconi[20], M. Franklin[59], G. Frattari[73a,73b], A. N. Fray[93], P. M. Freeman[21], B. Freund[110], W. S. Freund[81b], E. M. Freundlich[47], D. C. Frizzell[128], D. Froidevaux[36], J. A. Frost[134], M. Fujimoto[126], C. Fukunaga[164], E. Fullana Torregrosa[174], T. Fusayasu[116], J. Fuster[174], A. Gabrielli[23a,23b], A. Gabrielli[36], S. Gadatsch[54], P. Gadow[115], G. Gagliardi[55a,55b], L. G. Gagnon[110], G. E. Gallardo[134], E. J. Gallas[134], B. J. Gallop[143], R. Gamboa Goni[93], K. K. Gan[127], S. Ganguly[180], J. Gao[60a], Y. Gao[50], Y. S. Gao[31,m], F. M. Garay Walls[146a], C. García[174], J. E. García Navarro[174], J. A. García Pascual[15a], C. Garcia-Argos[52], M. Garcia-Sciveres[18], R. W. Gardner[37], N. Garelli[153], S. Gargiulo[52], C. A. Garner[167], V. Garonne[133], S. J. Gasiorowski[148], P. Gaspar[81b], A. Gaudiello[55a,55b], G. Gaudio[71a], P. Gauzzi[73a,73b], I. L. Gavrilenko[111], A. Gavrilyuk[124], C. Gay[175], G. Gaycken[46], E. N. Gazis[10], A. A. Geanta[27b], C. M. Gee[145], C. N. P. Gee[143], J. Geisen[97], M. Geisen[100], C. Gemme[55b], M. H. Genest[58], C. Geng[106], S. Gentile[73a,73b], S. George[94], T. Geralis[44], L. O. Gerlach[53], P. Gessinger-Befurt[100], G. Gessner[47], M. Ghasemi Bostanabad[176], M. Ghneimat[151], A. Ghosh[65], A. Ghosh[78], B. Giacobbe[23b], S. Giagu[73a,73b], N. Giangiacomi[167], P. Giannetti[72a], A. Giannini[70a,70b], G. Giannini[14], S. M. Gibson[94], M. Gignac[145], D. T. Gil[84b], B. J. Gilbert[39], D. Gillberg[34], G. Gilles[182], N. E. K. Gillwald[46], D. M. Gingrich[3,aj], M. P. Giordani[67a,67c], P. F. Giraud[144], G. Giugliarelli[67a,67c], D. Giugni[69a], F. Giuli[74a,74b], S. Gkaitatzis[162], I. Gkialas[9,h], E. L. Gkougkousis[14], P. Gkountoumis[10], L. K. Gladilin[113], C. Glasman[99], J. Glatzer[14], P. C. F. Glaysher[46], A. Glazov[46], G. R. Gledhill[131], I. Gnesi[41b,c], M. Goblirsch-Kolb[26], D. Godin[110], S. Goldfarb[105], T. Golling[54], D. Golubkov[123], A. Gomes[139a,139b], R. Goncalves Gama[53], R. Gonçalo[139a,139c], G. Gonella[131], L. Gonella[21], A. Gongadze[80], F. Gonnella[21], J. L. Gonski[39], S. González de la Hoz[174], S. Gonzalez Fernandez[14], R. Gonzalez Lopez[91], C. Gonzalez Renteria[18], R. Gonzalez Suarez[172], S. Gonzalez-Sevilla[54], G. R. Gonzalvo Rodriguez[174], L. Goossens[36], N. A. Gorasia[21], P. A. Gorbounov[124], H. A. Gordon[29], B. Gorini[36], E. Gorini[68a,68b], A. Gorišek[92], A. T. Goshaw[49], M. I. Gostkin[80], C. A. Gottardo[119], M. Gouighri[35b], A. G. Goussiou[148], N. Govender[33c], C. Goy[5], I. Grabowska-Bold[84a], E. C. Graham[91], J. Gramling[171], E. Gramstad[133], S. Grancagnolo[19], M. Grandi[156], V. Gratchev[137], P. M. Gravila[27f], F. G. Gravili[68a,68b], C. Gray[57], H. M. Gray[18], C. Grefe[24], K. Gregersen[97], I. M. Gregor[46], P. Grenier[153], K. Grevtsov[46], C. Grieco[14], N. A. Grieser[128], A. A. Grillo[145], K. Grimm[31,l], S. Grinstein[14,w], J.-F. Grivaz[65], S. Groh[100], E. Gross[180], J. Grosse-Knetter[53], Z. J. Grout[95], C. Grud[106],

A. Grummer[118], J. C. Grundy[134], L. Guan[106], W. Guan[181], C. Gubbels[175], J. Guenther[77], A. Guerguichon[65], J. G. R. Guerrero Rojas[174], F. Guescini[115], D. Guest[77], R. Gugel[100], A. Guida[46], T. Guillemin[5], S. Guindon[36], J. Guo[60c], W. Guo[106], Y. Guo[60a], Z. Guo[102], R. Gupta[46], S. Gurbuz[12c], G. Gustavino[128], M. Guth[52], P. Gutierrez[128], C. Gutschow[95], C. Guyot[144], C. Gwenlan[134], C. B. Gwilliam[91], E. S. Haaland[133], A. Haas[125], C. Haber[18], H. K. Hadavand[8], A. Hadef[100], M. Haleem[177], J. Haley[129], J. J. Hall[149], G. Halladjian[107], G. D. Hallewell[102], K. Hamano[176], H. Hamdaoui[35e], M. Hamer[24], G. N. Hamity[50], K. Han[60a], L. Han[15c], L. Han[60a], S. Han[18], Y. F. Han[167], K. Hanagaki[82,u], M. Hance[145], D. M. Handl[114], M. D. Hank[37], R. Hankache[135], E. Hansen[97], J. B. Hansen[40], J. D. Hansen[40], M. C. Hansen[24], P. H. Hansen[40], E. C. Hanson[101], K. Hara[169], T. Harenberg[182], S. Harkusha[108], P. F. Harrison[178], N. M. Hartman[153], N. M. Hartmann[114], Y. Hasegawa[150], A. Hasib[50], S. Hassani[144], S. Haug[20], R. Hauser[107], M. Havranek[141], C. M. Hawkes[21], R. J. Hawkings[36], S. Hayashida[117], D. Hayden[107], C. Hayes[106], R. L. Hayes[175], C. P. Hays[134], J. M. Hays[93], H. S. Hayward[91], S. J. Haywood[143], F. He[60a], Y. He[165], M. P. Heath[50], V. Hedberg[97], A. L. Heggelund[133], N. D. Hehir[93], C. Heidegger[52], K. K. Heidegger[52], W. D. Heidorn[79], J. Heilman[34], S. Heim[46], T. Heim[18], B. Heinemann[46,ah], J. G. Heinlein[136], J. J. Heinrich[131], L. Heinrich[36], J. Hejbal[140], L. Helary[46], A. Held[125], S. Hellesund[133], C. M. Helling[145], S. Hellman[45a,45b], C. Helsens[36], R. C. W. Henderson[90], L. Henkelmann[32], A. M. Henriques Correia[36], H. Herde[26], Y. Hernández Jiménez[33e], H. Herr[100], M. G. Herrmann[114], T. Herrmann[48], G. Herten[52], R. Hertenberger[114], L. Hervas[36], G. G. Hesketh[95], N. P. Hessey[168a], H. Hibi[83], S. Higashino[82], E. Higón-Rodriguez[174], K. Hildebrand[37], J. C. Hill[32], K. K. Hill[29], K. H. Hiller[46], S. J. Hillier[21], M. Hils[48], I. Hinchliffe[18], F. Hinterkeuser[24], M. Hirose[132], S. Hirose[169], D. Hirschbuehl[182], B. Hiti[92], O. Hladik[140], J. Hobbs[155], R. Hobincu[27e], N. Hod[180], M. C. Hodgkinson[149], A. Hoecker[36], D. Hohn[52], D. Hohov[65], T. Holm[24], T. R. Holmes[37], M. Holzbock[115], L. B. A. H. Hommels[32], T. M. Hong[138], J. C. Honig[52], A. Hönle[115], B. H. Hooberman[173], W. H. Hopkins[6], Y. Horii[117], P. Horn[48], L. A. Horyn[37], S. Hou[158], A. Hoummada[35a], J. Howarth[57], J. Hoya[89], M. Hrabovsky[130], J. Hrivnac[65], A. Hrynevich[109], T. Hryn'ova[5], P. J. Hsu[64], S.-C. Hsu[148], Q. Hu[39], S. Hu[60c], Y. F. Hu[15a,15d,al], D. P. Huang[95], X. Huang[15c], Y. Huang[60a], Y. Huang[15a], Z. Hubacek[141], F. Hubaut[102], M. Huebner[24], F. Huegging[24], T. B. Huffman[134], M. Huhtinen[36], R. Hulsken[58], R. F. H. Hunter[34], N. Huseynov[80,ab], J. Huston[107], J. Huth[59], R. Hyneman[153], S. Hyrych[28a], G. Iacobucci[54], G. Iakovidis[29], I. Ibragimov[151], L. Iconomidou-Fayard[65], P. Iengo[36], R. Ignazzi[40], R. Iguchi[163], T. Iizawa[54], Y. Ikegami[82], M. Ikeno[82], N. Ilic[119,167,aa], F. Iltzsche[48], H. Imam[35a], G. Introzzi[71a,71b], M. Iodice[75a], K. Iordanidou[168a], V. Ippolito[73a,73b], M. F. Isacson[172], M. Ishino[163], W. Islam[129], C. Issever[19,46], S. Istin[160], J. M. Iturbe Ponce[63a], R. Iuppa[76a,76b], A. Ivina[180], J. M. Izen[43], V. Izzo[70a], P. Jacka[140], P. Jackson[1], R. M. Jacobs[46], B. P. Jaeger[152], V. Jain[2], G. Jäkel[182], K. B. Jakobi[100], K. Jakobs[52], T. Jakoubek[180], J. Jamieson[57], K. W. Janas[84a], R. Jansky[54], M. Janus[53], P. A. Janus[84a], G. Jarlskog[97], A. E. Jaspan[91], N. Javadov[80,ab], T. Javůrek[36], M. Javurkova[103], F. Jeanneau[144], L. Jeanty[131], J. Jejelava[159a], P. Jenni[52,d], N. Jeong[46], S. Jézéquel[5], J. Jia[155], Z. Jia[15c], H. Jiang[79], Y. Jiang[60a], Z. Jiang[153], S. Jiggins[52], F. A. Jimenez Morales[38], J. Jimenez Pena[115], S. Jin[15c], A. Jinaru[27b], O. Jinnouchi[165], H. Jivan[33e], P. Johansson[149], K. A. Johns[7], C. A. Johnson[66], E. Jones[178], R. W. L. Jones[90], S. D. Jones[156], T. J. Jones[91], J. Jovicevic[36], X. Ju[18], J. J. Junggeburth[115], A. Juste Rozas[14,w], A. Kaczmarska[85], M. Kado[73a,73b], H. Kagan[127], M. Kagan[153], A. Kahn[39], C. Kahra[100], T. Kaji[179], E. Kajomovitz[160], C. W. Kalderon[29], A. Kaluza[100], A. Kamenshchikov[123], M. Kaneda[163], N. J. Kang[145], S. Kang[79], Y. Kano[117], J. Kanzaki[82], L. S. Kaplan[181], D. Kar[33e], K. Karava[134], M. J. Kareem[168b], I. Karkanias[162], S. N. Karpov[80], Z. M. Karpova[80], V. Kartvelishvili[90], A. N. Karyukhin[123], E. Kasimi[162], A. Kastanas[45a,45b], C. Kato[60d], J. Katzy[46], K. Kawade[150], K. Kawagoe[88], T. Kawaguchi[117], T. Kawamoto[144], G. Kawamura[53], E. F. Kay[176], F. I. Kaya[170], S. Kazakos[14], V. F. Kazanin[122a,122b], J. M. Keaveney[33a], R. Keeler[176], J. S. Keller[34], E. Kellermann[97], D. Kelsey[156], J. J. Kempster[21], J. Kendrick[21], K. E. Kennedy[39], O. Kepka[140], S. Kersten[182], B. P. Kerševan[92], S. Ketabchi Haghighat[167], F. Khalil-Zada[13], M. Khandoga[144], A. Khanov[129], A. G. Kharlamov[122a,122b], T. Kharlamova[122a,122b], E. E. Khoda[175], T. J. Khoo[77], G. Khoriauli[177], E. Khramov[80], J. Khubua[159b], S. Kido[83], M. Kiehn[36], E. Kim[165], Y. K. Kim[37], N. Kimura[95], A. Kirchhoff[53], D. Kirchmeier[48], J. Kirk[143], A. E. Kiryunin[115], T. Kishimoto[163], D. P. Kisliuk[167], V. Kitali[46], C. Kitsaki[10], O. Kivernyk[24], T. Klapdor-Kleingrothaus[52], M. Klassen[61a], C. Klein[34], M. H. Klein[106], M. Klein[91], U. Klein[91], K. Kleinknecht[100], P. Klimek[36], A. Klimentov[29], F. Klimpel[36], T. Klingl[24], T. Klioutchnikova[36], F. F. Klitzner[114], P. Kluit[120], S. Kluth[115], E. Kneringer[77], E. B. F. G. Knoops[102], A. Knue[52], D. Kobayashi[88], M. Kobel[48], M. Kocian[153], T. Kodama[163], P. Kodys[142], D. M. Koeck[156],

P. T. Koenig[24], T. Koffas[34], N. M. Köhler[36], M. Kolb[144], I. Koletsou[5], T. Komarek[130], T. Kondo[82], K. Köneke[52], A. X. Y. Kong[1], A. C. König[119], T. Kono[126], V. Konstantinides[95], N. Konstantinidis[95], B. Konya[97], R. Kopeliansky[66], S. Koperny[84a], K. Korcyl[85], K. Kordas[162], G. Koren[161], A. Korn[95], I. Korolkov[14], E. V. Korolkova[149], N. Korotkova[113], O. Kortner[115], S. Kortner[115], V. V. Kostyukhin[149,166], A. Kotsokechagia[65], A. Kotwal[49], A. Koulouris[10], A. Kourkoumeli-Charalampidi[71a,71b], C. Kourkoumelis[9], E. Kourlitis[6], V. Kouskoura[29], R. Kowalewski[176], W. Kozanecki[101], A. S. Kozhin[123], V. A. Kramarenko[113], G. Kramberger[92], D. Krasnopevtsev[60a], M. W. Krasny[135], A. Krasznahorkay[36], D. Krauss[115], J. A. Kremer[100], J. Kretzschmar[91], K. Kreul[19], P. Krieger[167], F. Krieter[114], S. Krishnamurthy[103], A. Krishnan[61b], M. Krivos[142], K. Krizka[18], K. Kroeninger[47], H. Kroha[115], J. Kroll[140], J. Kroll[136], K. S. Krowpman[107], U. Kruchonak[80], H. Krüger[24], N. Krumnack[79], M. C. Kruse[49], J. A. Krzysiak[85], A. Kubota[165], O. Kuchinskaia[166], S. Kuday[4b], D. Kuechler[46], J. T. Kuechler[46], S. Kuehn[36], T. Kuhl[46], V. Kukhtin[80], Y. Kulchitsky[108,ad], S. Kuleshov[146b], Y. P. Kulinich[173], M. Kuna[58], A. Kupco[140], T. Kupfer[47], O. Kuprash[52], H. Kurashige[83], L. L. Kurchaninov[168a], Y. A. Kurochkin[108], A. Kurova[112], M. G. Kurth[15a,15d], E. S. Kuwertz[36], M. Kuze[165], A. K. Kvam[148], J. Kvita[130], T. Kwan[104], C. Lacasta[174], F. Lacava[73a,73b], D. P. J. Lack[101], H. Lacker[19], D. Lacour[135], E. Ladygin[80], R. Lafaye[5], B. Laforge[135], T. Lagouri[146c], S. Lai[53], I. K. Lakomiec[84a], J. E. Lambert[128], S. Lammers[66], W. Lampl[7], C. Lampoudis[162], E. Lançon[29], U. Landgraf[52], M. P. J. Landon[93], V. S. Lang[52], J. C. Lange[53], R. J. Langenberg[103], A. J. Lankford[171], F. Lanni[29], K. Lantzsch[24], A. Lanza[71a], A. Lapertosa[55a,55b], J. F. Laporte[144], T. Lari[69a], F. Lasagni Manghi[23a,23b], M. Lassnig[36], V. Latonova[140], T. S. Lau[63a], A. Laudrain[100], A. Laurier[34], M. Lavorgna[70a,70b], S. D. Lawlor[94], M. Lazzaroni[69a,69b], B. Le[101], E. Le Guirriec[102], A. Lebedev[79], M. LeBlanc[7], T. LeCompte[6], F. Ledroit-Guillon[58], A. C. A. Lee[95], C. A. Lee[29], G. R. Lee[17], L. Lee[59], S. C. Lee[158], S. Lee[79], B. Lefebvre[168a], H. P. Lefebvre[94], M. Lefebvre[176], C. Leggett[18], K. Lehmann[152], N. Lehmann[20], G. Lehmann Miotto[36], W. A. Leight[46], A. Leisos[162,v], M. A. L. Leite[81c], C. E. Leitgeb[114], R. Leitner[142], K. J. C. Leney[42], T. Lenz[24], S. Leone[72a], C. Leonidopoulos[50], A. Leopold[135], C. Leroy[110], R. Les[107], C. G. Lester[32], M. Levchenko[137], J. Levêque[5], D. Levin[106], L. J. Levinson[180], D. J. Lewis[21], B. Li[15b], B. Li[106], C-Q. Li[60c,60d], F. Li[60c], H. Li[60a], H. Li[60b], J. Li[60c], K. Li[148], L. Li[60c], M. Li[15a,15d], Q. Y. Li[60a], S. Li[60d,60c,b], X. Li[46], Y. Li[46], Z. Li[60b], Z. Li[134], Z. Li[104], Z. Li[91], Z. Liang[15a], M. Liberatore[46], B. Liberti[74a], K. Lie[63c], S. Lim[29], C. Y. Lin[32], K. Lin[107], R. A. Linck[66], R. E. Lindley[7], J. H. Lindon[21], A. Linss[46], A. L. Lionti[54], E. Lipeles[136], A. Lipniacka[17], T. M. Liss[173,ai], A. Lister[175], J. D. Little[8], B. Liu[79], B. X. Liu[152], H. B. Liu[29], J. B. Liu[60a], J. K. K. Liu[37], K. Liu[60d], M. Liu[60a], M. Y. Liu[60a], P. Liu[15a], X. Liu[60a], Y. Liu[46], Y. Liu[15a,15d], Y. L. Liu[106], Y. W. Liu[60a], M. Livan[71a,71b], A. Lleres[58], J. Llorente Merino[152], S. L. Lloyd[93], C. Y. Lo[63b], E. M. Lobodzinska[46], P. Loch[7], S. Loffredo[74a,74b], T. Lohse[19], K. Lohwasser[149], M. Lokajicek[140], J. D. Long[173], R. E. Long[90], I. Longarini[73a,73b], L. Longo[36], I. Lopez Paz[101], A. Lopez Solis[149], J. Lorenz[114], N. Lorenzo Martinez[5], A. M. Lory[114], A. Lösle[52], X. Lou[45a,45b], X. Lou[15a], A. Lounis[65], J. Love[6], P. A. Love[90], J. J. Lozano Bahilo[174], M. Lu[60a], Y. J. Lu[64], H. J. Lubatti[148], C. Luci[73a,73b], F. L. Lucio Alves[15c], A. Lucotte[58], F. Luehring[66], I. Luise[155], L. Luminari[73a], B. Lund-Jensen[154], N. A. Luongo[131], M. S. Lutz[161], D. Lynn[29], H. Lyons[91], R. Lysak[140], E. Lytken[97], F. Lyu[15a], V. Lyubushkin[80], T. Lyubushkina[80], H. Ma[29], L. L. Ma[60b], Y. Ma[95], D. M. Mac Donell[176], G. Maccarrone[51], C. M. Macdonald[149], J. C. MacDonald[149], J. Machado Miguens[136], R. Madar[38], W. F. Mader[48], M. Madugoda Ralalage Don[129], N. Madysa[48], J. Maeda[83], T. Maeno[29], M. Maerker[48], V. Magerl[52], N. Magini[79], J. Magro[67a,67c,r], D. J. Mahon[39], C. Maidantchik[81b], A. Maio[139a,139b,139d], K. Maj[84a], O. Majersky[28a], S. Majewski[131], Y. Makida[82], N. Makovec[65], B. Malaescu[135], Pa. Malecki[85], V. P. Maleev[137], F. Malek[58], D. Malito[41a,41b], U. Mallik[78], C. Malone[32], S. Maltezos[10], S. Malyukov[80], J. Mamuzic[174], G. Mancini[51], J. P. Mandalia[93], I. Mandić[92], L. Manhaes de Andrade Filho[81a], I. M. Maniatis[162], J. Manjarres Ramos[48], K. H. Mankinen[97], A. Mann[114], A. Manousos[77], B. Mansoulie[144], I. Manthos[162], S. Manzoni[120], A. Marantis[162], G. Marceca[30], L. Marchese[134], G. Marchiori[135], M. Marcisovsky[140], L. Marcoccia[74a,74b], C. Marcon[97], M. Marjanovic[128], Z. Marshall[18], M. U. F. Martensson[172], S. Marti-Garcia[174], C. B. Martin[127], T. A. Martin[178], V. J. Martin[50], B. Martin dit Latour[17], L. Martinelli[75a,75b], M. Martinez[14,w], P. Martinez Agullo[174], V. I. Martinez Outschoorn[103], S. Martin-Haugh[143], V. S. Martoiu[27b], A. C. Martyniuk[95], A. Marzin[36], S. R. Maschek[115], L. Masetti[100], T. Mashimo[163], R. Mashinistov[111], J. Masik[101], A. L. Maslennikov[122a,122b], L. Massa[23a,23b], P. Massarotti[70a,70b], P. Mastrandrea[72a,72b], A. Mastroberardino[41a,41b], T. Masubuchi[163], D. Matakias[29], A. Matic[114], N. Matsuzawa[163], P. Mättig[24], J. Maurer[27b], B. Maček[92], D. A. Maximov[122a,122b],

R. Mazini[158], I. Maznas[162], S. M. Mazza[145], J. P. Mc Gowan[104], S. P. Mc Kee[106], T. G. McCarthy[115], W. P. McCormack[18], E. F. McDonald[105], A. E. McDougall[120], J. A. Mcfayden[18], G. Mchedlidze[159b], M. A. McKay[42], K. D. McLean[176], S. J. McMahon[143], P. C. McNamara[105], C. J. McNicol[178], R. A. McPherson[176,aa], J. E. Mdhluli[33e], Z. A. Meadows[103], S. Meehan[36], T. Megy[38], S. Mehlhase[114], A. Mehta[91], B. Meirose[43], D. Melini[160], B. R. Mellado Garcia[33e], J. D. Mellenthin[53], M. Melo[28a], F. Meloni[46], A. Melzer[24], E. D. Mendes Gouveia[139a,139e], A. M. Mendes Jacques Da Costa[21], H. Y. Meng[167], L. Meng[36], X. T. Meng[106], S. Menke[115], E. Meoni[41a,41b], S. Mergelmeyer[19], S. A. M. Merkt[138], C. Merlassino[134], P. Mermod[54], L. Merola[70a,70b], C. Meroni[69a], G. Merz[106], O. Meshkov[113,111], J. K. R. Meshreki[151], J. Metcalfe[6], A. S. Mete[6], C. Meyer[66], J-P. Meyer[144], M. Michetti[19], R. P. Middleton[143], L. Mijović[50], G. Mikenberg[180], M. Mikestikova[140], M. Mikuž[92], H. Mildner[149], A. Milic[167], C. D. Milke[42], D. W. Miller[37], L. S. Miller[34], A. Milov[180], D. A. Milstead[45a,45b], A. A. Minaenko[123], I. A. Minashvili[159b], L. Mince[57], A. I. Mincer[125], B. Mindur[84a], M. Mineev[80], Y. Minegishi[163], Y. Mino[86], L. M. Mir[14], M. Mironova[134], T. Mitani[179], J. Mitrevski[114], V. A. Mitsou[174], M. Mittal[60c], O. Miu[167], A. Miucci[20], P. S. Miyagawa[93], A. Mizukami[82], J. U. Mjörnmark[97], T. Mkrtchyan[61a], M. Mlynarikova[121], T. Moa[45a,45b], S. Mobius[53], K. Mochizuki[110], P. Moder[46], P. Mogg[114], S. Mohapatra[39], R. Moles-Valls[24], K. Mönig[46], E. Monnier[102], A. Montalbano[152], J. Montejo Berlingen[36], M. Montella[95], F. Monticelli[89], S. Monzani[69a], N. Morange[65], A. L. Moreira De Carvalho[139a], D. Moreno[22a], M. Moreno Llácer[174], C. Moreno Martinez[14], P. Morettini[55b], M. Morgenstern[160], S. Morgenstern[48], D. Mori[152], M. Morii[59], M. Morinaga[179], V. Morisbak[133], A. K. Morley[36], G. Mornacchi[36], A. P. Morris[95], L. Morvaj[36], P. Moschovakos[36], B. Moser[120], M. Mosidze[159b], T. Moskalets[144], P. Moskvitina[119], J. Moss[31,n], E. J. W. Moyse[103], S. Muanza[102], J. Mueller[138], R. S. P. Mueller[114], D. Muenstermann[90], G. A. Mullier[97], D. P. Mungo[69a,69b], J. L. Munoz Martinez[14], F. J. Munoz Sanchez[101], P. Murin[28b], W. J. Murray[178,143], A. Murrone[69a,69b], J. M. Muse[128], M. Muškinja[18], C. Mwewa[33a], A. G. Myagkov[123,ae], A. A. Myers[138], G. Myers[66], J. Myers[131], M. Myska[141], B. P. Nachman[18], O. Nackenhorst[47], A.Nag Nag[48], K. Nagai[134], K. Nagano[82], Y. Nagasaka[62], J. L. Nagle[29], E. Nagy[102], A. M. Nairz[36], Y. Nakahama[117], K. Nakamura[82], T. Nakamura[163], H. Nanjo[132], F. Napolitano[61a], R. F. Naranjo Garcia[46], R. Narayan[42], I. Naryshkin[137], M. Naseri[34], T. Naumann[46], G. Navarro[22a], P. Y. Nechaeva[111], F. Nechansky[46], T. J. Neep[21], A. Negri[71a,71b], M. Negrini[23b], C. Nellist[119], C. Nelson[104], M. E. Nelson[45a,45b], S. Nemecek[140], M. Nessi[36,f], M. S. Neubauer[173], F. Neuhaus[100], M. Neumann[182], R. Newhouse[175], P. R. Newman[21], C. W. Ng[138], Y. S. Ng[19], Y. W. Y. Ng[171], B. Ngair[35e], H. D. N. Nguyen[102], T. Nguyen Manh[110], E. Nibigira[38], R. B. Nickerson[134], R. Nicolaidou[144], D. S. Nielsen[40], J. Nielsen[145], M. Niemeyer[53], N. Nikiforou[11], V. Nikolaenko[123,ae], I. Nikolic-Audit[135], K. Nikolopoulos[21], P. Nilsson[29], H. R. Nindhito[54], A. Nisati[73a], N. Nishu[60c], R. Nisius[115], I. Nitsche[47], T. Nitta[179], T. Nobe[163], D. L. Noel[32], Y. Noguchi[86], I. Nomidis[135], M. A. Nomura[29], M. Nordberg[36], J. Novak[92], T. Novak[92], O. Novgorodova[48], R. Novotny[118], L. Nozka[130], K. Ntekas[171], E. Nurse[95], F. G. Oakham[34,aj], J. Ocariz[135], A. Ochi[83], I. Ochoa[139a], J. P. Ochoa-Ricoux[146a], K. O'Connor[26], S. Oda[88], S. Odaka[82], S. Oerdek[53], A. Ogrodnik[84a], A. Oh[101], C. C. Ohm[154], H. Oide[165], R. Oishi[163], M. L. Ojeda[167], H. Okawa[169], Y. Okazaki[86], M. W. O'Keefe[91], Y. Okumura[163], A. Olariu[27b], L. F. Oleiro Seabra[139a], S. A. Olivares Pino[146a], D. Oliveira Damazio[29], J. L. Oliver[1], M. J. R. Olsson[171], A. Olszewski[85], J. Olszowska[85], Ö.O. Öncel[24], D. C. O'Neil[152], A. P. O'neill[134], A. Onofre[139a,139e], P. U. E. Onyisi[11], H. Oppen[133], R. G. Oreamuno Madriz[121], M. J. Oreglia[37], G. E. Orellana[89], D. Orestano[75a,75b], N. Orlando[14], R. S. Orr[167], V. O'Shea[57], R. Ospanov[60a], G. Otero y Garzon[30], H. Otono[88], P. S. Ott[61a], G. J. Ottino[18], M. Ouchrif[35d], J. Ouellette[29], F. Ould-Saada[133], A. Ouraou[144,*], Q. Ouyang[15a], M. Owen[57], R. E. Owen[143], V. E. Ozcan[12c], N. Ozturk[8], J. Pacalt[130], H. A. Pacey[32], K. Pachal[49], A. Pacheco Pages[14], C. Padilla Aranda[14], S. Pagan Griso[18], G. Palacino[66], S. Palazzo[50], S. Palestini[36], M. Palka[84b], P. Palni[84a], C. E. Pandini[54], J. G. Panduro Vazquez[94], P. Pani[46], G. Panizzo[67a,67c], L. Paolozzi[54], C. Papadatos[110], K. Papageorgiou[9,h], S. Parajuli[42], A. Paramonov[6], C. Paraskevopoulos[10], D. Paredes Hernandez[63b], S. R. Paredes Saenz[134], B. Parida[180], T. H. Park[167], A. J. Parker[31], M. A. Parker[32], F. Parodi[55a,55b], E. W. Parrish[121], J. A. Parsons[39], U. Parzefall[52], L. Pascual Dominguez[135], V. R. Pascuzzi[18], J. M. P. Pasner[145], F. Pasquali[120], E. Pasqualucci[73a], S. Passaggio[55b], F. Pastore[94], P. Pasuwan[45a,45b], S. Pataraia[100], J. R. Pater[101], A. Pathak[181,j], J. Patton[91], T. Pauly[36], J. Pearkes[153], M. Pedersen[133], L. Pedraza Diaz[119], R. Pedro[139a], T. Peiffer[53], S. V. Peleganchuk[122a,122b], O. Penc[140], C. Peng[63b], H. Peng[60a], B. S. Peralva[81a], M. M. Perego[65], A. P. Pereira Peixoto[139a], L. Pereira Sanchez[45a,45b], D. V. Perepelitsa[29], E. Perez Codina[168a], L. Perini[69a,69b], H. Pernegger[36], S. Perrella[36], A. Perrevoort[120], K. Peters[46],

R. F. Y. Peters[101], B. A. Petersen[36], T. C. Petersen[40], E. Petit[102], V. Petousis[141], C. Petridou[162], F. Petrucci[75a,75b], M. Pettee[183], N. E. Pettersson[103], K. Petukhova[142], A. Peyaud[144], R. Pezoa[146d], L. Pezzotti[71a,71b], T. Pham[105], P. W. Phillips[143], M. W. Phipps[173], G. Piacquadio[155], E. Pianori[18], A. Picazio[103], R. H. Pickles[101], R. Piegaia[30], D. Pietreanu[27b], J. E. Pilcher[37], A. D. Pilkington[101], M. Pinamonti[67a,67c], J. L. Pinfold[3], C. Pitman Donaldson[95], M. Pitt[161], L. Pizzimento[74a,74b], A. Pizzini[120], M.-A. Pleier[29], V. Plesanovs[52], V. Pleskot[142], E. Plotnikova[80], P. Podberezko[122a,122b], R. Poettgen[97], R. Poggi[54], L. Poggioli[135], I. Pogrebnyak[107], D. Pohl[24], I. Pokharel[53], G. Polesello[71a], A. Poley[152,168a], A. Policicchio[73a,73b], R. Polifka[142], A. Polini[23b], C. S. Pollard[46], V. Polychronakos[29], D. Ponomarenko[112], L. Pontecorvo[36], S. Popa[27a], G. A. Popeneciu[27d], L. Portales[5], D. M. Portillo Quintero[58], S. Pospisil[141], K. Potamianos[46], I. N. Potrap[80], C. J. Potter[32], H. Potti[11], T. Poulsen[97], J. Poveda[174], T. D. Powell[149], G. Pownall[46], M. E. Pozo Astigarraga[36], A. Prades Ibanez[174], P. Pralavorio[102], M. M. Prapa[44], S. Prell[79], D. Price[101], M. Primavera[68a], M. L. Proffitt[148], N. Proklova[112], K. Prokofiev[63c], F. Prokoshin[80], S. Protopopescu[29], J. Proudfoot[6], M. Przybycien[84a], D. Pudzha[137], A. Puri[173], P. Puzo[65], D. Pyatiizbyantseva[112], J. Qian[106], Y. Qin[101], A. Quadt[53], M. Queitsch-Maitland[36], G. Rabanal Bolanos[59], M. Racko[28a], F. Ragusa[69a,69b], G. Rahal[98], J. A. Raine[54], S. Rajagopalan[29], A. Ramirez Morales[93], K. Ran[15a,15d], D. F. Rassloff[61a], D. M. Rauch[46], F. Rauscher[114], S. Rave[100], B. Ravina[57], I. Ravinovich[180], J. H. Rawling[101], M. Raymond[36], A. L. Read[133], N. P. Readioff[149], M. Reale[68a,68b], D. M. Rebuzzi[71a,71b], G. Redlinger[29], K. Reeves[43], D. Reikher[161], A. Reiss[100], A. Rej[151], C. Rembser[36], A. Renardi[46], M. Renda[27b], M. B. Rendel[115], A. G. Rennie[57], S. Resconi[69a], E. D. Resseguie[18], S. Rettie[95], B. Reynolds[127], E. Reynolds[21], O. L. Rezanova[122a,122b], P. Reznicek[142], E. Ricci[76a,76b], R. Richter[115], S. Richter[46], E. Richter-Was[84b], M. Ridel[135], P. Rieck[115], O. Rifki[46], M. Rijssenbeek[155], A. Rimoldi[71a,71b], M. Rimoldi[46], L. Rinaldi[23b], T. T. Rinn[173], G. Ripellino[154], I. Riu[14], P. Rivadeneira[46], J. C. Rivera Vergara[176], F. Rizatdinova[129], E. Rizvi[93], C. Rizzi[36], S. H. Robertson[104,aa], M. Robin[46], D. Robinson[32], C. M. Robles Gajardo[146d], M. Robles Manzano[100], A. Robson[57], A. Rocchi[74a,74b], C. Roda[72a,72b], S. Rodriguez Bosca[174], A. Rodriguez Rodriguez[52], A. M. Rodríguez Vera[168b], S. Roe[36], J. Roggel[182], O. Røhne[133], R. Röhrig[115], R. A. Rojas[146d], B. Roland[52], C. P. A. Roland[66], J. Roloff[29], A. Romaniouk[112], M. Romano[23a,23b], N. Rompotis[91], M. Ronzani[125], L. Roos[135], S. Rosati[73a], G. Rosin[103], B. J. Rosser[136], E. Rossi[46], E. Rossi[75a,75b], E. Rossi[70a,70b], L. P. Rossi[55b], L. Rossini[46], R. Rosten[14], M. Rotaru[27b], B. Rottler[52], D. Rousseau[65], G. Rovelli[71a,71b], A. Roy[11], D. Roy[33e], A. Rozanov[102], Y. Rozen[160], X. Ruan[33e], T. A. Ruggeri[1], F. Rühr[52], A. Ruiz-Martinez[174], A. Rummler[36], Z. Rurikova[52], N. A. Rusakovich[80], H. L. Russell[104], L. Rustige[38,47], J. P. Rutherfoord[7], E. M. Rüttinger[149], M. Rybar[142], G. Rybkin[65], E. B. Rye[133], A. Ryzhov[123], J. A. Sabater Iglesias[46], P. Sabatini[174], L. Sabetta[73a,73b], S. Sacerdoti[65], H.F-W. Sadrozinski[145], R. Sadykov[80], F. Safai Tehrani[73a], B. Safarzadeh Samani[156], M. Safdari[153], P. Saha[121], S. Saha[104], M. Sahinsoy[115], A. Sahu[182], M. Saimpert[36], M. Saito[163], T. Saito[163], H. Sakamoto[163], D. Salamani[54], G. Salamanna[75a,75b], A. Salnikov[153], J. Salt[174], A. Salvador Salas[14], D. Salvatore[41a,41b], F. Salvatore[156], A. Salvucci[63a], A. Salzburger[36], J. Samarati[36], D. Sammel[52], D. Sampsonidis[162], D. Sampsonidou[60d,60c], J. Sánchez[174], A. Sanchez Pineda[67a,36,67c], H. Sandaker[133], C. O. Sander[46], I. G. Sanderswood[90], M. Sandhoff[182], C. Sandoval[22b], D. P. C. Sankey[143], M. Sannino[55a,55b], Y. Sano[117], A. Sansoni[51], C. Santoni[38], H. Santos[139a,139b], S. N. Santpur[18], A. Santra[174], K. A. Saoucha[149], A. Sapronov[80], J. G. Saraiva[139a,139d], O. Sasaki[82], K. Sato[169], F. Sauerburger[52], E. Sauvan[5], P. Savard[167,aj], R. Sawada[163], C. Sawyer[143], L. Sawyer[96], I. Sayago Galvan[174], C. Sbarra[23b], A. Sbrizzi[67a,67c], T. Scanlon[95], J. Schaarschmidt[148], P. Schacht[115], D. Schaefer[37], L. Schaefer[136], U. Schäfer[100], A. C. Schaffer[65], D. Schaile[114], R. D. Schamberger[155], E. Schanet[114], C. Scharf[19], N. Scharmberg[101], V. A. Schegelsky[137], D. Scheirich[142], F. Schenck[19], M. Schernau[171], C. Schiavi[55a,55b], L. K. Schildgen[24], Z. M. Schillaci[26], E. J. Schioppa[68a,68b], M. Schioppa[41a,41b], K. E. Schleicher[52], S. Schlenker[36], K. R. Schmidt-Sommerfeld[115], K. Schmieden[100], C. Schmitt[100], S. Schmitt[46], L. Schoeffel[144], A. Schoening[61b], P. G. Scholer[52], E. Schopf[134], M. Schott[100], J. F. P. Schouwenberg[119], J. Schovancova[36], S. Schramm[54], F. Schroeder[182], A. Schulte[100], H-C. Schultz-Coulon[61a], M. Schumacher[52], B. A. Schumm[145], Ph. Schune[144], A. Schwartzman[153], T. A. Schwarz[106], Ph. Schwemling[144], R. Schwienhorst[107], A. Sciandra[145], G. Sciolla[26], F. Scuri[72a], F. Scutti[105], L. M. Scyboz[115], C. D. Sebastiani[91], K. Sedlaczek[47], P. Seema[19], S. C. Seidel[118], A. Seiden[145], B. D. Seidlitz[29], T. Seiss[37], C. Seitz[46], J. M. Seixas[81b], G. Sekhniaidze[70a], S. J. Sekula[42], N. Semprini-Cesari[23a,23b], S. Sen[49], C. Serfon[29], L. Serin[65], L. Serkin[67a,67b], M. Sessa[60a], H. Severini[128], S. Sevova[153], F. Sforza[55a,55b], A. Sfyrla[54], E. Shabalina[53], J. D. Shahinian[136], N. W. Shaikh[45a,45b],

D. Shaked Renous[180], L. Y. Shan[15a], M. Shapiro[18], A. Sharma[36], A. S. Sharma[1], P. B. Shatalov[124], K. Shaw[156], S. M. Shaw[101], M. Shehade[180], Y. Shen[128], A. D. Sherman[25], P. Sherwood[95], L. Shi[95], C. O. Shimmin[183], Y. Shimogama[179], M. Shimojima[116], J. D. Shinner[94], I. P. J. Shipsey[134], S. Shirabe[165], M. Shiyakova[80,y], J. Shlomi[180], A. Shmeleva[111], M. J. Shochet[37], J. Shojaii[105], D. R. Shope[154], S. Shrestha[127], E. M. Shrif[33e], M. J. Shroff[176], E. Shulga[180], P. Sicho[140], A. M. Sickles[173], E. Sideras Haddad[33e], O. Sidiropoulou[36], A. Sidoti[23a,23b], F. Siegert[48], Dj. Sijacki[16], M. Jr. Silva[181], M. V. Silva Oliveira[36], S. B. Silverstein[45a], S. Simion[65], R. Simoniello[100], C. J. Simpson-allsop[21], S. Simsek[12b], P. Sinervo[167], V. Sinetckii[113], S. Singh[152], S. Sinha[33e], M. Sioli[23a,23b], I. Siral[131], S. Yu. Sivoklokov[113], J. Sjölin[45a,45b], A. Skaf[53], E. Skorda[97], P. Skubic[128], M. Slawinska[85], K. Sliwa[170], V. Smakhtin[180], B. H. Smart[143], J. Smiesko[28b], N. Smirnov[112], S. Yu. Smirnov[112], Y. Smirnov[112], L. N. Smirnova[113,s], O. Smirnova[97], E. A. Smith[37], H. A. Smith[134], M. Smizanska[90], K. Smolek[141], A. Smykiewicz[85], A. A. Snesarev[111], H. L. Snoek[120], I. M. Snyder[131], S. Snyder[29], R. Sobie[176,aa], A. Soffer[161], A. Søgaard[50], F. Sohns[53], C. A. Solans Sanchez[36], E. Yu. Soldatov[112], U. Soldevila[174], A. A. Solodkov[123], A. Soloshenko[80], O. V. Solovyanov[123], V. Solovyev[137], P. Sommer[149], H. Son[170], A. Sonay[14], W. Song[143], W. Y. Song[168b], A. Sopczak[141], A. L. Sopio[95], F. Sopkova[28b], S. Sottocornola[71a,71b], R. Soualah[67a,67c], A. M. Soukharev[122a,122b], D. South[46], S. Spagnolo[68a,68b], M. Spalla[115], M. Spangenberg[178], F. Spanò[94], D. Sperlich[52], T. M. Spieker[61a], G. Spigo[36], M. Spina[156], D. P. Spiteri[57], M. Spousta[142], A. Stabile[69a,69b], B. L. Stamas[121], R. Stamen[61a], M. Stamenkovic[120], A. Stampekis[21], E. Stanecka[85], B. Stanislaus[134], M. M. Stanitzki[46], M. Stankaityte[134], B. Stapf[120], E. A. Starchenko[123], G. H. Stark[145], J. Stark[58], P. Staroba[140], P. Starovoitov[61a], S. Stärz[104], R. Staszewski[85], G. Stavropoulos[44], M. Stegler[46], P. Steinberg[29], A. L. Steinhebel[131], B. Stelzer[152,168a], H. J. Stelzer[138], O. Stelzer-Chilton[168a], H. Stenzel[56], T. J. Stevenson[156], G. A. Stewart[36], M. C. Stockton[36], G. Stoicea[27b], M. Stolarski[139a], S. Stonjek[115], A. Straessner[48], J. Strandberg[154], S. Strandberg[45a,45b], M. Strauss[128], T. Strebler[102], P. Strizenec[28b], R. Ströhmer[177], D. M. Strom[131], L. R. Strom[46], R. Stroynowski[42], A. Strubig[45a,45b], S. A. Stucci[29], B. Stugu[17], J. Stupak[128], N. A. Styles[46], D. Su[153], W. Su[60d,148,60c], X. Su[60a], N. B. Suarez[138], V. V. Sulin[111], M. J. Sullivan[91], D. M. S. Sultan[54], S. Sultansoy[4c], T. Sumida[86], S. Sun[106], X. Sun[101], C. J. E. Suster[157], M. R. Sutton[156], S. Suzuki[82], M. Svatos[140], M. Swiatlowski[168a], S. P. Swift[2], T. Swirski[177], A. Sydorenko[100], I. Sykora[28a], M. Sykora[142], T. Sykora[142], D. Ta[100], K. Tackmann[46,x], J. Taenzer[161], A. Taffard[171], R. Tafirout[168a], E. Tagiev[123], R. H. M. Taibah[135], R. Takashima[87], K. Takeda[83], T. Takeshita[150], E. P. Takeva[50], Y. Takubo[82], M. Talby[102], A. A. Talyshev[122a,122b], K. C. Tam[63b], N. M. Tamir[161], J. Tanaka[163], R. Tanaka[65], S. Tapia Araya[173], S. Tapprogge[100], A. Tarek Abouelfadl Mohamed[107], S. Tarem[160], K. Tariq[60b], G. Tarna[27b,e], G. F. Tartarelli[69a], P. Tas[142], M. Tasevsky[140], E. Tassi[41a,41b], G. Tateno[163], A. Tavares Delgado[139a], Y. Tayalati[35e], A. J. Taylor[50], G. N. Taylor[105], W. Taylor[168b], H. Teagle[91], A. S. Tee[90], R. Teixeira De Lima[153], P. Teixeira-Dias[94], H. Ten Kate[36], J. J. Teoh[120], K. Terashi[163], J. Terron[99], S. Terzo[14], M. Testa[51], R. J. Teuscher[167,aa], N. Themistokleous[50], T. Theveneaux-Pelzer[19], D. W. Thomas[94], J. P. Thomas[21], E. A. Thompson[46], P. D. Thompson[21], E. Thomson[136], E. J. Thorpe[93], V. O. Tikhomirov[111,af], Yu. A. Tikhonov[122a,122b], S. Timoshenko[112], P. Tipton[183], S. Tisserant[102], K. Todome[23a,23b], S. Todorova-Nova[142], S. Todt[48], J. Tojo[88], S. Tokár[28a], K. Tokushuku[82], E. Tolley[127], R. Tombs[32], K. G. Tomiwa[33e], M. Tomoto[82,117], L. Tompkins[153], P. Tornambe[103], E. Torrence[131], H. Torres[48], E. Torró Pastor[174], M. Toscani[30], C. Tosciri[134], J. Toth[102,z], D. R. Tovey[149], A. Traeet[17], C. J. Treado[125], T. Trefzger[177], F. Tresoldi[156], A. Tricoli[29], I. M. Trigger[168a], S. Trincaz-Duvoid[135], D. A. Trischuk[175], W. Trischuk[167], B. Trocmé[58], A. Trofymov[65], C. Troncon[69a], F. Trovato[156], L. Truong[33c], M. Trzebinski[85], A. Trzupek[85], F. Tsai[46], P. V. Tsiareshka[108,ad], A. Tsirigotis[162,v], V. Tsiskaridze[155], E. G. Tskhadadze[159a], M. Tsopoulou[162], I. I. Tsukerman[124], V. Tsulaia[18], S. Tsuno[82], D. Tsybychev[155], Y. Tu[63b], A. Tudorache[27b], V. Tudorache[27b], A. N. Tuna[36], S. Turchikhin[80], D. Turgeman[180], I. Turk Cakir[4b,t], R. J. Turner[21], R. Turra[69a], P. M. Tuts[39], S. Tzamarias[162], E. Tzovara[100], K. Uchida[163], F. Ukegawa[169], G. Unal[36], M. Unal[11], A. Undrus[29], G. Unel[171], F. C. Ungaro[105], Y. Unno[82], K. Uno[163], J. Urban[28b], P. Urquijo[105], G. Usai[8], Z. Uysal[12d], V. Vacek[141], B. Vachon[104], K. O. H. Vadla[133], T. Vafeiadis[36], A. Vaidya[95], C. Valderanis[114], E. Valdes Santurio[45a,45b], M. Valente[168a], S. Valentinetti[23a,23b], A. Valero[174], L. Valéry[46], R. A. Vallance[21], A. Vallier[36], J. A. Valls Ferrer[174], T. R. Van Daalen[14], P. Van Gemmeren[6], S. Van Stroud[95], I. Van Vulpen[120], M. Vanadia[74a,74b], W. Vandelli[36], M. Vandenbroucke[144], E. R. Vandewall[129], D. Vannicola[73a,73b], R. Vari[73a], E. W. Varnes[7], C. Varni[55a,55b], T. Varol[158], D. Varouchas[65], K. E. Varvell[157], M. E. Vasile[27b], G. A. Vasquez[176], F. Vazeille[38], D. Vazquez Furelos[14], T. Vazquez Schroeder[36], J. Veatch[53], V. Vecchio[101], M. J. Veen[120], L. M. Veloce[167],

F. Veloso[139a,139c], S. Veneziano[73a], A. Ventura[68a,68b], A. Verbytskyi[115], V. Vercesi[71a], M. Verducci[72a,72b], C. M. Vergel Infante[79], C. Vergis[24], W. Verkerke[120], A. T. Vermeulen[120], J. C. Vermeulen[120], C. Vernieri[153], P. J. Verschuuren[94], M. C. Vetterli[152,aj], N. Viaux Maira[146d], T. Vickey[149], O. E. Vickey Boeriu[149], G. H. A. Viehhauser[134], L. Vigani[61b], M. Villa[23a,23b], M. Villaplana Perez[174], E. M. Villhauer[50], E. Vilucchi[51], M. G. Vincter[34], G. S. Virdee[21], A. Vishwakarma[50], C. Vittori[23a,23b], I. Vivarelli[156], M. Vogel[182], P. Vokac[141], J. Von Ahnen[46], S. E. von Buddenbrock[33e], E. Von Toerne[24], V. Vorobel[142], K. Vorobev[112], M. Vos[174], J. H. Vossebeld[91], M. Vozak[101], N. Vranjes[16], M. Vranjes Milosavljevic[16], V. Vrba[141], M. Vreeswijk[120], N. K. Vu[102], R. Vuillermet[36], I. Vukotic[37], S. Wada[169], P. Wagner[24], W. Wagner[182], J. Wagner-Kuhr[114], S. Wahdan[182], H. Wahlberg[89], R. Wakasa[169], V. M. Walbrecht[115], J. Walder[143], R. Walker[114], S. D. Walker[94], W. Walkowiak[151], V. Wallangen[45a,45b], A. M. Wang[59], A. Z. Wang[181], C. Wang[60a], C. Wang[60c], H. Wang[18], H. Wang[3], J. Wang[63a], P. Wang[42], Q. Wang[128], R.-J. Wang[100], R. Wang[60a], R. Wang[6], S. M. Wang[158], W. T. Wang[60a], W. Wang[15c], W. X. Wang[60a], Y. Wang[60a], Z. Wang[106], C. Wanotayaroj[46], A. Warburton[104], C. P. Ward[32], R. J. Ward[21], N. Warrack[57], A. T. Watson[21], M. F. Watson[21], G. Watts[148], B. M. Waugh[95], A. F. Webb[11], C. Weber[29], M. S. Weber[20], S. A. Weber[34], S. M. Weber[61a], Y. Wei[134], A. R. Weidberg[134], J. Weingarten[47], M. Weirich[100], C. Weiser[52], P. S. Wells[36], T. Wenaus[29], B. Wendland[47], T. Wengler[36], S. Wenig[36], N. Wermes[24], M. Wessels[61a], T. D. Weston[20], K. Whalen[131], A. M. Wharton[90], A. S. White[106], A. White[8], M. J. White[1], D. Whiteson[171], B. W. Whitmore[90], W. Wiedenmann[181], C. Wiel[48], M. Wielers[143], N. Wieseotte[100], C. Wiglesworth[40], L. A. M. Wiik-Fuchs[52], H. G. Wilkens[36], L. J. Wilkins[94], D. M. Williams[39], H. H. Williams[136], S. Williams[32], S. Willocq[103], P. J. Windischhofer[134], I. Wingerter-Seez[5], E. Winkels[156], F. Winklmeier[131], B. T. Winter[52], M. Wittgen[153], M. Wobisch[96], A. Wolf[100], R. Wölker[134], J. Wollrath[52], M. W. Wolter[85], H. Wolters[139a,139c], V. W. S. Wong[175], A. F. Wongel[46], N. L. Woods[145], S. D. Worm[46], B. K. Wosiek[85], K. W. Woźniak[85], K. Wraight[57], S. L. Wu[181], X. Wu[54], Y. Wu[60a], J. Wuerzinger[134], T. R. Wyatt[101], B. M. Wynne[50], S. Xella[40], L. Xia[178], J. Xiang[63c], X. Xiao[106], X. Xie[60a], I. Xiotidis[156], D. Xu[15a], H. Xu[60a], H. Xu[60a], L. Xu[29], R. Xu[136], T. Xu[144], W. Xu[106], Y. Xu[15b], Z. Xu[60b], Z. Xu[153], B. Yabsley[157], S. Yacoob[33a], D. P. Yallup[95], N. Yamaguchi[88], Y. Yamaguchi[165], A. Yamamoto[82], M. Yamatani[163], T. Yamazaki[163], Y. Yamazaki[83], J. Yan[60c], Z. Yan[25], H. J. Yang[60c,60d], H. T. Yang[18], S. Yang[60a], T. Yang[63c], X. Yang[60a], X. Yang[58,60b], Y. Yang[163], Z. Yang[60a], W-M. Yao[18], Y. C. Yap[46], H. Ye[15c], J. Ye[42], S. Ye[29], I. Yeletskikh[80], M. R. Yexley[90], E. Yigitbasi[25], P. Yin[39], K. Yorita[179], K. Yoshihara[79], C. J. S. Young[36], C. Young[153], J. Yu[79], R. Yuan[60b,i], X. Yue[61a], M. Zaazoua[35e], B. Zabinski[85], G. Zacharis[10], E. Zaffaroni[54], J. Zahreddine[135], A. M. Zaitsev[123,ae], T. Zakareishvili[159b], N. Zakharchuk[34], S. Zambito[36], D. Zanzi[36], S. V. Zeißner[47], C. Zeitnitz[182], G. Zemaityte[134], J. C. Zeng[173], O. Zenin[123], T. Ženiš[28a], D. Zerwas[65], M. Zgubič[134], B. Zhang[15c], D. F. Zhang[15b], G. Zhang[15b], J. Zhang[6], Kaili. Zhang[15a], L. Zhang[15c], L. Zhang[60a], M. Zhang[173], R. Zhang[181], S. Zhang[106], X. Zhang[60c], X. Zhang[60b], Y. Zhang[15a,15d], Z. Zhang[63a], Z. Zhang[65], P. Zhao[49], Y. Zhao[145], Z. Zhao[60a], A. Zhemchugov[80], Z. Zheng[106], D. Zhong[173], B. Zhou[106], C. Zhou[181], H. Zhou[7], M. Zhou[155], N. Zhou[60c], Y. Zhou[7], C. G. Zhu[60b], C. Zhu[15a,15d], H. L. Zhu[60a], H. Zhu[15a], J. Zhu[106], Y. Zhu[60a], X. Zhuang[15a], K. Zhukov[111], V. Zhulanov[122a,122b], D. Zieminska[66], N. I. Zimine[80], S. Zimmermann[52], Z. Zinonos[115], M. Ziolkowski[151], L. Živković[16], G. Zobernig[181], A. Zoccoli[23a,23b], K. Zoch[53], T. G. Zorbas[149], R. Zou[37], L. Zwalinski[36]

[1] Department of Physics, University of Adelaide, Adelaide, Australia
[2] Physics Department, SUNY Albany, Albany, NY, USA
[3] Department of Physics, University of Alberta, Edmonton, AB, Canada
[4] [(a)]Department of Physics, Ankara University, Ankara, Turkey; [(b)]Istanbul Aydin University, Application and Research Center for Advanced Studies, Istanbul, Turkey; [(c)]Division of Physics, TOBB University of Economics and Technology, Ankara, Turkey
[5] LAPP, Université Grenoble Alpes, Université Savoie Mont Blanc, CNRS/IN2P3, Annecy, France
[6] High Energy Physics Division, Argonne National Laboratory, Argonne, IL, USA
[7] Department of Physics, University of Arizona, Tucson, AZ, USA
[8] Department of Physics, University of Texas at Arlington, Arlington, TX, USA
[9] Physics Department, National and Kapodistrian University of Athens, Athens, Greece
[10] Physics Department, National Technical University of Athens, Zografou, Greece
[11] Department of Physics, University of Texas at Austin, Austin, TX, USA

[12] [(a)]Bahcesehir University, Faculty of Engineering and Natural Sciences, Istanbul, Turkey; [(b)]Istanbul Bilgi University, Faculty of Engineering and Natural Sciences, Istanbul, Turkey; [(c)]Department of Physics, Bogazici University, Istanbul, Turkey; [(d)]Department of Physics Engineering, Gaziantep University, Gaziantep, Turkey
[13] Institute of Physics, Azerbaijan Academy of Sciences, Baku, Azerbaijan
[14] Institut de Física d'Altes Energies (IFAE), Barcelona Institute of Science and Technology, Barcelona, Spain
[15] [(a)]Institute of High Energy Physics, Chinese Academy of Sciences, Beijing, China; [(b)]Physics Department, Tsinghua University, Beijing, China; [(c)]Department of Physics, Nanjing University, Nanjing, China; [(d)]University of Chinese Academy of Science (UCAS), Beijing, China
[16] Institute of Physics, University of Belgrade, Belgrade, Serbia
[17] Department for Physics and Technology, University of Bergen, Bergen, Norway
[18] Physics Division, Lawrence Berkeley National Laboratory and University of California, Berkeley, CA, USA
[19] Institut für Physik, Humboldt Universität zu Berlin, Berlin, Germany
[20] Albert Einstein Center for Fundamental Physics and Laboratory for High Energy Physics, University of Bern, Bern, Switzerland
[21] School of Physics and Astronomy, University of Birmingham, Birmingham, UK
[22] [(a)]Facultad de Ciencias y Centro de Investigaciónes, Universidad Antonio Nariño, Bogotá, Colombia; [(b)]Departamento de Física, Universidad Nacional de Colombia, Bogotá, Colombia
[23] [(a)]Dipartimento di Fisica, INFN Bologna and Universita' di Bologna, Bologna, Italy; [(b)]INFN Sezione di Bologna, Bologna, Italy
[24] Physikalisches Institut, Universität Bonn, Bonn, Germany
[25] Department of Physics, Boston University, Boston, MA, USA
[26] Department of Physics, Brandeis University, Waltham, MA, USA
[27] [(a)]Transilvania University of Brasov, Brasov, Romania; [(b)]Horia Hulubei National Institute of Physics and Nuclear Engineering, Bucharest, Romania; [(c)]Department of Physics, Alexandru Ioan Cuza University of Iasi, Iasi, Romania ; [(d)]Physics Department, National Institute for Research and Development of Isotopic and Molecular Technologies, Cluj-Napoca, Romania; [(e)]University Politehnica Bucharest, Bucharest, Romania; [(f)]West University in Timisoara, Timisoara, Romania
[28] [(a)]Faculty of Mathematics, Physics and Informatics, Comenius University, Bratislava, Slovak Republic; [(b)]Department of Subnuclear Physics, Institute of Experimental Physics of the Slovak Academy of Sciences, Kosice, Slovak Republic
[29] Physics Department, Brookhaven National Laboratory, Upton, NY, USA
[30] Departamento de Física, Universidad de Buenos Aires, Buenos Aires, Argentina
[31] California State University, CA, USA
[32] Cavendish Laboratory, University of Cambridge, Cambridge, UK
[33] [(a)]Department of Physics, University of Cape Town, Cape Town, South Africa; [(b)]iThemba Labs, Western Cape, South Africa; [(c)]Department of Mechanical Engineering Science, University of Johannesburg, Johannesburg, South Africa; [(d)]Department of Physics, University of South Africa, Pretoria, South Africa; [(e)]School of Physics, University of the Witwatersrand, Johannesburg, South Africa
[34] Department of Physics, Carleton University, Ottawa, ON, Canada
[35] [(a)]Faculté des Sciences Ain Chock, Réseau Universitaire de Physique des Hautes Energies-Université Hassan II, Casablanca, Morocco; [(b)]Faculté des Sciences, Université Ibn-Tofail, Kénitra, Morocco; [(c)]Faculté des Sciences Semlalia, Université Cadi Ayyad, LPHEA-Marrakech, Morocco; [(d)]Faculté des Sciences, Université Mohamed Premier and LPTPM, Oujda, Morocco; [(e)]Faculté des sciences, Université Mohammed V, Rabat, Morocco
[36] CERN, Geneva, Switzerland
[37] Enrico Fermi Institute, University of Chicago, Chicago, IL, USA
[38] LPC, Université Clermont Auvergne, CNRS/IN2P3, Clermont-Ferrand, France
[39] Nevis Laboratory, Columbia University, Irvington, NY, USA
[40] Niels Bohr Institute, University of Copenhagen, Copenhagen, Denmark
[41] [(a)]Dipartimento di Fisica, Università della Calabria, Rende, Italy; [(b)]INFN Gruppo Collegato di Cosenza, Laboratori Nazionali di Frascati, Frascati, Italy
[42] Physics Department, Southern Methodist University, Dallas, TX, USA
[43] Physics Department, University of Texas at Dallas, Richardson, TX, USA
[44] National Centre for Scientific Research "Demokritos", Agia Paraskevi, Greece
[45] [(a)]Department of Physics, Stockholm University, Stockholm, Sweden; [(b)]Oskar Klein Centre, Stockholm, Sweden

[46] Deutsches Elektronen-Synchrotron DESY, Hamburg and Zeuthen, Germany
[47] Lehrstuhl für Experimentelle Physik IV, Technische Universität Dortmund, Dortmund, Germany
[48] Institut für Kern- und Teilchenphysik, Technische Universität Dresden, Dresden, Germany
[49] Department of Physics, Duke University, Durham, NC, USA
[50] SUPA-School of Physics and Astronomy, University of Edinburgh, Edinburgh, UK
[51] INFN e Laboratori Nazionali di Frascati, Frascati, Italy
[52] Physikalisches Institut, Albert-Ludwigs-Universität Freiburg, Freiburg, Germany
[53] II. Physikalisches Institut, Georg-August-Universität Göttingen, Göttingen, Germany
[54] Département de Physique Nucléaire et Corpusculaire, Université de Genève, Geneva, Switzerland
[55] [(a)]Dipartimento di Fisica, Università di Genova, Genoa, Italy; [(b)]INFN Sezione di Genova, Genoa, Italy
[56] II. Physikalisches Institut, Justus-Liebig-Universität Giessen, Giessen, Germany
[57] SUPA-School of Physics and Astronomy, University of Glasgow, Glasgow, UK
[58] LPSC, Université Grenoble Alpes, CNRS/IN2P3, Grenoble INP, Grenoble, France
[59] Laboratory for Particle Physics and Cosmology, Harvard University, Cambridge, MA, USA
[60] [(a)]Department of Modern Physics and State Key Laboratory of Particle Detection and Electronics, University of Science and Technology of China, Hefei, China; [(b)]Institute of Frontier and Interdisciplinary Science and Key Laboratory of Particle Physics and Particle Irradiation (MOE), Shandong University, Qingdao, China; [(c)]School of Physics and Astronomy,, Shanghai Jiao Tong University, KLPPAC-MoE, SKLPPC, Shanghai, China; [(d)]Tsung-Dao Lee Institute, Shanghai, China
[61] [(a)]Kirchhoff-Institut für Physik, Ruprecht-Karls-Universität Heidelberg, Heidelberg, Germany; [(b)]Physikalisches Institut, Ruprecht-Karls-Universität Heidelberg, Heidelberg, Germany
[62] Faculty of Applied Information Science, Hiroshima Institute of Technology, Hiroshima, Japan
[63] [(a)]Department of Physics, Chinese University of Hong Kong, Shatin N.T., Hong Kong, China; [(b)]Department of Physics, University of Hong Kong, Hong Kong, China; [(c)]Department of Physics and Institute for Advanced Study, Hong Kong University of Science and Technology, Clear Water Bay, Kowloon, Hong Kong, China
[64] Department of Physics, National Tsing Hua University, Hsinchu, Taiwan
[65] IJCLab, Université Paris-Saclay, CNRS/IN2P3, 91405 Orsay, France
[66] Department of Physics, Indiana University, Bloomington, IN, USA
[67] [(a)]INFN Gruppo Collegato di Udine, Sezione di Trieste, Udine, Italy; [(b)]ICTP, Trieste, Italy; [(c)]Dipartimento Politecnico di Ingegneria e Architettura, Università di Udine, Udine, Italy
[68] [(a)]INFN Sezione di Lecce, Lecce, Italy; [(b)]Dipartimento di Matematica e Fisica, Università del Salento, Lecce, Italy
[69] [(a)]INFN Sezione di Milano, Milan, Italy; [(b)]Dipartimento di Fisica, Università di Milano, Milan, Italy
[70] [(a)]INFN Sezione di Napoli, Naples, Italy; [(b)]Dipartimento di Fisica, Università di Napoli, Naples, Italy
[71] [(a)]INFN Sezione di Pavia, Pavia, Italy; [(b)]Dipartimento di Fisica, Università di Pavia, Pavia, Italy
[72] [(a)]INFN Sezione di Pisa, Pisa, Italy; [(b)]Dipartimento di Fisica E. Fermi, Università di Pisa, Pisa, Italy
[73] [(a)]INFN Sezione di Roma, Rome, Italy; [(b)]Dipartimento di Fisica, Sapienza Università di Roma, Rome, Italy
[74] [(a)]INFN Sezione di Roma Tor Vergata, Rome, Italy; [(b)]Dipartimento di Fisica, Università di Roma Tor Vergata, Rome, Italy
[75] [(a)]INFN Sezione di Roma Tre, Rome, Italy; [(b)]Dipartimento di Matematica e Fisica, Università Roma Tre, Rome, Italy
[76] [(a)]INFN-TIFPA, Povo, Italy; [(b)]Università degli Studi di Trento, Trento, Italy
[77] Institut für Astro- und Teilchenphysik, Leopold-Franzens-Universität, Innsbruck, Austria
[78] University of Iowa, Iowa City, IA, USA
[79] Department of Physics and Astronomy, Iowa State University, Ames, IA, USA
[80] Joint Institute for Nuclear Research, Dubna, Russia
[81] [(a)]Departamento de Engenharia Elétrica, Universidade Federal de Juiz de Fora (UFJF), Juiz de Fora, Brazil; [(b)]Universidade Federal do Rio De Janeiro COPPE/EE/IF, Rio de Janeiro, Brazil; [(c)]Instituto de Física, Universidade de São Paulo, São Paulo, Brazil
[82] KEK, High Energy Accelerator Research Organization, Tsukuba, Japan
[83] Graduate School of Science, Kobe University, Kobe, Japan
[84] [(a)]AGH University of Science and Technology, Faculty of Physics and Applied Computer Science, Kraków, Poland; [(b)]Marian Smoluchowski Institute of Physics, Jagiellonian University, Kraków, Poland
[85] Institute of Nuclear Physics Polish Academy of Sciences, Kraków, Poland
[86] Faculty of Science, Kyoto University, Kyoto, Japan

[87] Kyoto University of Education, Kyoto, Japan
[88] Research Center for Advanced Particle Physics and Department of Physics, Kyushu University, Fukuoka , Japan
[89] Instituto de Física La Plata, Universidad Nacional de La Plata and CONICET, La Plata, Argentina
[90] Physics Department, Lancaster University, Lancaster, UK
[91] Oliver Lodge Laboratory, University of Liverpool, Liverpool, UK
[92] Department of Experimental Particle Physics, Jožef Stefan Institute and Department of Physics, University of Ljubljana, Ljubljana, Slovenia
[93] School of Physics and Astronomy, Queen Mary University of London, London, UK
[94] Department of Physics, Royal Holloway University of London, Egham, UK
[95] Department of Physics and Astronomy, University College London, London, UK
[96] Louisiana Tech University, Ruston, LA, USA
[97] Fysiska institutionen, Lunds universitet, Lund, Sweden
[98] Centre de Calcul de l'Institut National de Physique Nucléaire et de Physique des Particules (IN2P3), Villeurbanne, France
[99] Departamento de Física Teorica C-15 and CIAFF, Universidad Autónoma de Madrid, Madrid, Spain
[100] Institut für Physik, Universität Mainz, Mainz, Germany
[101] School of Physics and Astronomy, University of Manchester, Manchester, UK
[102] CPPM, Aix-Marseille Université, CNRS/IN2P3, Marseille, France
[103] Department of Physics, University of Massachusetts, Amherst, MA, USA
[104] Department of Physics, McGill University, Montreal, QC, Canada
[105] School of Physics, University of Melbourne, Melbourne, VIC, Australia
[106] Department of Physics, University of Michigan, Ann Arbor, MI, USA
[107] Department of Physics and Astronomy, Michigan State University, East Lansing, MI, USA
[108] B.I. Stepanov Institute of Physics, National Academy of Sciences of Belarus, Minsk, Belarus
[109] Research Institute for Nuclear Problems of Byelorussian State University, Minsk, Belarus
[110] Group of Particle Physics, University of Montreal, Montreal, QC, Canada
[111] P.N. Lebedev Physical Institute of the Russian Academy of Sciences, Moscow, Russia
[112] National Research Nuclear University MEPhI, Moscow, Russia
[113] D.V. Skobeltsyn Institute of Nuclear Physics, M.V. Lomonosov Moscow State University, Moscow, Russia
[114] Fakultät für Physik, Ludwig-Maximilians-Universität München, Munich, Germany
[115] Max-Planck-Institut für Physik (Werner-Heisenberg-Institut), Munich, Germany
[116] Nagasaki Institute of Applied Science, Nagasaki, Japan
[117] Graduate School of Science and Kobayashi-Maskawa Institute, Nagoya University, Nagoya, Japan
[118] Department of Physics and Astronomy, University of New Mexico, Albuquerque, NM, USA
[119] Institute for Mathematics, Astrophysics and Particle Physics, Radboud University Nijmegen/Nikhef, Nijmegen, The Netherlands
[120] Nikhef National Institute for Subatomic Physics and University of Amsterdam, Amsterdam, The Netherlands
[121] Department of Physics, Northern Illinois University, DeKalb, IL, USA
[122] [(a)]Budker Institute of Nuclear Physics and NSU, SB RAS, Novosibirsk, Russia; [(b)]Novosibirsk State University Novosibirsk, Novosibirsk, Russia
[123] Institute for High Energy Physics of the National Research Centre Kurchatov Institute, Protvino, Russia
[124] Institute for Theoretical and Experimental Physics named by A.I. Alikhanov of National Research Centre "Kurchatov Institute", Moscow, Russia
[125] Department of Physics, New York University, New York, NY, USA
[126] Ochanomizu University, Otsuka, Bunkyo-ku, Tokyo, Japan
[127] Ohio State University, Columbus, OH, USA
[128] Homer L. Dodge Department of Physics and Astronomy, University of Oklahoma, Norman, OK, USA
[129] Department of Physics, Oklahoma State University, Stillwater, OK, USA
[130] Palacký University, RCPTM, Joint Laboratory of Optics, Olomouc, Czech Republic
[131] Institute for Fundamental Science, University of Oregon, Eugene, OR, USA
[132] Graduate School of Science, Osaka University, Osaka, Japan
[133] Department of Physics, University of Oslo, Oslo, Norway
[134] Department of Physics, Oxford University, Oxford, UK

[135] LPNHE, Sorbonne Université, Université de Paris, CNRS/IN2P3, Paris, France
[136] Department of Physics, University of Pennsylvania, Philadelphia, PA, USA
[137] Konstantinov Nuclear Physics Institute of National Research Centre "Kurchatov Institute", PNPI, St. Petersburg, Russia
[138] Department of Physics and Astronomy, University of Pittsburgh, Pittsburgh, PA, USA
[139] [(a)]Laboratório de Instrumentação e Física Experimental de Partículas-LIP, Lisboa, Portugal; [(b)]Departamento de Física, Faculdade de Ciências, Universidade de Lisboa, Lisbon, Portugal; [(c)]Departamento de Física, Universidade de Coimbra, Coimbra, Portugal; [(d)]Centro de Física Nuclear da Universidade de Lisboa, Lisbon, Portugal; [(e)]Departamento de Física, Universidade do Minho, Braga, Portugal; [(f)]Departamento de Física Teórica y del Cosmos, Universidad de Granada, Granada, Spain; [(g)]Dep Física and CEFITEC of Faculdade de Ciências e Tecnologia, Universidade Nova de Lisboa, Caparica, Portugal; [(h)]Instituto Superior Técnico, Universidade de Lisboa, Lisbon, Portugal
[140] Institute of Physics of the Czech Academy of Sciences, Prague, Czech Republic
[141] Czech Technical University in Prague, Prague, Czech Republic
[142] Charles University, Faculty of Mathematics and Physics, Prague, Czech Republic
[143] Particle Physics Department, Rutherford Appleton Laboratory, Didcot, UK
[144] IRFU, CEA, Université Paris-Saclay, Gif-sur-Yvette, France
[145] Santa Cruz Institute for Particle Physics, University of California Santa Cruz, Santa Cruz, CA, USA
[146] [(a)]Departamento de Física, Pontificia Universidad Católica de Chile, Santiago, Chile; [(b)]Department of Physics, Universidad Andres Bello, Santiago, Chile; [(c)]Instituto de Alta Investigación, Universidad de Tarapacá, Santiago, Chile; [(d)]Departamento de Física, Universidad Técnica Federico Santa María, Valparaíso, Chile
[147] Universidade Federal de São João del Rei (UFSJ), São João del Rei, Brazil
[148] Department of Physics, University of Washington, Seattle, WA, USA
[149] Department of Physics and Astronomy, University of Sheffield, Sheffield, UK
[150] Department of Physics, Shinshu University, Nagano, Japan
[151] Department Physik, Universität Siegen, Siegen, Germany
[152] Department of Physics, Simon Fraser University, Burnaby, BC, Canada
[153] SLAC National Accelerator Laboratory, Stanford, CA, USA
[154] Physics Department, Royal Institute of Technology, Stockholm, Sweden
[155] Departments of Physics and Astronomy, Stony Brook University, Stony Brook, NY, USA
[156] Department of Physics and Astronomy, University of Sussex, Brighton, UK
[157] School of Physics, University of Sydney, Sydney, Australia
[158] Institute of Physics, Academia Sinica, Taipei, Taiwan
[159] [(a)]E. Andronikashvili Institute of Physics, Iv. Javakhishvili Tbilisi State University, Tbilisi, Georgia; [(b)]High Energy Physics Institute, Tbilisi State University, Tbilisi, Georgia
[160] Department of Physics, Technion, Israel Institute of Technology, Haifa, Israel
[161] Raymond and Beverly Sackler School of Physics and Astronomy, Tel Aviv University, Tel Aviv, Israel
[162] Department of Physics, Aristotle University of Thessaloniki, Thessaloniki, Greece
[163] International Center for Elementary Particle Physics and Department of Physics, University of Tokyo, Tokyo, Japan
[164] Graduate School of Science and Technology, Tokyo Metropolitan University, Tokyo, Japan
[165] Department of Physics, Tokyo Institute of Technology, Tokyo, Japan
[166] Tomsk State University, Tomsk, Russia
[167] Department of Physics, University of Toronto, Toronto, ON, Canada
[168] [(a)]TRIUMF, Vancouver, BC, Canada; [(b)]Department of Physics and Astronomy, York University, Toronto, ON, Canada
[169] Division of Physics and Tomonaga Center for the History of the Universe, Faculty of Pure and Applied Sciences, University of Tsukuba, Tsukuba, Japan
[170] Department of Physics and Astronomy, Tufts University, Medford, MA, USA
[171] Department of Physics and Astronomy, University of California Irvine, Irvine, CA, USA
[172] Department of Physics and Astronomy, University of Uppsala, Uppsala, Sweden
[173] Department of Physics, University of Illinois, Urbana, IL, USA
[174] Instituto de Física Corpuscular (IFIC), Centro Mixto Universidad de Valencia - CSIC, Valencia, Spain
[175] Department of Physics, University of British Columbia, Vancouver, BC, Canada
[176] Department of Physics and Astronomy, University of Victoria, Victoria, BC, Canada
[177] Fakultät für Physik und Astronomie, Julius-Maximilians-Universität Würzburg, Würzburg, Germany

[178] Department of Physics, University of Warwick, Coventry, UK
[179] Waseda University, Tokyo, Japan
[180] Department of Particle Physics and Astrophysics, Weizmann Institute of Science, Rehovot, Israel
[181] Department of Physics, University of Wisconsin, Madison, WI, USA
[182] Fakultät für Mathematik und Naturwissenschaften, Fachgruppe Physik, Bergische Universität Wuppertal, Wuppertal, Germany
[183] Department of Physics, Yale University, New Haven, CT, USA

[a] Also at Borough of Manhattan Community College, City University of New York, New York, NY, USA
[b] Also at Center for High Energy Physics, Peking University, China
[c] Also at Centro Studi e Ricerche Enrico Fermi, Rome, Italy
[d] Also at CERN, Geneva, Switzerland
[e] Also at CPPM, Aix-Marseille Université, CNRS/IN2P3, Marseille, France
[f] Also at Département de Physique Nucléaire et Corpusculaire, Université de Genève, Geneva, Switzerland
[g] Also at Departament de Fisica de la Universitat Autonoma de Barcelona, Barcelona, Spain
[h] Also at Department of Financial and Management Engineering, University of the Aegean, Chios, Greece
[i] Also at Department of Physics and Astronomy, Michigan State University, East Lansing, MI, USA
[j] Also at Department of Physics and Astronomy, University of Louisville, Louisville, KY, USA
[k] Also at Department of Physics, Ben Gurion University of the Negev, Beer Sheva, Israel
[l] Also at Department of Physics, California State University, East Bay, USA
[m] Also at Department of Physics, California State University, Fresno, USA
[n] Also at Department of Physics, California State University, Sacramento, USA
[o] Also at Department of Physics, King's College London, London, UK
[p] Also at Department of Physics, St. Petersburg State Polytechnical University, St. Petersburg, Russia
[q] Also at Department of Physics, University of Fribourg, Fribourg, Switzerland
[r] Also at Dipartimento di Matematica, Informatica e Fisica, Università di Udine, Udine, Italy
[s] Also at Faculty of Physics, M.V. Lomonosov Moscow State University, Moscow, Russia
[t] Also at Giresun University, Faculty of Engineering, Giresun, Turkey
[u] Also at Graduate School of Science, Osaka University, Osaka, Japan
[v] Also at Hellenic Open University, Patras, Greece
[w] Also at Institucio Catalana de Recerca i Estudis Avancats, ICREA, Barcelona, Spain
[x] Also at Institut für Experimentalphysik, Universität Hamburg, Hamburg, Germany
[y] Also at Institute for Nuclear Research and Nuclear Energy (INRNE) of the Bulgarian Academy of Sciences, Sofia, Bulgaria
[z] Also at Institute for Particle and Nuclear Physics, Wigner Research Centre for Physics, Budapest, Hungary
[aa] Also at Institute of Particle Physics (IPP), Victoria, Canada
[ab] Also at Institute of Physics, Azerbaijan Academy of Sciences, Baku, Azerbaijan
[ac] Also at Instituto de Fisica Teorica, IFT-UAM/CSIC, Madrid, Spain
[ad] Also at Joint Institute for Nuclear Research, Dubna, Russia
[ae] Also at Moscow Institute of Physics and Technology State University, Dolgoprudny, Russia
[af] Also at National Research Nuclear University MEPhI, Moscow, Russia
[ag] Also at Physics Department, An-Najah National University, Nablus, Palestine
[ah] Also at Physikalisches Institut, Albert-Ludwigs-Universität Freiburg, Freiburg, Germany
[ai] Also at The City College of New York, New York, NY, USA
[aj] Also at TRIUMF, Vancouver, BC, Canada
[ak] Also at Universita di Napoli Parthenope, Naples, Italy
[al] Also at University of Chinese Academy of Sciences (UCAS), Beijing, China
* Deceased